Integrated Electromechanical Wind Turbine Control for Power System Operation and Load Reduction

Fan Zhang

Industrial Control Centre,
Department of Electronic and Electrical Engineering,
University of Strathclyde,
204 George Street,
Glasgow G1 1XW

Thesis submitted to the University of Strathclyde for the degree of Doctor of Philosophy

July 2013

This thesis is the result of the author's original research. It has been composed by the author and has not been previously submitted for examination which has led to the award of a degree.

The copyright of this thesis belongs to the author under the terms of the United Kingdom Copyright Acts as qualified by University of Strathclyde Regulation 3.50. Due acknowledgement must always be made of the use of any material contained in, or derived from, this thesis.

ABSTRACT

With the penetration level of wind power in electric power networks increasing rapidly all over the world, modern wind turbines are challenged to provide the same grid services as conventional synchronous power plants. The dynamic interaction between wind turbines and grid has to be assessed first before replacing large amount of conventional power plants by wind power. Over the last few years many power system operators have revised their grid codes and established more demanding requirements for wind power connection. In the past, when wind turbines were small, they were allowed to simply disconnect during a grid fault/disturbance. However, as wind turbine size has increased considerably, their fault ride-through capability has to be improved if the penetration of wind power is to be further increased. Wind turbine design and control need to be improved to optimize the compatibility of wind power and the grid.

Among the various requirements that wind turbines have to meet, fault ride-through is of great importance and a very challenging one. Grid faults cause transients not only in the electrical system, but also in the wind turbine mechanical system. The dynamic performance of wind turbines is determined by both mechanical and electrical systems. From the mechanical point of view, the grid disturbance adds extra loads on wind turbine components. Severe grid faults may even lead to wind turbine emergency shut-down. From the electrical point of view, wind farms may lose power generation during a grid fault, which deteriorates the fault impact and slows down the fault recovery. Advanced control and active damping is required to improve wind turbine operation and assist it to remain connected during a grid fault. The novelty of this research is the study of the interaction between mechanical and electrical systems of the wind turbine. The detailed modelling of both the wind turbine mechanical and electrical dynamics not only helps to identify possible

problems that wind turbines encounter during grid faults, but also allows adopting a combined approach to design the wind turbine controller.

This thesis aims at improving the wind turbine fault ride-through capability and the ability of wind turbine to provide network support during grid disturbances. The main contents are as follows:

- The detailed model of wind turbine and grid including wind turbine mechanical model, wind turbine controller, synchronous and induction generator model, doubly fed induction generator (DFIG) controller and a generic network model are presented.

- A wind turbine fault ride-through strategy considering structural loads alleviation is proposed.

- A controller for asymmetrical fault ride-through of DFIG wind turbines is presented.

- The effect of having Power System Stabilizer (PSS) on wind turbine is investigated. A multi-band PSS controller for DFIG wind turbine is demonstrated.

ACKNOWLEDGEMENT

First of all, I would like to express my deep gratitude to my supervisor Professor Bill Leithead who has taken me in and guided me through my PhD study. His advice has helped me a lot on my research. I would also like to thank my second supervisor Dr. Olimpo Anaya-lara for his technical guidance. The time he spent to discuss my work with me is greatly appreciated.

I would like to thank UK-China Joint Research Consortium on Sustainable Electric Power Supply for providing financial support for this research project. Many thanks for holding the annual PhD summer school/conference where I had great experiences and gained lots of innovative ideas.

Furthermore, Many thanks to my colleagues in the Industrial Control Centre of the University of Strathclyde. I had an enjoyable work environment and great time.

Finally, I would like to thank my parents for their love and support throughout my life.

TABLE OF CONTENTS

LIST OF FIGURES

LIST OF TABLES

ABBREVIATIONS AND NOMENCLATURE

AVR	Active Voltage Regulator
DFIG	Doubly Fed Induction Generator
DRF	Dual Reference Frame
FRC	Fully Rated Converter
FRT	Fault Ride-Through
FSWT	Fixed Speed Wind Turbine
KCL	Kirchhoff's Current Law
KVL	Kirchhoff's Voltage Law
LVRT	Low Voltage Ride-Through
PCC	Point of Common Coupling
PMG	Permanent Magnet Generator
PSS	Power System Stabilizer
SCIG	Squirrel-Cage Induction Generator
SFO	Stator Flux Oriented
SRF	Single Reference Frame
SVO	Stator Voltage Oriented
TSO	Transmission System Operator
VSWT	Variable Speed Wind Turbine

Wind turbine

Ω	Rotor speed
C_p	Power coefficient
T_H	Hub torque
T_1	Gearbox torque
β	Pitch angle

λ	Tip speed ratio

Electrical system

V	Voltage vector
I	Current vector
ψ	Flux vector
$R_{s,}$ R_r	Stator, rotor resistance
L_s, L_r, L_{ls}, L_{lr}	Stator, rotor self and leakage inductance
L_m	Mutual inductance
s	Slip
ω_s, ω_r	Stator, rotor speed
P, Q	Active, reactive power
α, β	α, β axis subscripts
d, q	d, q axis subscripts

CHAPTER 1: BACKGROUND

There is great interest in the development of renewable energy worldwide due to concerns over the environment and shortness of fossil fuels. The Intergovernmental Panel on Climate Change (IPCC) estimates that global temperature will increase by $1.4^{\circ}C$ to $5.8^{\circ}C$ from 1900 to 2100 [1]. To protect life on Earth from the danger of global warming, the Kyoto Protocol was adopted on 11th December 1997 to limit the emission of greenhouse gases [2]. It is expected that using energy more efficiently and increasing renewable energy generation will help reduce most emissions. Judging by the current consumption of conventional energy, the reserves of fossil fuel will only be able to last another 200 years. Natural gas will run out in about 50 years and oil in 30 years. The most viable solution to the imminent energy crisis is to develop renewable energy technology and shift the energy structure from using non-renewable resources to renewable energy.

Among various types of renewable energy, a promising and popular one is wind power, which currently has the largest penetration level on electricity networks compared to other renewable energy sources. According to Renewable UK [3], wind energy supplies 5% of the UK national electricity by 2012. By the end of 2014, the percentage is expected to increase to 10%, which means the amount of wind power will double in two years. In 2016 wind power is expected to take the place of nuclear power and become the second largest electricity supply after natural gas. There are currently about 7 GW wind capacity in operation in the UK and 4 GW under construction. Another 5 GW wind power is approved and waiting for construction. At present onshore wind generation capacity dominates over offshore in the UK. However, offshore wind farms are growing at a faster pace, as wind speeds offshore are higher and less turbulent.

The rapid growth of wind power is not only happening in the UK but also in many other countries around the world. In the past decade, the share of the wind power capacity in power networks increased from 2.2% to 10% in Europe which makes wind the major renewable energy resource followed by solar PV [4]. The target is that in 2020 wind power will supply 20% of the overall European electricity. China is dominating in both the amount and the growing speed of the installed wind power capacity. By the end of 2011 China had installed 62 GW wind capacity while the plan is in 2015 the number will increase to 100 GW. The United States installed about 7 GW of wind power generation system and remains the second largest country in installed wind capacity [5]. According to a report by the Global Wind Energy Association (GWEA), there were in total 40.5 GW wind power connected to power systems in 2011 which represents 6% of market growth compared to 2010 despite a relatively bad economic environment [6]. The total installed wind power in the world increased to 238 GW by the end of 2011 thanks to the continuing fast growth of wind energy. The top10 countries in the installed wind power capacity are shown in Figure 1-1 and Table 1-1.

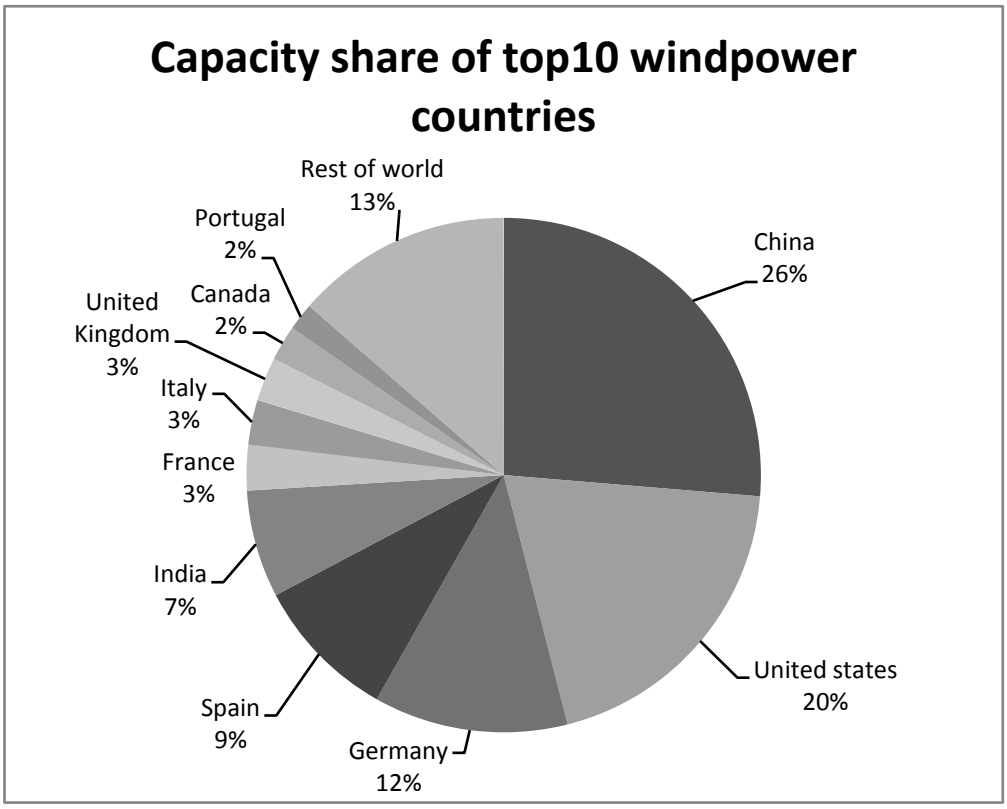

Figure 1-1: Wind power capacity share of top10 countries.[7]

It can be seen from Figure 1-1 that China has the largest wind power capacity, which is 26% of the total wind power in the world. The United States market kept its fast growth and remains in second place. Due to its framework and long-term plan of the for renewable energy development, the European market is stable as usual, and is about the same size as the sum of Chinese and US markets. However, the installed capacity does not necessarily mean the actual power generated. The online time of wind farms is limited by many factors. China is facing a lot of wind power integration problems. The large and complex Chinese power grid is not able to adapt to the sudden inrush of wind power. Although China has the most wind power installed, the actual production from wind is only half that of the US wind power generation in 2010. US wind power development is highly dependent on policy issues. The Federal Production Tax credit (PTC) has significantly speeded up the growth of wind power in the past few years in US but the continuity of the policy

cannot be guaranteed in the coming years. Once the policy is stopped, a large decrease of wind power generation construction can be expected. Europe is a good example of the stable wind power market. The support from the government and relatively strong grid has guaranteed the efficient usage of the installed wind power capacity. Table 1-1 shows the difference between the installed capacity and the electricity generation of the top10 wind power countries in 2010.

Table 1-1: Capacity and generated power of top10 wind power countries.[8]

Countries	Installed capacity (MW)		Countries	Electricity generation (TWh)
China	44733		China	55.5
USA	40180		USA	94.65
Germany	27215		Germany	35.90
Spain	20676		Spain	41.5
India	13065		India	20.6
Italy	5797		France	9.20
France	5660		Italy	8.0
UK	5204		UK	9.7
Canada	4008		Canada	5.5
Portugal	3702		Portugal	8.6
World total	196630		World total	327.85

It is noticed from Table 1-1 that in developed countries, the efficiency of generating electricity by existing wind farms is significantly higher than in developing countries. One reason is that wind turbines used in developed countries are more advanced and have a larger size, which increases efficiency. However, wind turbine design and

manufacturing techniques in developing countries such as China and India are under fast development in recent years and the wind turbines installed in these countries are able to operate with satisfactory performance. The major reason for the low energy production is that the power systems in these countries are weaker compared to others. The large amount of wind power integration causes various power system operation problems such as frequency and peak-load regulation. Strong grids also face same problems if more wind power is to be connected. Most countries in the world have large ambition on developing wind power therefore the compatibility between the wind turbine and the power system must be further investigated and improved.

CHAPTER 2: INTRODUCTION

2.1 Review of connection requirements for wind energy

Transmission system operators (TSOs) have been updating the requirements for wind farms to be connected to power systems to accommodate the increase in penetration level of wind power. In the early years when wind turbines were of small sizes and the effect they had on power system operation was not significant, most TSOs did not expect wind farms to contribute to any kind of power system control activity, therefore did not specify the requirement for wind power integration in their grid codes. Wind turbines were considered as a kind of embedded generator and free to connect to the grid. However, due to the fluctuating nature of wind power generation and lack of control to assist the stable operation of a power system, wind farms are normally the first that get disconnected during abnormal grid events such as frequency variation, voltage collapse and large power flow. Since wind power only accounts for a small portion of total power in the grid, the disconnection of wind farms helps TSOs to simplify the situation during grid events by eliminating uncontrolled power plants.

Over recent years, considerable amount of wind power capacity is installed all over the world. Wind power plants are having larger impact on the stability of power systems. TSOs decide that wind farms cannot be simply disconnected during grid events, as the sudden loss of large amount of power would deteriorate the grid disturbance. The requirements for wind power integration into power systems are added to grid codes and wind farms are obliged to contribute to power system stability under these requirements. At present, all the existing grid codes have included fault ride-through and frequency support requirements from wind farms [9].

The level of the contribution that wind turbines should be able to provide to the grid varies from country to country as the grid strength and the penetration level of wind power is different. A commonly accepted understanding is that wind power plants should be able to provide similar grid services as synchronous generators, which are used in conventional power plants. Synchronous generators have been maintaining the power system stability well by assisting in the grid frequency, reactive power and voltage control and transient stability [10]. Wind turbines that use induction generators, such as DFIG, and permanent-magnet synchronous generators with fully-rated converters, are also required by grid codes to provide support in these aspects. It is necessary to review the requirements set for wind power integration in grid codes so that wind turbines can be designed to comply with the requirements of TSOs.

All grid codes have similar requirements for wind power connection but differ in the details. The grid code of certain representative countries in wind energy are selected and reviewed here.

- GB National Grid [11] (including the Scottish connection requirements [12]) are reviewed because of the high potential of wind power, especially offshore wind power, in the UK. The detailed regulation for non-synchronous machines in this code is of great interest in the context of the study of wind turbine.

- Denmark is the country with the highest wind power penetration level in the world. The requirement for wind turbine connection is explained in separate sections in the Danish grid codes [13, 14]. It is also the only grid code that has different requirements based on voltage level.

- Wind power is an important energy source in the German power system and the German system operator EON Netz started issuing a grid code containing requirements for wind farms very early [15]. The code is often used as a

reference when drafting other grid codes. A file which specifies the requirements for offshore wind turbines are provided as a supplement to the grid code [16].

- China, as the country with the largest installed wind power capacity, has not issued an official grid code that explains the requirements for wind farm integration. However, a technical regulation draft [17] has been issued as reference for wind farms construction.

- The US Federal Energy Regulatory Commission issued the rules for wind energy interconnection in June 2005 [18]. The US code is chosen as a representation of North America.

A large number of grid codes reviews for wind turbine interconnection can be found in the open literature, as they are the foundation work for large-scale wind power integration [10, 19-27]. These grid codes, especially the parts related to wind turbine interconnection, are revised frequently in recent years to fit the wind power increase. A brief review of the most up-to-date grid codes is given here as a design basis for the research presented in this thesis.

2.1.1 Fault Ride-Through Capability

A grid fault is normally caused by the short circuit of one or more phases in a power system. The occurrence and removal of the grid fault results in the temporary abnormal voltage over the entire grid. The fault can propagate through long distances especially in weak power systems. A study on the GB power system shows that a large number of wind farms can be affected when a grid fault happens [28]. Synchronous generators are directly coupled to the grid and have greater damping than asynchronous generators, therefore by nature have better fault ride-through performance than asynchronous generators which is widely used for wind energy generation. In a power system with large amount of wind turbines equipped with

asynchronous generators, it is generally expected that wind turbines can achieve the same fault ride-through performance as synchronous generators.

2.1.1.1 Fault/Low voltage ride-through requirements

The situation where the wind turbine must stay connected during the grid fault can be defined by the voltage profile. The voltage profile shows at which voltage level wind turbine should be able to remain connected and for how long. Figure 2-1 shows the fault ride-through requirements for reviewed grid codes of different countries. Wind farms are required to remain connected for voltage dips above the pre-defined voltage-time line in Figure 2-1. The voltage refers to the voltage level at the point of common coupling (PCC) of wind farms.

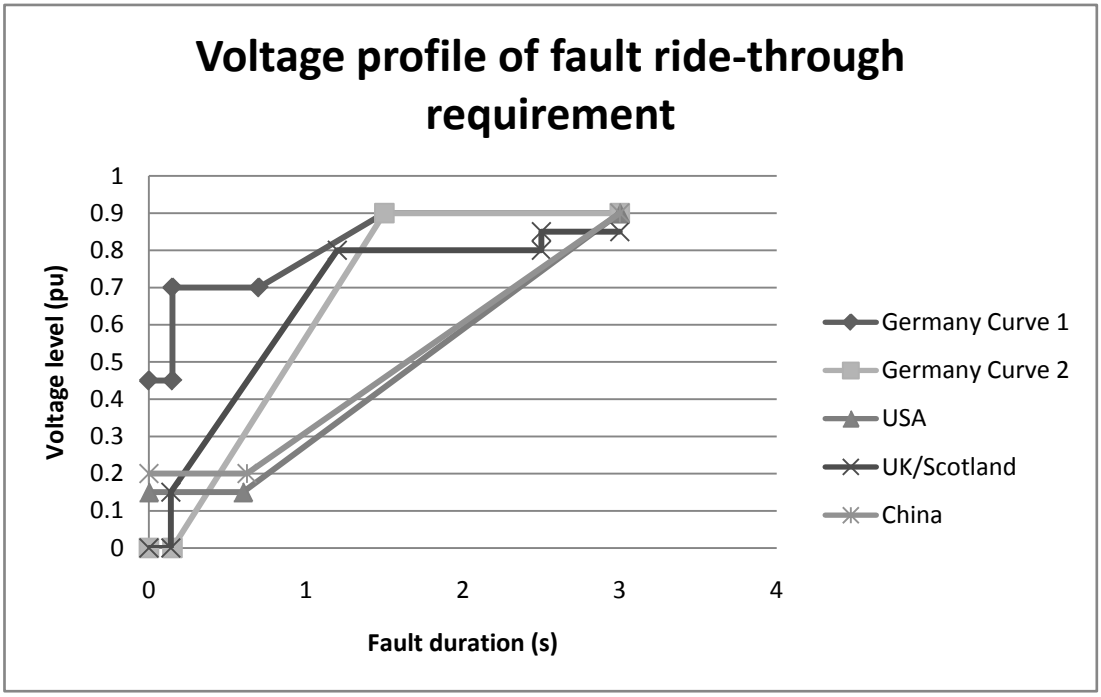

Figure 2-1: Fault ride-through requirements for wind energy integration.

The German TSO E.ON sets up two limiting voltage profiles to regulate wind turbine behaviour under a fault. Above curve 1 is when wind turbine must stay connected during the grid fault and be able to recover by 20% per second of its rated power after

the re-closure of the circuit breaker. Wind turbine is permitted to go offline for less than 2 seconds when the voltage is between curve 1 and curve 2. After the reconnection, the wind turbine must be able to resume the power output with the speed of 10% per second of the rated power. Below curve 2 is where wind turbine is free to decouple from the grid. The E.ON grid code gives wind turbine certain degree of freedom to decide if it shall disconnect or not. The hard limit (curve 1) is set to a loose level. However, curve 2, which is the suggested fault ride-through ability for wind turbine, is strict. Under such requirements, wind turbine can avoid going into the unstable range by short-term disconnection but have to guarantee fast reconnection.

It should be noticed that although it is shown on the graph that wind turbine can disconnect from grid under below 90% of nominal voltage after 1.5 seconds of fault occurrence, the decision should only be made by the automatic protection system. The disconnection order that automatic protection system gives is normally with a long time delay, e.g. after 2.4 seconds. From the wind turbine design perspective, the wind turbine must be able to fully ride-through this voltage level for any demanded time without becoming unstable. The long-term fault ride-through requirement may be even more difficult to meet than the short-term one. Wind turbine mechanical components are able to provide sufficient damping for short-term oscillations because of their large mass. However, the wind turbine slowly deviates from its optimum operational condition if the demanded torque cannot be produced for a period of time. This issue will be discussed in detail in Chapter 4.

National Grid and Scottish grid code have the same low voltage limit for wind turbine fault ride-through [11, 20]. Among all the reviewed grid codes, the GB grid code is the most demanding one on the wind turbine fault ride-through capability. It is the only grid code that requires zero fault ride-through as shown in Figure 2-1. The generator can produce no reaction torque under zero voltage no matter what control

or protection device is employed. The wind turbine must be able to withstand 140ms with rotor speed acceleration, and drive train and tower oscillations. The zero-voltage fault ride-through problem can only be countered by the mechanical design or control. Unlike the strict requirement for short-term low-voltage criterion, the GB grid code allows wind turbine to shut down at relatively high voltage that lasts longer time. The challenge that the GB grid code raises is more on the mechanical design of the wind turbine rather than on the successful fault ride-through strategy. National Grid gives a sharp power production recovery curve. Wind turbines are required to produce 90% of their rated power within one second. The reason of having such onerous requirement is likely to result from the weak grid that Britain has compared to other countries. A faster power restore rate is needed in a more islanded power system. The fault ride-through performance in post fault phase rather than during fault is where wind turbine manufactures are able to improve to meet the GB grid code better.

As the country with the highest wind power penetration level, Denmark gives very detailed requirements for wind turbine interconnection under grid fault. The requirements are categorised by the grid voltage level. Different documents are issued for below and above 110kV. In spite of the voltage profile illustrated in Figure 2-1, Denmark TSO also defined fault ride-through demands for each fault criterion including symmetrical and asymmetrical faults [29]. It is also the only grid code that sets up high voltage ride-through requirements. Some large-scale grid collapse events mentioned in [30] indicate that high voltage ride-through ability of wind turbine should also be considered in future grid codes.

The low voltage ride-through voltage curve is identical to former E.ON requirement. This voltage versus time curve has proved to be effective in the German grid for many years and taken as reference by many countries including Ireland and Canada when making first regulations document on wind farm integration. Most new grid

codes increased the standard of wind power connection requirements. It can be foreseen that with the penetration of wind power increasing, the fault ride-through ability of wind turbines will need to be further enhanced.

The Chinese fault ride-through code is similar to the US code but has slightly higher standard for short duration FRT for wind turbine. However, compared to the UK grid code, the Chinese grid code has relatively low requirement within 200ms but higher requirement for long duration fault. The active power recovery rate, which is 10% per second, is also low compared to other grid codes. Although China and the US have large amounts of wind power capacity installed, the penetration level of wind power is low due to their large-scale power systems. Therefore a high standard on wind turbine fault ride-through capability is not needed in these countries.

Combining the most onerous requirement over the entire time scale of all reviewed grid codes, a fault ride through requirement suitable for all countries is provided in Figure 2-2.

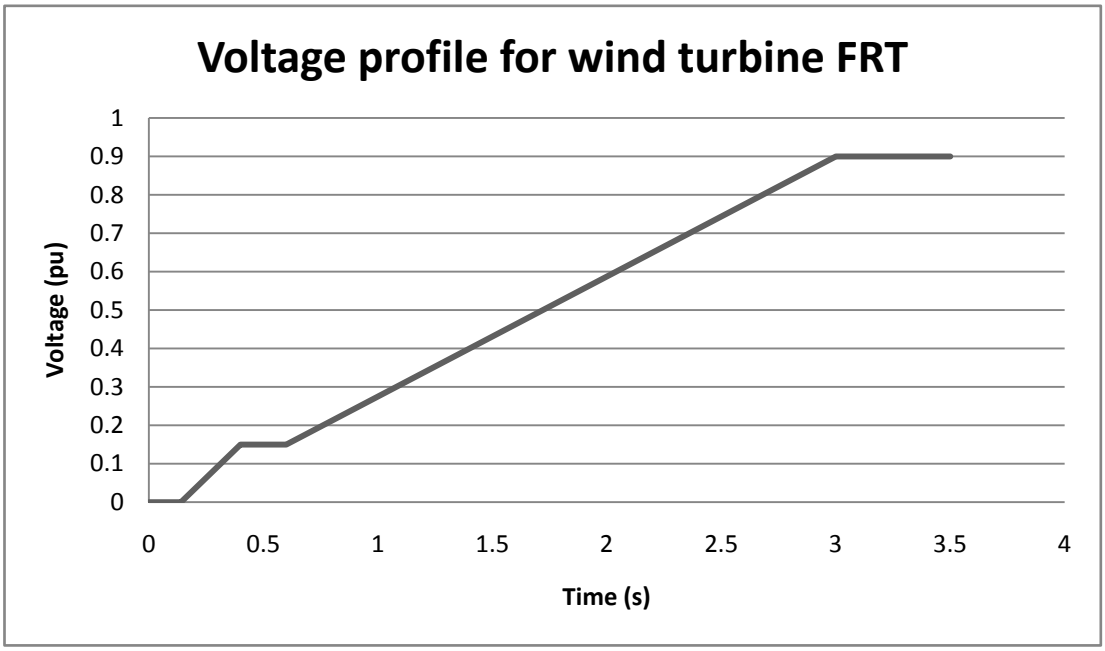

Figure 2-2: Generic requirement for wind turbine FRT

The major challenge for wind turbine fault ride-through is shown in Figure 2-2. For the grid fault with short duration, a wind turbine should be able to stay connected under zero voltage; for voltage sag over long period, a wind turbine should be able to operate under 90% of the rated voltage without decrease in performance. After fault clearance, the wind turbine should be able to recover 90% of its rated power within one second.

2.1.1.2 Active power control

The essential task of a power system is to supply electricity to the customer whenever needed. The real-time balance between power production and demand is very important for the stable and consistent operation of a power system. Control over active power output of power plants in order to maintain system frequency within acceptable range, regulate power flow, prevent transmission line from overloading, meet power quality standards and avoid current and voltage surge is required by system operators [31, 32].

At the early stages of wind power development, control of active power output was poor mainly because of the technology being used, that is, turbines such as fixed speed induction generators limited the performance of the wind turbine power control. Wind farms were not considered as power plants with controllable output but as consumers with negative demand. With the increase of wind power in the power system, many TSOs have determined that wind turbine should also be able to regulate the active power output to some extent. Although arbitrary power control of wind power plants is still not demanded due to the nature of the wind energy harvest, which mandates maximum power extraction, some simple control to ensure that the wind turbine does not cause system instability is indicated by some grid codes.

In grid codes using the early E.ON code as a reference like China and US codes, the active power control was not explicitly defined. The power control of wind farms

was still operated by TSO operators who simply controlled the output by shutting down and reconnecting wind farms. In codes that define the active power control standard, the requirements are mostly on the ability of wind turbine active power curtailment. As the upper limit of wind turbine output is determined by the availability of wind resource, the increase in the active power output is not always possible. However, the ability of power production reduction can assist power system operation in many cases. The German grid code requires wind farms to be able to reduce active power output with a ramp rate of 10% per minute. The Danish code has similar requirements but the speed of power reduction is to be decided by TSOs. The GB grid code does not give any specific requirement on wind turbine power control. However, some interesting requirements can be found in the Irish and Scottish regulation documents. Ireland requires the speed of power curtailment of 1 MW to 30 MW per minute, which is easier for large wind farms but for smaller wind farms with less capacity, a higher response speed is required. Scotland issued separate requirements for large and small-scale wind farms. Wind farms with less than 15 MW capacities should be able to reduce active power output of 3MW within 1 minute. For larger wind farms the requirement is 20% of the registered capacity. It is also defined in many codes that during the start-up and shutdown of wind turbine, the ramp rate limit should not be exceeded [33].

It should be noted that unlike LVRT requirements, the active power control requirements are applied on the whole wind farm rather than single wind turbines. It is possible to meet requirements by shutting down a single turbine thus avoiding the need to change wind turbine control in order to fulfil grid codes. Nevertheless, precise control cannot be achieved in this manner and in the future the ability of a temporary increase of wind power output may be needed with more wind power connected to the power system. The ability of a wind turbine to control its output power according to a TSO’s order or automatically in response to a change of power system variables is a key technique to enable large-scale wind power integration.

2.1.2 Grid frequency related issues

2.1.2.1 Operational frequency range

It is specified in most grid codes which range of grid frequency wind turbines should be capable to withstand. The frequency range and the abnormal frequency time duration for Germany, Denmark, UK and China is shown in Table 2-1. Scotland shares the same frequency ride-through requirement with the national grid code.

Table 2-1: Frequency range for wind turbine to remain connected

Frequency (HZ)	**Ride-through duration**			
	Germany	**Denmark**	**UK**	**China**
52-53	disconnection	0.2	disconnection	disconnection
51.5-52	disconnection	0.2	continuous	disconnection
51-51.5	30 minutes	0.2	continuous	2 minutes
50.5-51	30 minutes	continuous	continuous	2 minutes
50-50.5	continuous	continuous	continuous	10 minutes
49.5-50	continuous	continuous	continuous	continuous
49-49.5	continuous	continuous	continuous	10 minutes
48.5-49	30 minutes	continuous	continuous	10 minutes
48-48.5	20 minutes	25 minutes	continuous	10 minutes
47.5-48	10 minutes	5 minutes	continuous	disconnection
47-47.5	10 seconds	10 seconds	20 seconds	disconnection

2.1.2.2 Frequency control

The power system transmits energy from a prime mover (steam turbine, wind turbine, hydro etc.) to consumers. The demanded power at the consumer end is not always the same as the generated power at the generator end. The system frequency is an indicator of the mismatch between power generation and consumption. In a well-regulated power system, the frequency is normally controlled to 50±0.1Hz and rarely falls out of 49-50.3Hz for a system with 50Hz nominal frequency [34].

The widely adopted method to keep frequency within the acceptable range is to equip some synchronous generators with frequency sensitive control to adjust the output of these generators thus bringing the system frequency back to around the rated frequency. There are generally two types of frequency control applied in power system, namely primary and secondary control. The primary control is able to adjust the generation in the time of 1 to 30 seconds to cope with the load change. The primary reserve needs to be restored after used to keep it effective in the long run. The secondary control is adopted to supply the consumed primary control capacity. The secondary control is in charge of the frequency variation between 10 to 15 minutes.

In current power systems, synchronous generators provide primary and secondary control. A major reason for this is that synchronous generators are strongly coupled to the grid. The electromagnetic link automatically counters the frequency deviation. Wind turbines were considered to have negative effect on system frequency control because a conventional wind turbine does not actively respond to the system frequency oscillation. To cope with the wind turbine integration, the conventional frequency control capacity has to be increased. There is a strong demand that wind turbines can participate in the frequency control of the power system.

The German frequency control requirement for wind turbines majorly lies in the over frequency range (>50 Hz). It is demanded that a wind farm reduces its output with a proportion no less than 40% per Hz when grid frequency exceeds 50.2 Hz. National Grid applies the same over frequency control requirement as Germany. Moreover, primary and secondary control abilities are expected from wind farms. Wind farms are required to increase or decrease the power output linearly against the grid frequency to assist the frequency maintenance within a frequency range which is defined by TSOs. When the grid frequency lies outside the pre-defined range where wind farms are required to provide frequency support, wind farms are free from the duty of providing frequency support to the power system [32]. The Danish grid code defines two curves to limit the frequency control range as shown in Figure 2-3. The frequency control can only reduce wind farm's production in the case of the solid line. When the production falls below the dotted line due to the frequency control demand, the wind turbine can also participate in frequency control by increasing the power production.

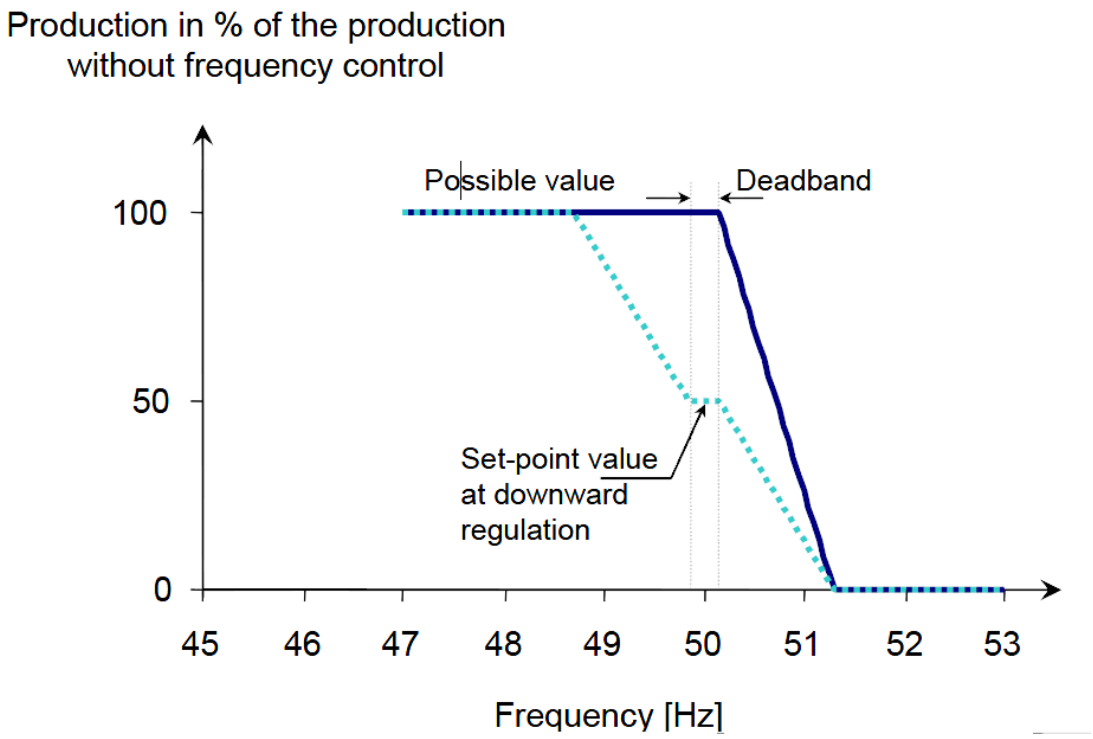

Figure 2-3: Danish frequency regulation limiting curve [14].

2.1.3 Reactive power control

Consumer utilities are designed to operate under a certain voltage range. One of the goals a power system needs to achieve is to avoid system voltage to deviate from rated value too far. The voltage at different nodes in the grid is traditionally controlled by centralized synchronous generators and voltage control devices like an automatic voltage regulator (AVR) [35].

The increasing number of wind turbines raised new challenge to the existing power system in terms of voltage control. Power system voltage is mainly affected by the reactive power flow. Most wind turbines, especially early models, are equipped with an induction machine, which draws reactive power for magnetization. The reactive power demand used to be met by the combination of localized reactive power compensation devices and the grid supply. With more wind power integrated to the grid, the percentage of conventional power plants is reduced accordingly. Voltage

control devices, which rely on synchronous generators to function properly are decreasing in number but more heavily burdened.

Wind farms are also required to provide reactive power support during grid fault in many grid codes. The German transmission code requires that “reactive current of 2% of rated current is provided per percent voltage drop up to 100% rated current and that this is provided within 20ms[32].” The Danish grid code[14] also has requirement defining the amount of reactive power wind farms have to produce in relation to the voltage drop level. However, a few grid codes including the UK grid code didn’t specify reactive power support requirement for wind turbine during faults.

Wind farms need to have a continuously operating voltage regulation system if large-scale integration of wind power is to be realized. The use of power electronic devices on wind turbine generators enables such a function. TSOs then set reasonable requirements for wind farms to contribute to power system voltage control.

The reactive power requirements are expressed in various manners such as power factor in relation to voltage (Germany code), reactive power in relation to active power (GB and Chinese codes) or reactive power in relation to power factor (GB offshore code), hence it is difficult to compare them directly. The demanded reactive power supply under different real power output levels varies according to national codes. However, one thing in common is that most countries including Denmark, UK, USA and China set the full load power factor to -0.95 to +0.95. This power factor range is chosen as the reference in this thesis for wind turbine reactive power supply investigation.

2.2 Wind turbine concepts

There are three major topologies of modern wind turbine in the market, namely fixed-speed induction generator, doubly-fed induction generator (DFIG) and fully-rated converter wind turbine (FRC), as shown in Figure 2-4.

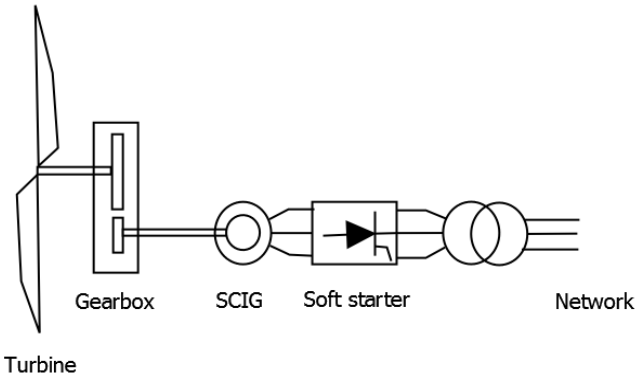

(a)

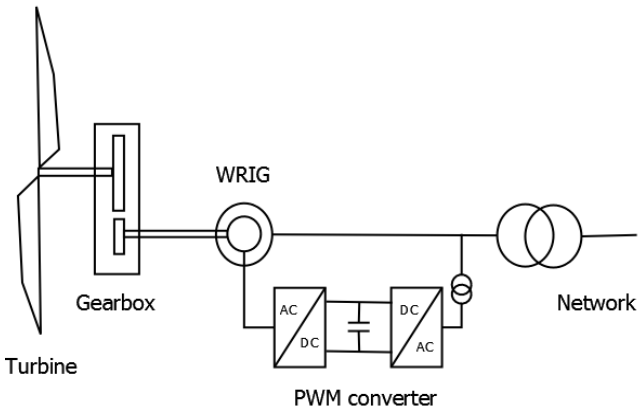

(b)

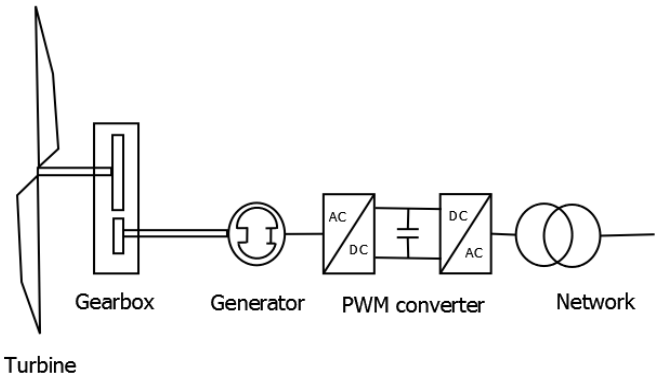

(c)

Figure 2-4: Wind turbine topologies:

(a) Fixed speed induction generator (b) Doubly fed induction generator (c) Full rated converter wind turbine generator

A fixed-speed wind turbine mainly appeared at the early stage of wind turbine development. This type of wind turbine normally adopts the squirrel-cage induction generator (SCIG) as the generation system [36, 37]. The stator of the SCIG is directly connected to the three-phase grid through a soft starter followed by a transformer. The rotor is connected to wind turbine rotor via a gearbox of fixed ratio. The rotor slip is fixed to a value slightly above synchronous speed. The rotor slip, and hence the rotor speed, varies with the amount of power generated. In this wind turbine concept the rotor speed variation is very small (typically 1%-2%).This is why this wind turbine concept is referred to as a fixed-speed wind turbine. The control of this type of wind turbine is limited as the rotational speed of wind turbine rotor is in effect a constant value. As the efficiency of wind turbine energy conversion is determined by tip-speed ratio [38], the wind turbine has to work under reduced efficiency with a fixed rotor speed. Pitch control can be implemented on this wind turbine concept. The power output of fixed-speed wind turbine suffers from large fluctuation due to the lack of flexibility of the manoeuvrability at generator side. The SCIG cannot adapt to a mechanical power change quickly leading to a potential unstable output which influences grid stability. Another issue related to this wind turbine type is that the SCIG has no excitation system and therefore needs to draw reactive power from the grid for magnetization. A reactive power compensation device has to be mounted in wind farms to balance the reactive power and maintain voltage at the connection point to the grid. The advantage of a fixed-speed wind turbine is the drive-train dynamics are well damped due to the fact that induction generator reaction torque naturally changes proportionally against rotational speed. The reaction torque of the fixe-speed induction generator automatically increases when the rotor speed increases and vice versa. The rotor speed variation of the FSIG is countered by the torque characteristic therefore the damping of such machine is relatively high without any additional damping devices. The mechanical side of this

wind turbine concept is protected from grid disturbances although the generator is not capable of assisting the grid.

The DFIG is the dominating concept in the wind turbine market currently. The stator of a DFIG is directly coupled with grid. The rotor of a DFIG is connected to the grid through converters. It has huge advantages compared to a fixed speed wind turbine with induction generator. The employment of power electronics enables the variable speed ability of wind turbine. Hence, the wind turbine can achieve maximum power extraction by adopting pitch control. The power electronics only handles rotor power which means the capacity of converters only need to be a part of the wind turbine rated power (usually 25% to 40%). The converters also enable the control of reactive power. They are not only able to supply reactive power needed for the generator but also can assist grid voltage control with an appropriate control strategy applied. The strong controllability and competitive price together makes the DFIG the most widely used wind turbine type nowadays in the world [39].

A fully-rated converter wind turbine requires large capacity power electronics (typically 120% rated power). However, the use of fully rated converter totally decouples the wind turbine from the grid. The electricity generation system on this wind turbine concept is a synchronous generator with large diameter. This structure allows the operation without gearbox. The synchronous generator is connected to grid via the inverter and converter. The generator produces AC current at the same frequency as the rotational speed of wind turbine hub, which is then converted to grid frequency by power electronic device. The grid requirements for wind turbine can be easily satisfied using this topology. With the price of power electronic components decreasing, this type of wind turbine is starting to gain more attention due to its powerful control capability.

2.3 Contributions of this thesis

The contributions of the thesis to the field and existing literature are:

- A detailed mathematical model of DFIG-based wind turbine and power system is developed and implemented in Matlab/Simulink. The model enables the observation of the interaction between the wind turbine mechanical and electrical system. The effect wind turbine mechanical oscillations and electrical transients has on each other can be assessed using the model. The induced structural load on wind turbine components by grid disturbances is well represented in the Simulink model.

- A DFIG rotor resistance controller is developed to achieve the DFIG fault ride-through while reducing mechanical loads on wind turbine drive-train. The controller has a smaller time constant than a PID-type rotor resistance controller by using feed-forward control and machine parameters so that the control over DFIG torque is achieved in the short duration of grid fault.

- An active tuning method for the wind turbine drive-train damping is proposed. The wind turbine drive-train damping is adjusted according to the grid voltage level for improved damping during grid faults.

- A pitch filter is designed to avoid the excessive blade pitching due to grid faults.

- An auxiliary control loop for the DFIG to ride-through asymmetrical grid faults based on the existing single reference frame DFIG control is presented. The high frequency torque and current oscillation in the wind turbine and DFIG resulting from an asymmetrical fault is suppressed by incorporating the proposed control loop.

- A multi-band PSS concept for wind turbine is proposed. The PSS allows wind turbines to provide enhanced damping on various mechanical and electrical modes without influencing the basic controller. The wind turbine is able to contribute to power system stability by this means.

2.4 Structure of the thesis

The structure of this thesis is outlined as below:

Chapter 1 – The background of the grid integration of wind power is presented.

Chapter 2 – The state-of-art wind turbine technology is introduced first. The wind turbine fault ride-through requirements in worldwide grid codes are summarized as the benchmark for fault ride-through strategy design.

Chapter 3 – The modelling of the wind turbine, DFIG, grid and corresponding controllers is shown in this chapter. Both the mathematical model and the Simulink implementations are presented.

Chapter 4 – A symmetrical fault ride-through strategy for wind turbines is explained in this chapter. A variable rotor resistance control scheme, which is able to limit DFIG over-current and control generator reaction torque for wind turbine drive-train load alleviation is proposed. A drive-train damping filter tuning method for drive-train active damping is presented. A filter designed to reduce the blade fatigue caused by grid faults is also introduced.

Chapter 5 – A DFIG rotor voltage compensation controller for wind turbine asymmetrical fault ride-through is established in this part. The controller effectively reduces the mechanical and electrical transients induced by asymmetrical grid fault.

Chapter 6 – A PSS for wind turbines with multi-band structure is demonstrated in this chapter. The proposed PSS aims to improve the damping of both mechanical and electrical modes of the wind turbine and power system so that the wind turbine can contribute to power system stability without reducing the structural damping.

Chapter 7 – The work and contribution presented in this thesis is summarized. Possible future work based on the research in this thesis is suggested.

2.5 List of Publications

1. ***F. Zhang****, W.E. Leithead, and O. Anaya-lara,* "Dynamic modelling of wind turbine and power system for fault ride-through analysis," European Academy of Wind Energy (EAWE) 6th PhD Seminar, Trondheim, 30-1 October

2. ***F. Zhang****, W.E. Leithead, and O. Anaya-lara,* "Wind turbine control design to enhance the fault ride-through capability," Renewable Power Generation (RPG 2011), IET Conference on, Edinburgh, 6-8 Sept. 2011

3. ***F. Zhang****, W.E. Leithead, and O. Anaya-lara,* "A combined controller design of power system stabilizer and wind turbine drive-train damping filter," Sustainable Power Generation and Supply (SUPERGEN 2012), International Conference on, Hangzhou, 8-9 Sept. 2012

4. ***F. Zhang****, W.E. Leithead, and O. Anaya-lara,* "Wind turbine symmetrical and asymmetrical fault ride-through strategy considering structural loads," IEEE Transactions on Energy Conversion, Submitted

5. ***F. Zhang****, W.E. Leithead, and O. Anaya-lara,* "A multi-band power system stabilizer concept for DFIG-based wind turbine," IEEE Transactions on Power Systems, Submitted

CHAPTER 3: WIND TURBINE MODELLING FOR POWER SYSTEM STUDIES

There are extensive research publications on the issue of the integration between the wind turbine and the power system. Most of them neglect details of the mechanical model of wind turbine and assume perfect pitch and torque control. It is often claimed that wind turbine mechanical side operation has minor effect on the electrical system transients [40]. Nevertheless, some literature shows that the wind turbine mechanical dynamics could influence the fault ride-through performance of the wind turbine [41]. The necessity of the detailed modelling of the mechanical system of wind turbine for power system study is arguable. Whether the model of the wind turbine mechanical dynamics is needed depends on the aim of the study. In this thesis, the wind turbine modelling has been conducting considering the following:

1. The impact of the fault in electrical systems on wind turbine components should be represented clearly.

2. How the wind turbine reacts to disturbances and hence affects the fault clearance and recovery should be shown in the model.

3. The wind turbine controller and protection system which decide the wind turbine emergent shut-down limit is to be included in the model.

Issue 1 requires the dynamics of wind turbine components to be modelled so that the effect of grid fault on wind turbine can be monitored. The structural loads and the deviation from wind turbine optimum operation point caused by the grid disturbance can be calculated by developing models that represents wind turbine mechanical dynamics. Issue 2 demands that wind turbine aerodynamics and wind speed must be included in the model. In many publications the wind speed is assumed to be

constant and aerodynamics neglected which is not actually true. The variation of aerodynamic torque also influences the performance of wind turbine during grid events. For example, wind turbine pitch control is employed by some researchers to counter grid disturbance. Such control strategy can only be validated with the aerodynamic model of wind turbine given. Issue 3 addresses the importance of the modelling of the wind turbine supervisory control and protection system.

Detailed wind turbine mechanical model and electrical system model are introduced in this chapter. The model enables the observation of wind turbine mechanical response to electrical disturbance. The interaction between wind turbine and grid events can be investigated so that the study of the fault ride-through issue of wind turbine is extended to the mechanical side of wind turbine. The model described in this chapter is implemented in Matlab/Simulink®. The Simulink® model of the wind turbine is validated against Bladed. The electrical models including synchronous generator and DFIGs are validated against the SimPowerSystems™ library in Simulink®. The mechanical part of the wind turbine is modelled in SI units and the electrical part modelled in per unit system.

3.1 Mechanical system model

The complete wind turbine mechanical model is comprised of the following components:

- Wind speed
- Aerodynamics
- Rotor dynamics
- Tower dynamics
- Drive-train dynamics

- Control dynamics

The wind speed model is described in detail in [42]. The wind turbine dynamic model is shown in [43, 44] and the controller of the wind turbine is developed in [45-47].

In this Chapter, the modelling of wind turbine components is introduced. The parameters of a 2-MW exemplar wind turbine adopted in the model are shown in Appendix B. The block diagram of the full wind turbine mechanical model is shown in Figure 3-1.

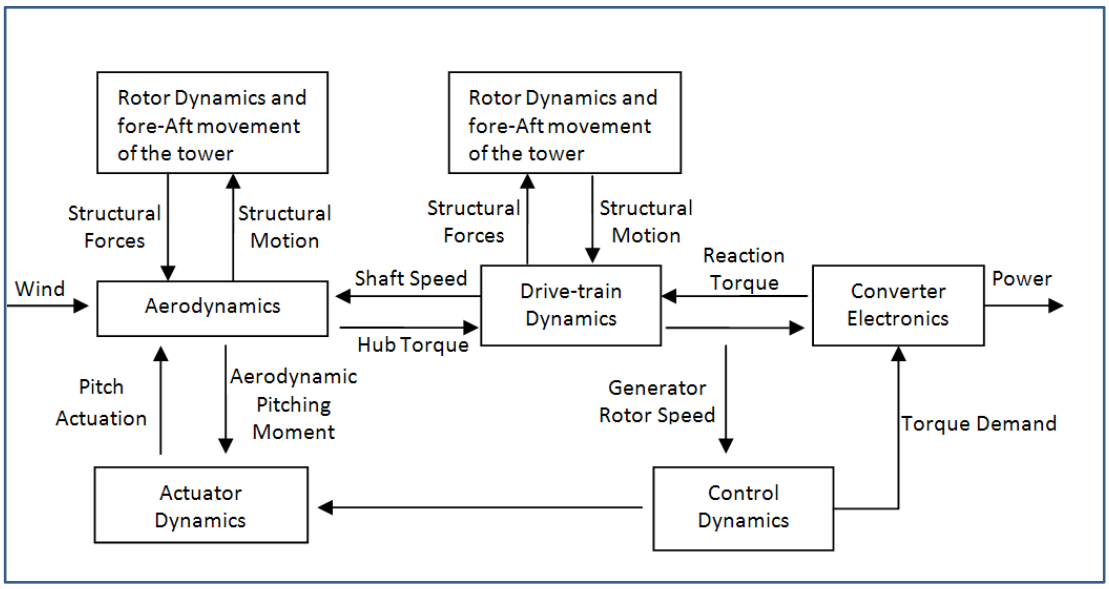

Figure 3-1: Wind turbine mechanical model.

3.1.1 Wind speed model

To investigate the wind energy conversion system, it is important to obtain a mathematical model of the wind speed. The wind speed in real-time is needed for control purposes. It is impossible to measure the wind speed directly since the wind speeds is time varying and different at each point over the rotor disc. The wind speed at one point cannot represent the overall effect that a wind field has on the rotor so it

is not suitable for wind turbine control. An alternative way is to use effective wind speed. An effective wind speed is the constant wind speed, which induces the same aerodynamic force as the spatially varying wind speed experienced by the wind turbine. The effective wind speed is obtained by filtering point wind speed. The model of the power spectrum of point wind speed is derived first.

For simulation of a few minutes, the wind speed can be described as equation (3-1):

$$V_w(t) = \hat{V}_w + \sum_{i=0}^{N} A_i \cos(\omega_i t + \varphi_i) \tag{3-1}$$

where the effective wind speed are divided into two components: the slowly varying mean wind speed $\hat{V}_w$ and N sinusoidal components with amplitude of A_i, frequency of ω_i and phase of φ_i [48].

There are several models of the turbulence component of the wind speed such as the Von Karman model and the Kaimal. The Von Karman model is the most appropriate model for the analysis of a few minutes [49]. The value of A_i, ω_i and φ_i are determined by the following filter:

$$S_v(w) = 0.476\sigma_v^2 \frac{\frac{L_t}{\hat{V}}}{\left(1+\left(\frac{wL_t}{\hat{V}}\right)^2\right)^{\frac{5}{6}}} \tag{3-2}$$

where $\hat{V}$ is the mean point wind speed, L_t is the turbulence length scale and σ_v is the turbulence intensity.

The 5/6-order filter requires long calculation time in real time simulation, to improve the simulation speed, equation (3-2) is approximated by a rational transfer function described in [50]:

$$S_p(s) = \frac{\sqrt{2} + \sigma(\hat{V})s}{\left(\sqrt{2} + \sqrt{a}\sigma(\hat{V})s\right)\left(1 + \frac{\sigma(\hat{V})s}{\sqrt{a}}\right)} \tag{3-3}$$

where $\sigma = \frac{\lambda R}{\hat{V}}$ and λ is the turbulent wind speed decay factor, which is a constant. From the expression of σ we can see that the spatial filter varies with wind speed.

The component representing slowly varying mean wind speed over time in (3-1) is produced by filtering the superposition of a constant wind speed and a white noise. The filter is

$$\frac{k}{\tau s + 1} \tag{3-4}$$

where τ is the filtering time and normally chosen to be 30s and k is the scaling factor.

For wind turbine control, the spectral peak is a crucial issue, which is not taken into consideration in the above model. To include spectral peaks, a component is added to the aerodynamic torque. The spectral peak at $n\Omega$ is modelled by[51]

$$Ln\Omega = \varepsilon_1 \cos(n\Omega t) + \varepsilon_2 \sin(n\Omega t) \tag{3-5}$$

where ε_1 and ε_2 are coloured noise.

To be applied on wind turbine, the effective wind speed needs to be further modified because the rotor and tower movement affect the actual wind speed experienced by the rotor. The modified effective wind speed is[51]:

$$v = \bar{w} - L\dot{\varphi}_R - H\dot{\varphi}_T \tag{3-6}$$

in which $\bar{w}$ is the original effective wind speed, $\dot{\varphi}_R$ and $\dot{\varphi}_T$ are rotor and tower angular displacement, L is the length of blade and H is hub height.

The wind speed model is implemented in Simulink by filtering the point wind speed, as shown in Figure 3-2.

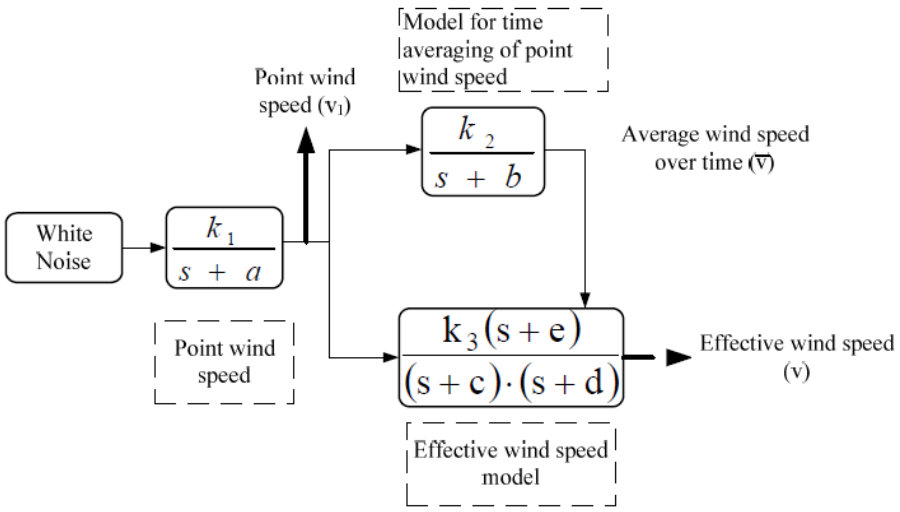

Figure 3-2: Effective wind speed model

The point wind speed filter is to eliminate the high frequency component in the constant wind speed with noise, the time averaging of the point wind speed refers to expression (3-4) and the effective wind speed model refers to (3-3).

3.1.2 Wind turbine aerodynamics

In the study of the interaction between wind turbine and power systems, the real-time energy production from wind turbine determines the limit of the active power support the wind turbine can produce and the reaction torque demand the wind turbine requires the power system to provide in order to maintain balanced operation. The wind turbine aerodynamics establishes the relationship between the effective wind speed and the mechanical torque produced by the wind turbine.

When the wind turbine is running, the blowing wind produces an aerodynamic torque on the rotor. The torque is

$$F_1 = \frac{1}{2} \cdot \frac{\rho \pi C_p(\lambda, \beta) R^2 v^2}{\lambda} \tag{3-7}$$

where the tip speed ratio

$$\lambda = \frac{R\Omega}{v} \tag{3-8}$$

R is the rotor radius, Ω is the rotor speed, v is the effective wind speed, ρ is the air density, β is the pitch angle, and C_p is the aerodynamic power coefficient.

The aerodynamic power coefficient depends on wind speed and pitch angle. This parameter is very important for wind turbine control. The maximum C_p value leads to the maximum power, which is what we want to achieve through control. By adjusting the rotational speed and pitch angle the wind turbine can be regulated to generate maximum power under all wind speed.

3.1.3 Drive-train model

The drive train of a wind turbine is composed by the rotor hub and low-speed shaft, gearbox, high-speed shaft and generator rotor. To study the fault ride-through of wind turbine, the behaviour of drive train needs to be investigated as it is connected directly to the generator and is affected by the power fluctuation in the grid. The model of wind turbine drive train is represented in Figure 3-3

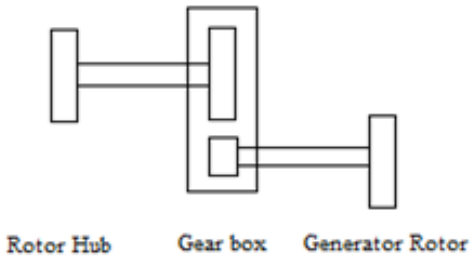

Figure 3-3: Wind turbine drive train.

In the model, the gear-train is represented in the low-speed shaft. The inertias of the low speed shaft and high-speed shaft are incorporated into the inertias of rotor hub and generator rotor.

At the low speed shaft end we get:

$$T_H = \left(K_E + I\dot{\theta}_R^2\right)\cdot\left[\left(\theta_R - \theta_H\right)\cos\beta - \left(\phi_R - \phi_T\right)\sin\beta\right]\cos\beta$$

$$+\left(K_F + I\dot{\theta}_R^2\right)\cdot\left[\left(\theta_R - \theta_H\right)\sin\beta - \left(\phi_R - \phi_T\right)\cos\beta\right]\sin\beta \qquad (3\text{-}9)$$

$$I_{Ls}\ddot{\theta}_H = T_H - T_1 - \gamma_{Ls}\dot{\theta}_H \qquad (3\text{-}10)$$

$$T_1 = K_{Ls}\left(\theta_H - \theta_1\right) \qquad (3\text{-}11)$$

where T_H, T_1 are the hub torque and gearbox torque at the low-speed shaft end. I is the rotor inertia and I_{Ls} is the hub inertia modified to include the low-speed shaft inertia. β is the pitch angle. θ_H and θ_1 are the angular displacement of the hub and the low-speed shaft gear. θ_R is the in-plane angular displacement of the centre of mass of the blade. ϕ_R is the out-of-plane angular displacement of the centre of mass of the blade. ϕ_T is the in-plane angular displacement of the tower. K_{Ls} is the low speed shaft stiffness. γ_{Ls} is the mechanical losses in the low speed end of the drive-train.

For the gearbox the following equations can be obtained:

$$T_1 = -NT_2 \tag{3-12}$$

$$\theta_2 = N\theta_1 \tag{3-13}$$

where T_2 is the gearbox torque at the high-speed shaft end and θ_2 is the angular displacement of the high-speed shaft gear.

At the generator side, we can get a similar dynamic equation as at the rotor side

$$T_2 = K_{Hs}\left(\theta_{gen} - \theta_2\right) \tag{3-14}$$

$$I_{Hs}\ddot{\theta}_{gen} = T_{gen} - T_2 - \gamma_{Hs}\dot{\theta}_g \tag{3-15}$$

where I_{Hs} is the generator rotor inertia plus the high-speed shaft inertia and the brake inertia. θ_{gen} is the angular displacement of the generator rotor. T_{gen} is the

output torque of generator. γ_{Hs} is the mechanical losses in the high speed end of the drive-train.

Considering the side-to-side displacement of the tower and gearbox, the following expressions can be derived

$$J_{Gb}\ddot{\theta}_{Gb} = -B_{Gb}\dot{\theta}_{Gb} - K_{Gb}\left(\theta_{Gb} - \theta_{TS}\right) - \left(N-1\right)T_2 \tag{3-16}$$

$$J_{Ts}\ddot{\theta}_{TS} = -B_{TS}\dot{\theta}_{TS} - K_{TS}\theta_{TS} - K_{Gb}\left(\theta_{TS} - \theta_{Gb}\right) \tag{3-17}$$

where J_{Gb} and J_{Ts} are inertia of gearbox and tower, respectively. θ_{Gb} and θ_{TS} are gearbox and tower side-to-side displacement. B_{Gb} and B_{TS} are damping of gearbox mounting and tower. K_{Gb} and K_{TS} are stiffness of gearbox and tower. Also the relationship of the rotational displacement of gears is changed to

$$\theta_2 = N\theta_1 - \left(N-1\right)\theta_{Gb} \tag{3-18}$$

which shows the effect of gearbox side-to-side movement on the gearbox.

The damping provided by the twisting of shafts, which is named material damping, can also be added to the model. It increases the total damping of the drive-train and attenuates the drive-train modes. The drive-train is normally very lightly damped hence increase of drive-train damping is desired.

The Simulink implementation of the drive-train is shown in Figure 3-4.

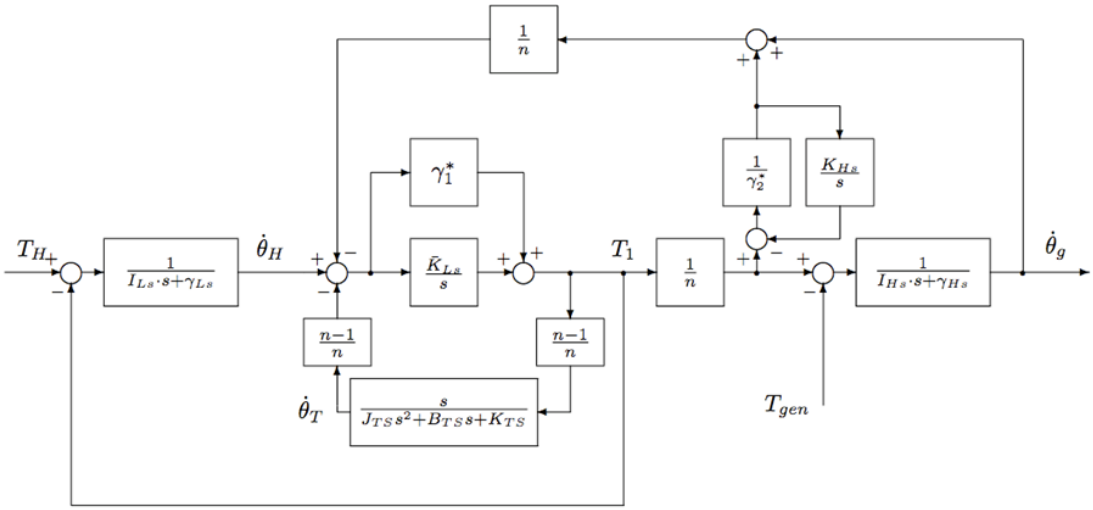

Figure 3-4: Drive-train block diagram

3.1.4 Rotor

The rotor dynamics of the wind turbine is essential in the wind turbine loads analysis. The rotor interacts with both the drive-train and the tower during operation and hence influences the overall wind turbine loads. The rotor of wind turbine consists of the blades and the wind turbine hub.

The rotor dynamics is dominated by the structural modes of each blade. There are two major rotor modes namely out-of-plane mode and in-plane mode. All blades moving in phase and contribute to the low frequency transients which affect drive-train loads. The out-of-plane mode of the rotor mainly contributes to wind turbine drive-train loads by modifying the wind speed while in-plane mode increases the compliance of the drive-train. The rotor dynamics is represented by the single blade modes in this thesis. The dynamic model of the single blade is

$$L_R = \frac{1}{2} J \dot{\theta}_R^2 + \frac{1}{2} J_T \dot{\phi}_T^2 + J_C \dot{\phi}_R \dot{\phi}_T - \frac{1}{2} K_E \left[\left(\theta_R - \theta_H \right) \cos\beta - \left(\phi_R - \phi_T \right) \sin\beta \right]^2$$

$$-\frac{1}{2}K_F\left[\left(\theta_R-\theta_H\right)\sin\beta+\left(\phi_R-\phi_T\right)\cos\beta\right]^2-\frac{1}{2}K_T\phi_T^2+D_T\phi_T+F_1\theta_R+F_2\phi_R$$

$$-\frac{1}{2}J\Omega_o^2\left(\theta_R-\theta_H\right)^2-\frac{1}{2}J\Omega_o^2\left(\varphi_R-\varphi_T\right)^2 \qquad (3\text{-}19)$$

θ_R - Blade in-plane angular displacement

K_E K_F - blade edge and flap-wise stiffness

φ_R - Blade out-plane angular displacement

Ω_o - Rotor angular velocity

φ_T - Fore-aft angular displacement of the tower

J_C - Tower/rotor cross-coupling inertia

θ_H - Side-to-side angular displacement of the hub

D_T - Fore-aft damping force

β - Pitch angle

J, J_T - Blade and tower inertia

F_1, F_2 - in and out-of-plane aerodynamic torques

K_T - Tower stiffness

The interaction between wind turbine blades and nacelle is also to be taken into consideration when modelling the wind turbine rotor. The first and second nacelle modes both contribute to rotor loads. The first nacelle mode refers to the fore-aft motion of the nacelle and the second mode refers to the nodding movement of the nacelle. The blade mode due to nacelle motion is

$$\begin{bmatrix} M_{T\theta_R} \\ M_{T\varphi_R} \end{bmatrix} = m_b l \begin{bmatrix} -\ddot{z}_R \\ \cos\varphi\cdot\ddot{y}_R \end{bmatrix} + J \begin{bmatrix} \dot{\Omega}_{yR} \\ \cos\varphi\cdot\dot{\Omega}_{zR} \end{bmatrix} \qquad (3\text{-}20)$$

$M_{T\theta_R}$ - Moment on the blade due to tower dynamics in the in-plane direction

$M_{T\varphi_R}$ - Moment on the blade due to tower dynamics in the out-plane direction

J - Inertia component of the blade

m_b - Mass of the blade

l - Distance of the centre of mass from the root

$\ddot{z}_R, \ddot{y}_R$ - Tower fore-aft and side-to-side linear accelerations

$\dot{\Omega}_{yR}, \dot{\Omega}_{zR}$ - Tower forward and side-to-side rotational accelerations

θ - Blade edgewise vibration angle

$M_{T\theta_R}, M_{T\varphi_R}$ - Moment on the blade due to tower dynamics in the in-plane and out-plane directions

$M_{A\theta}, M_{A\varphi}$ - In and out-plane aerodynamic loadings

$M_{I/P}, M_{O/P}$ - Blade in-plane and out-plane bending moments

θ_R, φ_R - Blade in-plane and out-plane vibration angles

ω_E, ω_F - Blade flap-wise and edge-wise frequencies

J - Inertia component of the blade

β - Pitch angle

3.1.5 Pitch actuator

The pitch actuator is included in the model to precisely simulate the limit and time delay on pitch angle changes. The actuator is essentially a low-pass filter. The third order model of the pitch actuator is

$$G_{act} = \frac{K_{A1}K_{A2}}{s^3 + as + K_{A2}s + K_{A1}K_{A2}} \tag{3-21}$$

To reduce the model complexity, the first order model is employed which produces similar performance as third order model. The first order pitch actuator model G_{act} is a basic low pass filter which only reflects the time delaying effect of the wind turbine pitch system.

$$G_{act} = \frac{a}{s+a} \tag{3-22}$$

The block diagram of the pitch actuator model is shown below:

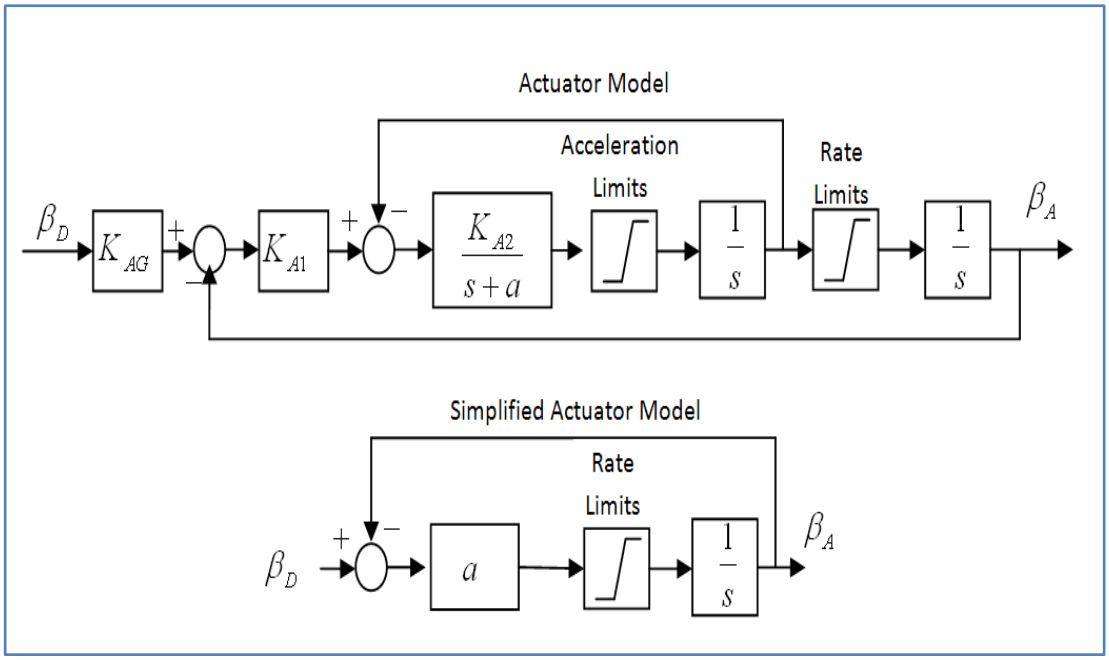

Figure 3-5: Block diagram of pitch actuator

3.1.6 Wind turbine control

3.1.6.1 Control objective

Small-scale wind turbines are able to run without a control system and generate unregulated power. However, with the increase of the wind turbine size, the requirement concerning economical and safe operation of the wind turbine increases

as well. Besides, power system operators have their own standards for any wind turbine to be connected to the grid. The controller objective is described below but with the development of wind turbine new objectives may be added.

3.1.6.1.1 Energy Capture

The power in a wind gust can be described by the following expression

$$P = \frac{1}{2}\rho A V^3 \tag{3-23}$$

where ρ is the air density, A is the area that the gust passes through and V is the wind speed. However, only a portion of the total power can be extracted from the wind. The maximum amount of power that can be extracted from the wind is 59.3%, which is known as the Betz Limit. The wind turbine should be able to extract as much energy as possible. Due to economic efficiency and safety issues, wind turbine limits its power output when the wind speed is too low or too high.

3.1.6.1.2 Load Alleviation

Wind turbines are subjected to mechanical loads when in operation. The loads can be categorized by their frequencies. The low frequency load, which is called the transient load, is induced by wind turbulence and gusts. The transient load becomes more significant as wind speed increases. It is the major reason why wind turbines cut out at high wind speed. The high frequency load is the load induced by the periodic rotation of rotor. Therefore the load usually concentrates around spectral peaks. For an N-bladed wind turbine rotating with speed Ω, 1Ω and $N\Omega$ spectral peaks are the most important for controller design.

Loads can also be classified by components that experience the load, namely drive-train load and structural load. The drive-train load is the variations in the net

aerodynamic torque that propagates down the drive-train and the structural load is due to the variations in the aerodynamic loads on the mechanical structure.

3.1.6.2 Control Strategy

The control strategy describes the way in which the wind turbine is regulated to achieve the control objective. Different types of wind turbines adopt different control strategies according to their features. The more components are included in the control action, the better the machine can be controlled. For instance, a fixed-speed fixed-pitch wind turbine has no potential for control at all. No active control action can be applied on a machine of this type thus the power output is totally unregulated and there is no way to alleviate the load on the machine. Rotor speed and pitch angle are two major parameters that can be manipulated for wind turbine control. The variable-speed feature provides wind turbines with several benefits including maximum energy capture, load alleviation and control of power production. However, due to the constraint of material and wind turbine structure, the rotor speed has to be limited within a certain range. Therefore when the wind speed goes too high the turbine has to be shut down. The pitching mechanism improves the performance of the wind turbine under high wind speed as wind turbine with pitch control can produce different aerodynamic torques under the same rotor speed. The variable-speed pitch-regulated wind turbine is the most popular wind turbine concept, although variable-speed fixed-pitch and fixed-speed pitch-regulated turbines are still used under certain circumstances for their relatively low price and simplicity of control system.

The most straightforward method to control a variable-speed wind turbine is to define the relationship between rotor speed and wind speed. However, the measured point wind speed is not the wind speed experienced by the wind turbine. The actual wind speed experienced by the wind turbine can only be derived from measurements

such as generated torque and electrical power. Since the relationship between aerodynamics and wind speed is not linear, the better approach is to control rotor speed based on other variables like torque.

For each wind turbine a rated wind speed is specified. In below-rated wind speed the controller priority is to maximize the energy capture. In above-rated wind speed the controller tries to shed the excess power in the wind. A typical power curve is shown in Figure 3-6.

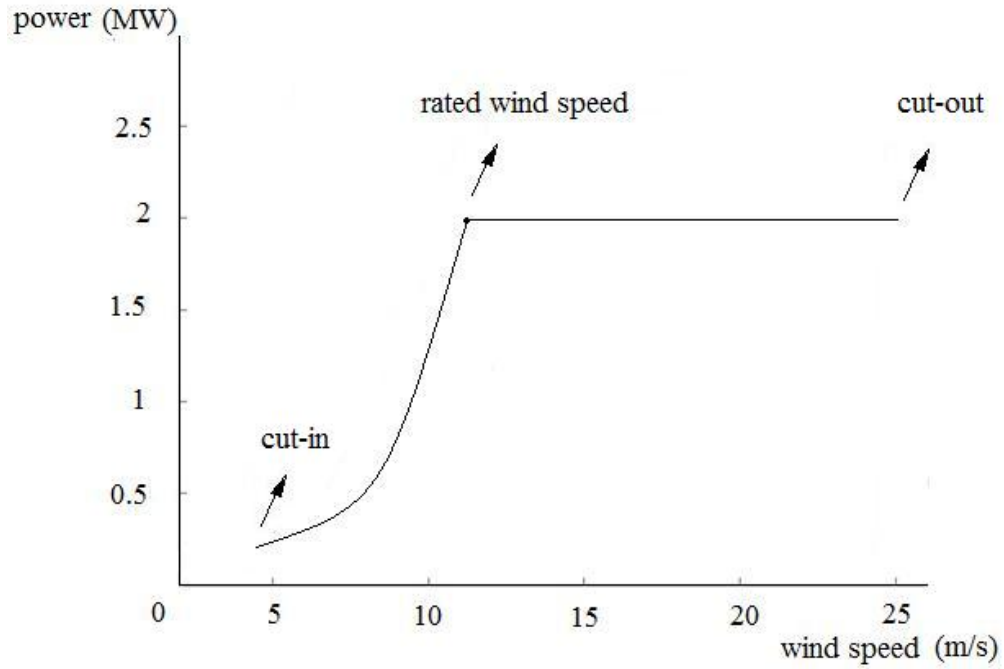

Figure 3-6: Power versus wind speed

From the power curve it can be seen that the wind turbine starts up at a predefined cut-in wind speed, below which the power production is too low to compensate the loss. The generated power keeps increasing with wind speed until the rated wind speed is reached. Above the rated wind speed the power is controlled to be constant. At the cut-out wind speed the wind turbine is shut down for safety reasons.

There are three modes in below-rated operation. Figure 3-7 shows the control strategy in the torque – rotor speed plane.

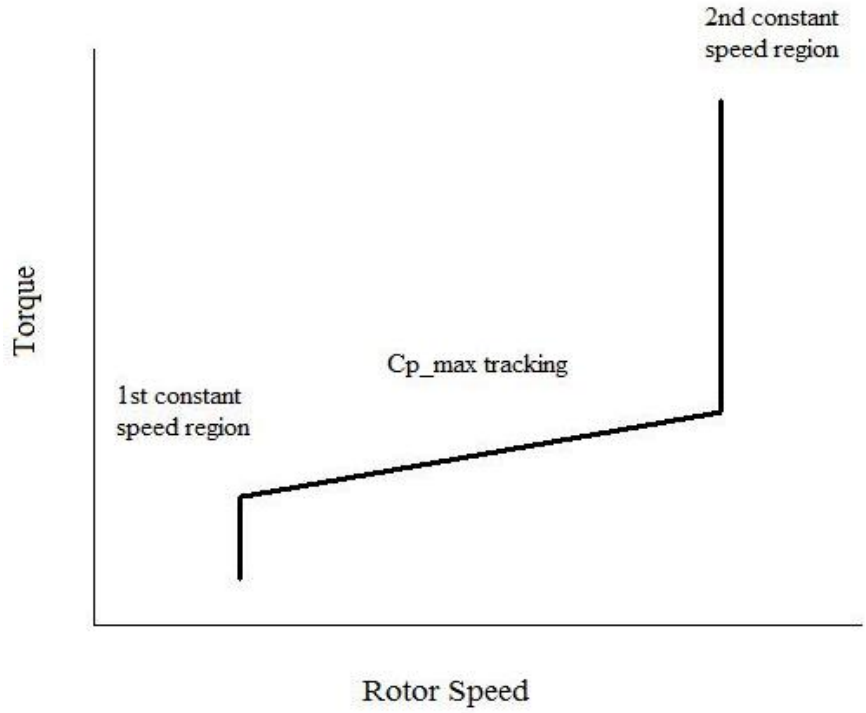

Figure 3-7: wind turbine operation modes

In the first constant region, the rotor speed is held constant while the aerodynamic torque keeps increasing until the C_{p_max} curve is reached. Then the controller is switched to the second mode which is maximum power tracking. The rotor speed is controlled to guarantee the maximum power production. The third mode is also constant rotor speed mode. In this region the rotor speed has reached its maximum value so the generator reaction torque is used to prevent rotor over-speed. Once the generator torque has reached its maximum value, the rotor blades need to start pitching to shed the power that exceeds the rated power.

3.1.6.3 Gain Scheduling

As discussed before, blade pitching controls the generator torque above rated wind speed. However, the relationship between aerodynamic torque and blade pitch angle

is nonlinear, which implies that the gain of the plant varies nonlinearly above rated. Therefore, compensation for the pitch demand is required. The aerodynamic torque is determined by rotor speed, wind speed and pitch angle.

It is proved that the aerodynamic torque can be divided into two components- one only depends on wind speed while the other depends on pitch angle and rotor speed [52]. This separation of aerodynamic torque simplified the linearization of the gain of plant because with the wind speed taken out of the expression, the nonlinearity of the wind turbine only depends on the pitch angle and the rotor speed.

The gain scheduling is implemented by placing the inverse of the nonlinear gain, which is scheduled on the pitch angle, in series with the controller.

3.1.6.4 Drive-Train Damping Filter

In the early type wind turbine, which is fixed speed with an asynchronous generator, the electrical grid provides damping to the generator rotor. Hence the damping for the wind turbine drive-train is satisfactory. In a variable-speed wind turbine an induction machine with power electronics is used so the damping from the grid is lost. The first drive-train mode is very lightly damped. Since the first drive-train mode is very resonant, the lack of damping can lead to very large torque oscillations, which affect the turbine life-time and safety [36].

The increase of damping of the first drive-train mode is achieved by feeding back the variation of the generator speed at the first drive-train mode frequency. Essentially this approach employs the wind turbine dynamics to damp the first drive-train mode. The block diagram is shown in Figure 3-8.

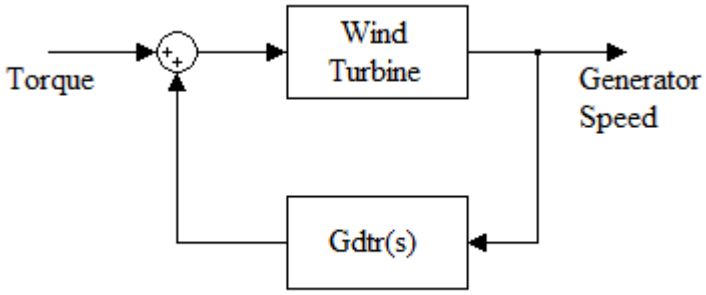

Figure 3-8: Drive-train damping filter

The drive-train damping filter is actually a band-pass filter. The frequency of the filter is not necessarily the first drive-train frequency as the gain of the plant at the first drive-train frequency is very high. Therefore, even if the filter frequency is biased a little, it is still able to filter the first drive-train mode properly.

3.1.6.5 Controller Design

The design of the wind turbine controller strongly influences the performance of the plant. With poor design the control objectives cannot be attained and the system may become unstable. The structural modes may be excited if the controller gain is chosen inappropriately. Proper stability, enough bandwidth and disturbance rejection is required in the controller design. A filter may be used at a certain frequency however it compromises the controller bandwidth.

The controller design for the wind turbine is carried out in the frequency domain. The spectral density of wind is described by von der Hoven spectra.

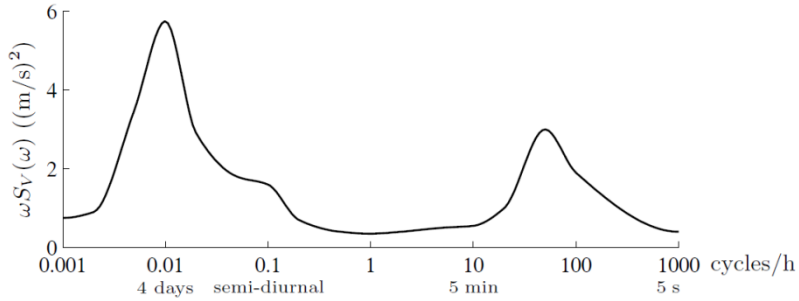

Figure 3-9: Von der Hoven spectra [36]

From the spectrum it can be seen that there are two spectral peaks. One is centred at the frequency of 4 days and the other is centred at high frequency. The high frequency component, which is induced by turbulence, is the one that control system is designed for. The controller should provide good stability margin and enough bandwidth to counter the spectral peak.

In the low frequency region the controller aims to maximize the bandwidth and increase the disturbance rejection as much as possible. In the high frequency region the controller should produce enough roll-off to reduce the actuator activity since frequent actuator action leads to large transient loads on the wind turbine components.

3.1.6.5.1 Wind turbine controller for below rated operation

The wind turbine rotational speed in below rated wind speed is regulated by the generator reaction torque. The system has the generator torque reference as input and generator speed as output. It is clear that the system has negative gain as the increase of the generator torque results in the decrease of the generator speed. The Bode plot of the wind turbine operating below rated wind speed is shown in Figure 3-10.

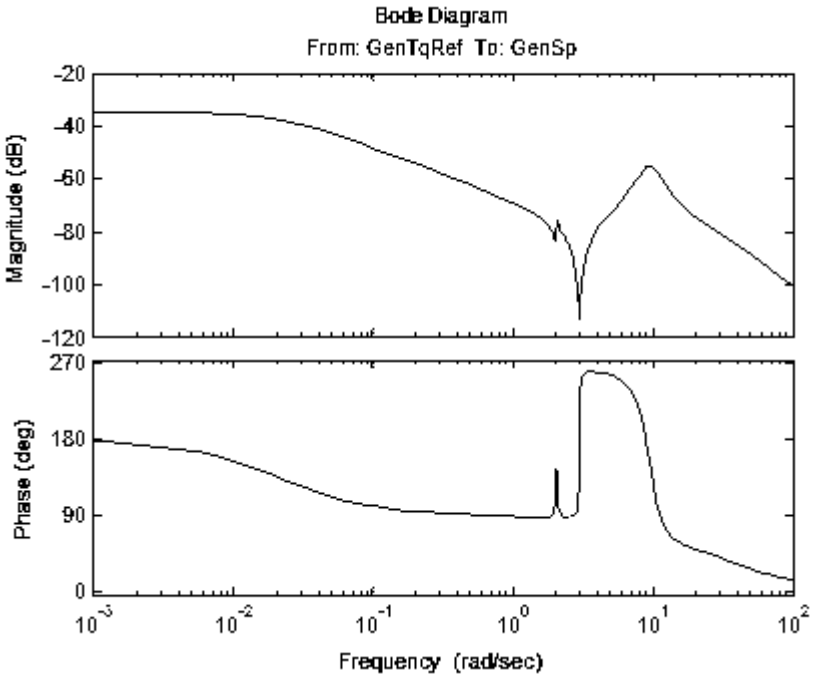

Figure 3-10: Bode plot of the transfer function from reference torque demand to generator speed in below rated wind speed

The wind turbine controller used in this thesis is described in [53]. The transfer function of the below rated controller is given by (3-24).

$$C_{br} = -5335.5\frac{s + 0.02218}{s} \tag{3-24}$$

The PI controller is designed to achieve the following goals: good disturbance rejection at low frequency, 1 rad/s bandwidth and good high frequency roll-off. The controller is adjusted to provide good stability margin and enough bandwidth to reject the higher frequency peak of the von der Hoven spectra shown in Figure 3-9. The low frequency shaping is employed to maximize the bandwidth and improves the disturbance rejection without compromising the stability. Enough roll-off at high frequency is provided to reduce the actuator activity. Additional filters can be added but that would imply a decay of phase and a reduction of the bandwidth. The Bode plot of the controller is shown in Figure 3-11.

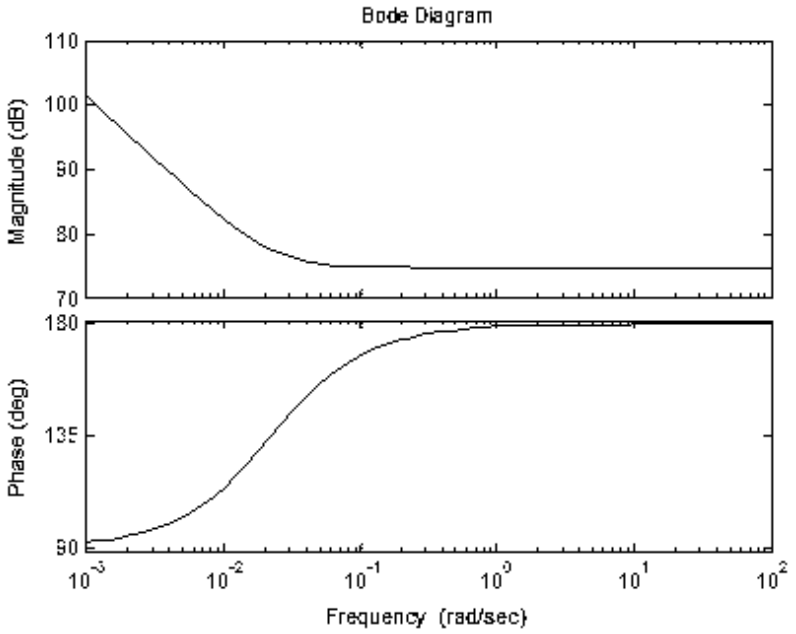

Figure 3-11: Bode plot of the wind turbine controller for below rated wind speed

The Bode plot of the controlled wind turbine in below rated wind speed is shown in Figure 3-12. It can be noticed that over 50 degree phase margin and 10dB gain margin is achieved. The sensitivity plot in Figure 3-13 shows that the designed controller for wind turbine below rated operation has relatively low gain and thus good disturbance rejection.

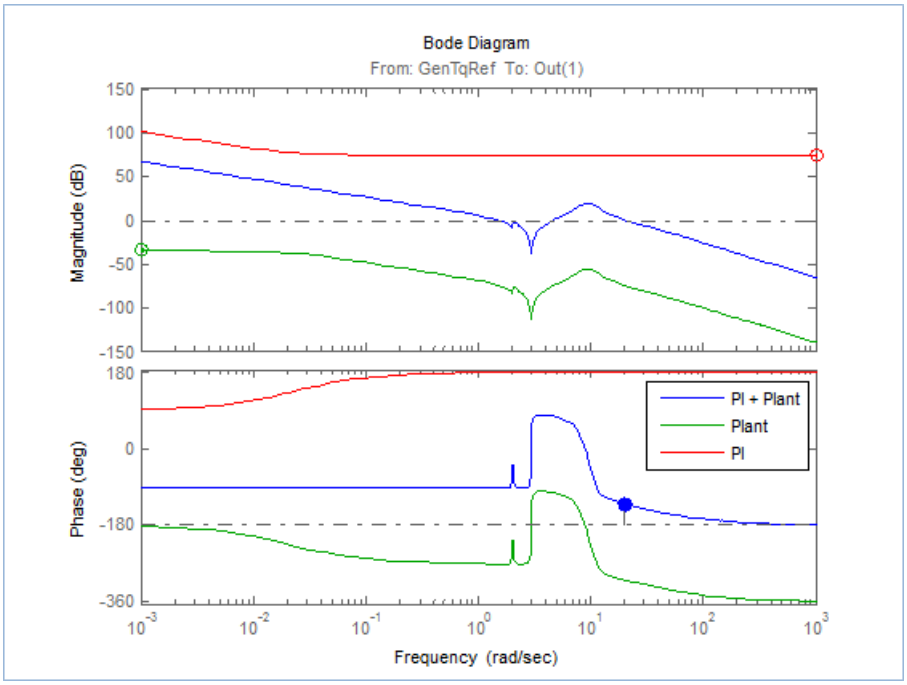

Figure 3-12: Bode plot of the wind turbine and controller in below rated wind speed

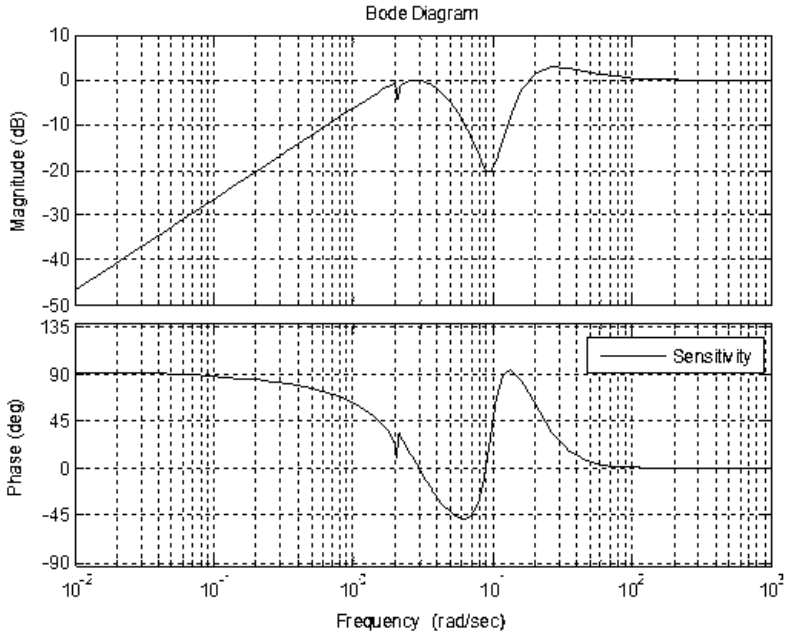

Figure 3-13: Bode plot of the sensitivity function of the wind turbine in below rated wind speed

The controller for the maximum power tracking of the wind turbine is given by (3-25). The drive-train and generator loss has to be taken into consideration when choosing the feedback gain K. As the 99% efficiency lines, see Figure 3-14, are quite far from the tracking curve, there is no need of a close loop control. An open loop control will be enough.

$$T = \frac{1}{2}\rho\pi R^5 \frac{\omega^2}{\lambda_{\max}} = K\omega^2 \tag{3-25}$$

where T is the torque. ρ is the air density. R is the blade radius. λ is the tip speed ratio and ω is the rotor speed.

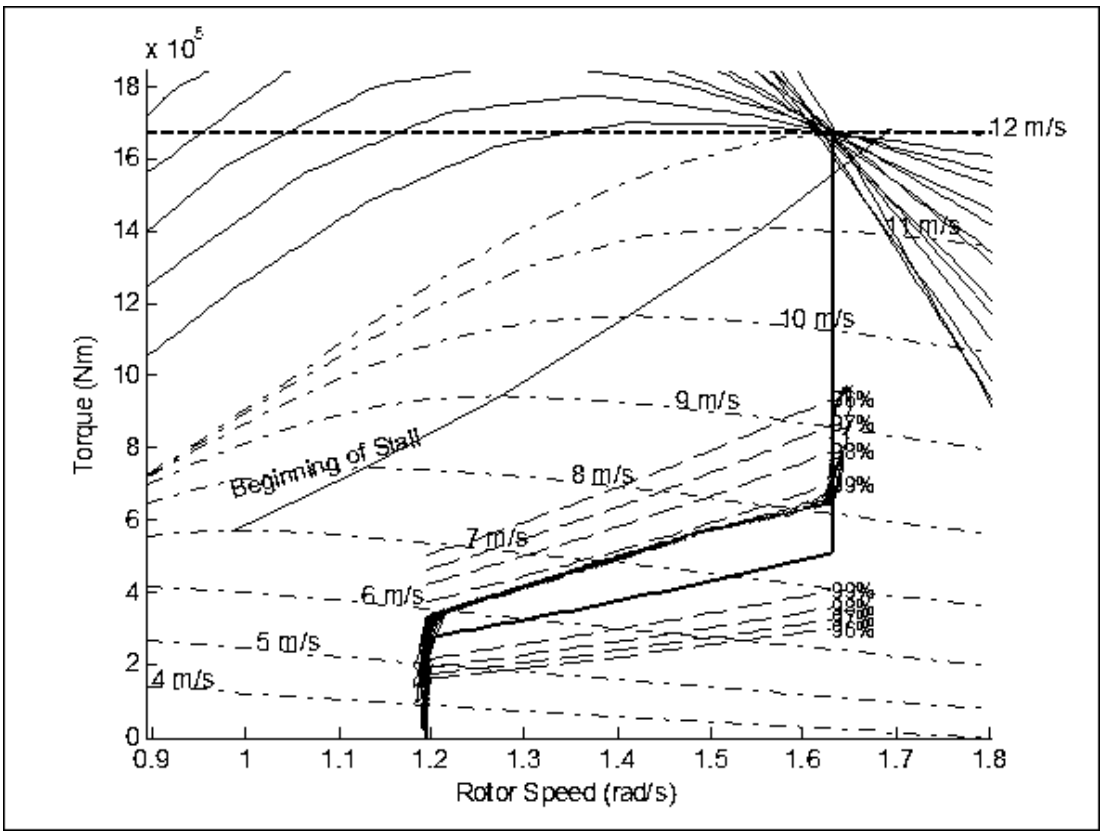

Figure 3-14: 99% efficiency line of wind turbine

3.1.6.5.2 Wind turbine controller for above rated operation

The gain scheduling technique introduced in section 3.1.6.3 is used in above rated controller design. The wind turbine plant changes in above rated wind speed as the aerodynamics varies. The gain scheduling compensates the aerodynamics so that only one controller needs to be designed for above rated.

The above rated controller operation has pitch position demand as input and generator speed as output. The system gain is negative as the increase of the pitch angle results in the decrease of rotor speed. The Bode plot of the plant is shown in Figure 3-15.

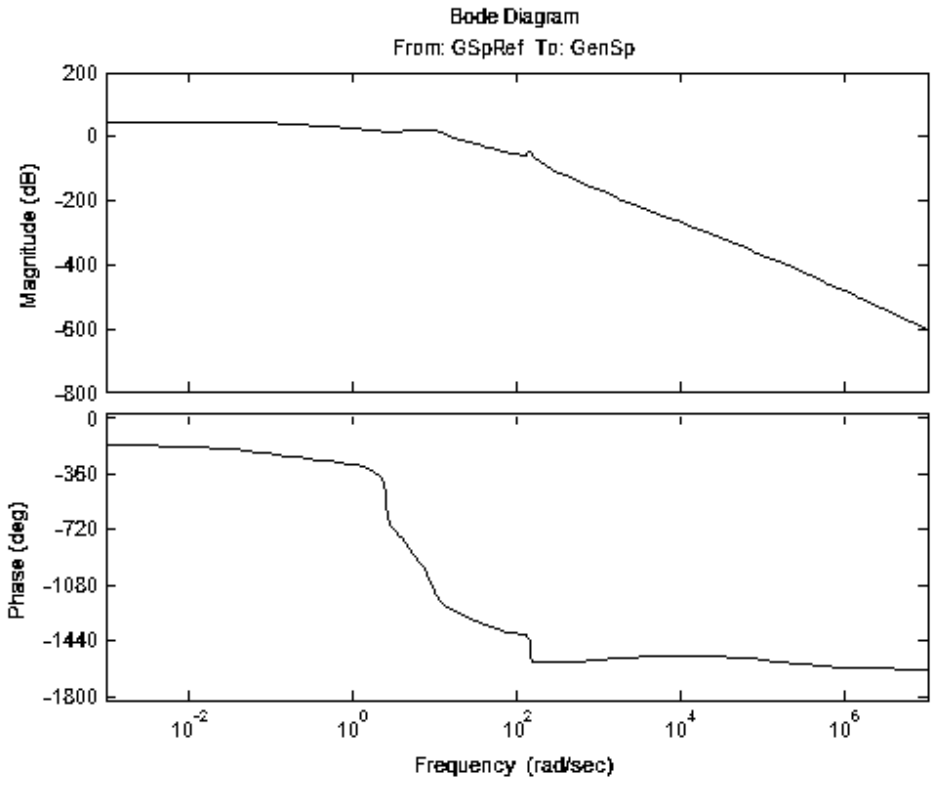

Figure 3-15: Bode plot of the above rated wind turbine

A PI controller defined by (3-26) is used for pitch control. The same criteria applied to the controller below rated operation should be applied to the controller above rated operation. The Bode plot of the above rated controller is shown in Figure 3-16.

$$C_{ar} = -0.026721\frac{s+0.02484}{s} \tag{3-26}$$

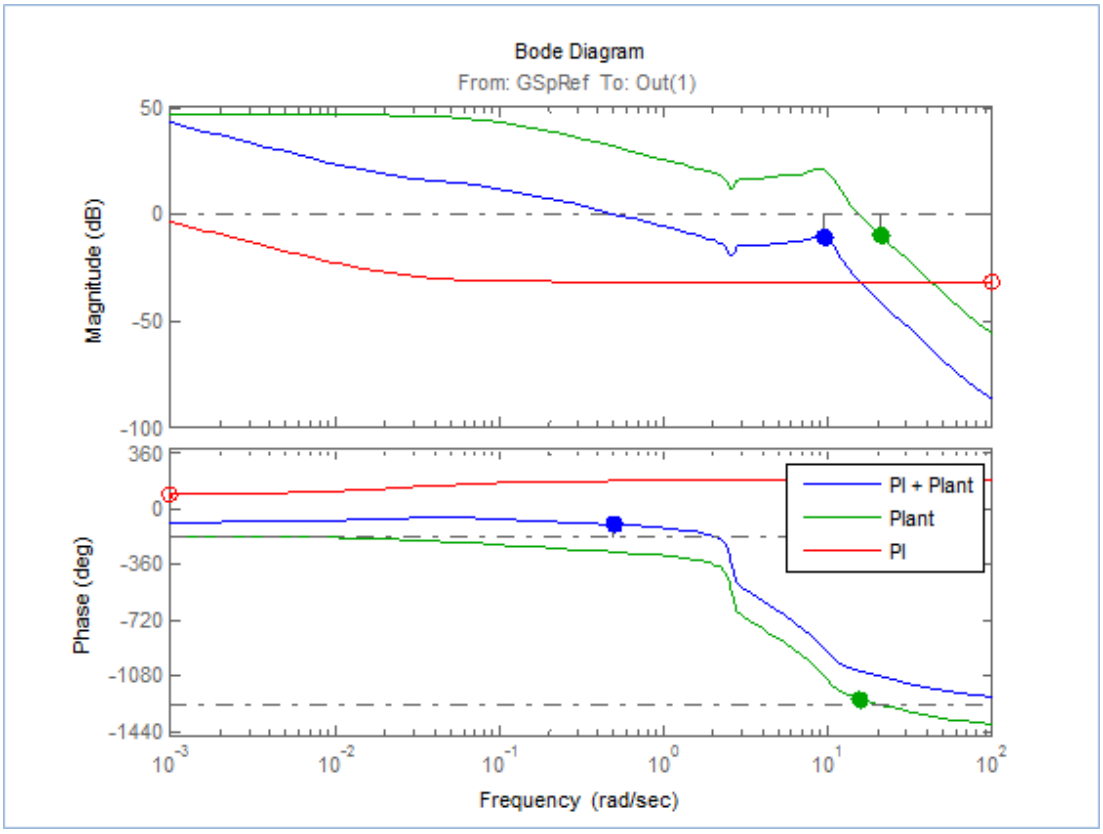

Figure 3-16: Bode plot of the above rated controller

The controller tuning is carried out in the frequency domain. By adjusting the proportional gain and the integral gain of the PI controller, the gain margin of 10.5 dB and phase margin of 80.3 degree is achieved. The sensitivity plot shown in Figure 3-17 indicates that the controller produces satisfactory disturbance rejection.

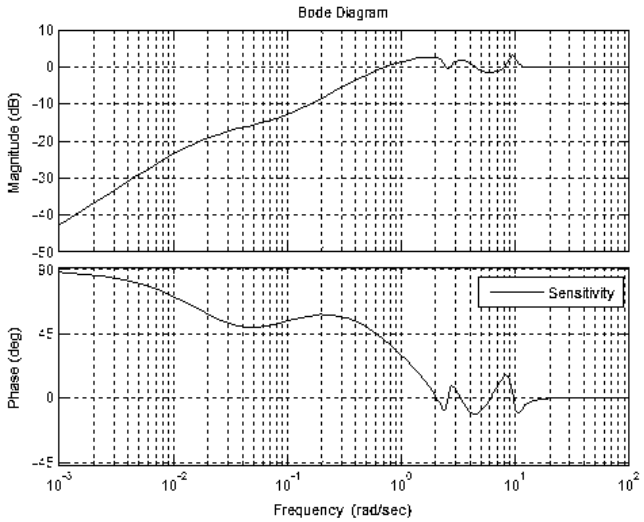

Figure 3-17: Bode plot of the disturbance rejection of wind turbine in above rated wind speed

3.1.6.6 Controller Switching

As the wind speed varies, wind turbines operate under different operation modes. Four modes of wind turbine operation are stated below:

- Mode 0: First constant speed mode
- Mode 1: C_{p_max} tracking mode
- Mode 2: Second constant speed mode
- Mode 3: Pitch control mode

The wind turbine controller should deliver the maximum power available below rated wind speed. Above rated wind speed, the power generated would exceed the nominal value and the controller is required to discard the extra energy. Besides, there are restrictions on the minimum and maximum rotor speed. Hence, an automatic controller switching system needs to be implemented to guarantee the smooth operation during mode transition. The control system is required to operate over the whole envelope of wind speeds. Close attention is given to the switching

strategy due to its impact on the overall performance of the controller. Even if all subsystems are stable, a poor switching strategy can lead to instabilities.

The scheme of the wind turbine controller switching strategy in below rated wind speed is shown in Figure 3-18.

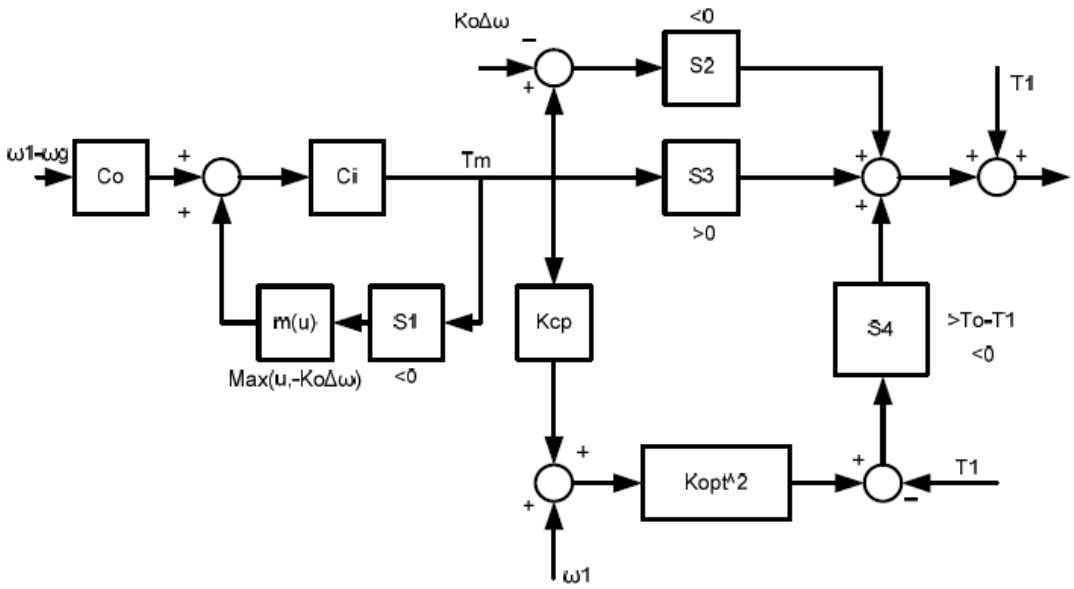

Figure 3-18: Scheme for the switching below rated [53]

PI controller is used for the torque demand in Mode 0 and Mode 2 to keep the rotor speed constant. In Mode 1 the generator speed is determined by the wind speed while generator torque is obtained from the generator speed and the C_{p_max} curve. Transitions between modes are realized by in effecting switching operation based on demanded generator reaction torque. The controller is designed in the manner that idle modes are saturated at the switching value to ensure smooth switching between different modes. In Figure 3-18, C_0 and C_i are designed such that $C_0C_i=C_{br}$ which is described in (3-24). The transfer function of C_0 and C_i are chosen in the manner that $\frac{C_0C_i}{1-C_i}$ is a low pass filter with a bandwidth of 3 rad/s.

3.1.6.6.1 Switching between mode 2 and mode 1

As mentioned before, mode 2 is the constant speed region where the generator torque is controlled so that generator speed is the fixed to a constant value ω_1. The output of the wind turbine in mode 1 is determined by the C_{p_max} curve directly. No active control is involved in this mode. The switching between mode 2 and mode 1 is explained below. ω_g is smaller than ω_1 in mode 1 so that the input to C_i is negative. T_m is negative as well therefore S1=1 which closes the loop while opening the switch S2. With S1 closed, the loop $\frac{C_0 C_i}{1-C_i}$ is basically a constant gain until 3rad/s. We have the wind turbine speed error ω_g -ω_1 at the output of K_{cp}. By adding ω_1 we get the estimated generator speed ω_g as the input to K_{opt} which defines the optimal power curve. The switching torque T_1 is subtracted from the output and the error is processed by S3 to make sure that the generator torque reference does not exceed the maximum torque in mode 1. T_1 is added back in after S3 so that the reference torque is generated.

When the rotational speed ω_1 is reached, ω_g -ω_1 will be positive which changes the states of S1, S2 and S3 so that $T_m=C_0C_i=C_{br}$ which is the wind turbine controller for below rated wind speed operation.

3.1.6.6.2 Switching between mode 1 and mode 0

When the wind speed drops so that the minimum rotational speed of the wind turbine ω_0 is reached, the controller has to be switched from mode 1 to mode 0. The switching is carried out with a similar method as between mode 2 and mode 1 but with calibrated set-point of the switching torque. The value of ω_1- ω_g is controlled to add an offset to the switching point. The value of the offset is

$$m(u) = -C_0(\omega_1 - \omega_0) = -K_0 \Delta\omega \qquad (3\text{-}27)$$

The value of T_m is therefore $-K_0\Delta\omega$.

3.1.6.6.3 Switching from below rated to above rated

When wind turbine switches to above rated, $\omega_g > \omega_{g0}$ therefore S1 is open. Loop 1 becomes $\frac{C_{br}}{1-C_{br}}$ which is basically an all-pass filter. S2 is also open because T_m is negative. Given these switch status, the output of the below rated controller is derived as

$$T_d = K_{opt}\left(K_{cp}T_m + \omega_{g0}\right) = K_{opt}\omega_g^2 \tag{3-28}$$

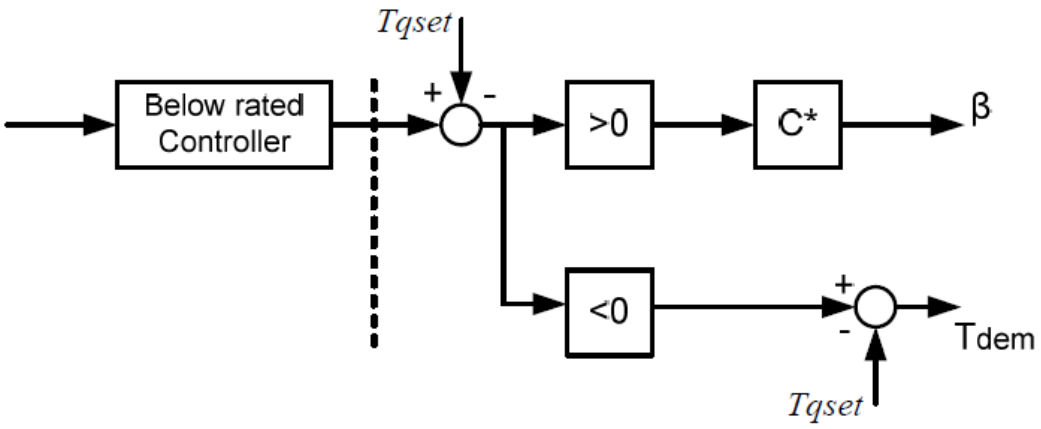

Figure 3-19: Structure for switching from below to above rated

3.2 DFIG system modelling

As an essential component of wind energy conversion system, the performance of the generator and its controller directly affects the transient stability of the wind turbine and the power system. A dynamic analytical mathematical model is needed for the investigation of the stability of wind turbine and power system. Only a DFIG model

is presented here as this thesis focuses on a wind turbine with this type of generator. Based on the reference frame used, the DFIG model can be divided into 3 categories namely:

- ABC reference frame model
- αβ reference frame model
- dq reference frame model

3.2.1 Mathematical model of DFIG

3.2.1.1 Mathematical model in the ABC reference frame

Following the nature of the three-phase power system, the most straightforward way to model a DFIG is in 3-phase reference frame, which is commonly referred to as the ABC frame. Earlier DFIG controller designs were based on this model [54]. The modelling of DFIGs in the ABC frame is introduced in many publications [55-58]. The model of a DFIG is of high order and strongly nonlinear. When developing the model the following assumptions are made: harmonics, magnetic saturation, iron core loss and resistance variation of stator and rotor are ignored. The rotor winding is represented in the stator winding equivalent. The variables of DFIG in the ABC frame are illustrated in Figure 3-20.

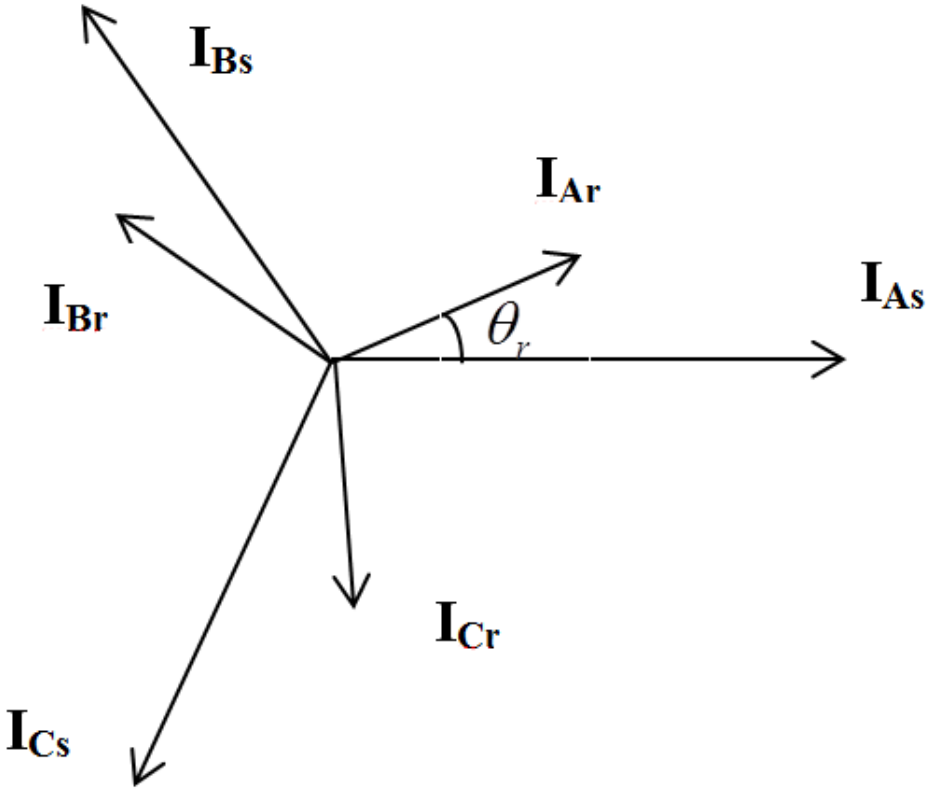

Figure 3-20: Vector diagram of DFIG current in the ABC frame

where 3 phases A B C are 120° apart from each other. The rotor winding vectors rotates with rotor. θ_r is the angle between phase *a* of rotor and phase *A* of stator.

Applying Kirchhoff's law and Lenz's law we can get the equation for both rotor and stator.

$$\boldsymbol{U} = R\boldsymbol{I} + \frac{d}{d_t}\boldsymbol{\psi} \tag{3-29}$$

where voltage vector $\boldsymbol{U} = \left[\boldsymbol{U}_A\ \boldsymbol{U}_B\ \boldsymbol{U}_C\ \boldsymbol{U}_a\ \boldsymbol{U}_b\ \boldsymbol{U}_c\right]^{\mathrm{T}}$, current vector $\boldsymbol{I} = \left[\boldsymbol{I}_A\ \boldsymbol{I}_B\ \boldsymbol{I}_C\ \boldsymbol{I}_a\ \boldsymbol{I}_b\ \boldsymbol{I}_c\right]^T$, resistance vector $R = diag\left[R_s\ R_s\ R_s\ R_r\ R_r\ R_r\ \right]$. $\boldsymbol{U_A}$, $\boldsymbol{U_B}$,

$\boldsymbol{U_C}$ represent stator voltage, $\boldsymbol{U_a}$, $\boldsymbol{U_b}$, $\boldsymbol{U_c}$ represent rotor voltage, $\boldsymbol{I_A}$, $\boldsymbol{I_B}$, $\boldsymbol{I_C}$ represent stator current, $\boldsymbol{I_a}$, $\boldsymbol{I_b}$, $\boldsymbol{I_c}$ represent rotor current, R_s represents stator resistance, R_r represents rotor resistance, ψ is the total flux which includes self-flux and mutual-flux[59]:

$$\begin{bmatrix} \boldsymbol{\psi_s} \\ \boldsymbol{\psi_r} \end{bmatrix} = \begin{bmatrix} L_{ss} & L_{sr} \\ L_{rs} & L_{rr} \end{bmatrix} \begin{bmatrix} \boldsymbol{I_s} \\ \boldsymbol{I_r} \end{bmatrix} = L\boldsymbol{I} \tag{3-30}$$

where $\boldsymbol{\psi_A}\ \boldsymbol{\psi_B}\ \boldsymbol{\psi_C}$ is the stator flux, $\boldsymbol{\psi_a}\ \boldsymbol{\psi_b}\ \boldsymbol{\psi_c}$ is the rotor flux, $\boldsymbol{\psi_s} = \left[\boldsymbol{\psi_A}\ \boldsymbol{\psi_B}\ \boldsymbol{\psi_C}\right]^T$, $\boldsymbol{\psi_r} = \left[\boldsymbol{\psi_a}\ \boldsymbol{\psi_b}\ \boldsymbol{\psi_c}\right]^T$, $\boldsymbol{I_s} = \left[\boldsymbol{I_A}\ \boldsymbol{I_B}\ \boldsymbol{I_C}\right]^T$, $\boldsymbol{I_r} = \left[\boldsymbol{I_a}\ \boldsymbol{I_b}\ \boldsymbol{I_c}\right]^T$ and[59]

$$L_{ss} = \begin{bmatrix} L_m + L_{ls} & -\frac{1}{2}L_m & -\frac{1}{2}L_m \\ -\frac{1}{2}L_m & L_m + L_{ls} & -\frac{1}{2}L_m \\ -\frac{1}{2}L_m & -\frac{1}{2}L_m & L_m + L_{ls} \end{bmatrix} \tag{3-31}$$

$$L_{ss} = \begin{bmatrix} L_m + L_{lr} & -\frac{1}{2}L_m & -\frac{1}{2}L_m \\ -\frac{1}{2}L_m & L_m + L_{lr} & -\frac{1}{2}L_m \\ -\frac{1}{2}L_m & -\frac{1}{2}L_m & L_m + L_{lr} \end{bmatrix} \tag{3-32}$$

$$L_{rs} = L_{sr}^T = L_m \begin{bmatrix} \cos\theta_r & \cos\left(\theta_r - 120^\circ\right) & \cos\left(\theta_r + 120^\circ\right) \\ \cos\left(\theta_r + 120^\circ\right) & \cos\theta_r & \cos\left(\theta_r - 120^\circ\right) \\ \cos\left(\theta_r - 120^\circ\right) & \cos\left(\theta_r + 120^\circ\right) & \cos\theta_r \end{bmatrix} \tag{3-33}$$

in which L_m is the mutual inductance, L_{ls} is the stator leakage inductance, L_{lr} is the rotor leakage inductance.

Substituting (3-30) into (3-29):

$$\boldsymbol{U} = R\boldsymbol{I} + \dot{L}\frac{d\boldsymbol{I}}{dt} + \frac{dL}{dt}\boldsymbol{I} \tag{3-34}$$

The generator torque of the DFIG in the ABC frame can be expressed as:

$$T_e = \frac{1}{2} n_p \boldsymbol{I}^T \begin{bmatrix} 0 & \frac{d}{d\theta_r} L_{sr} \\ \frac{d}{d\theta_r} L_{rs} & 0 \end{bmatrix} \boldsymbol{I} \tag{3-35}$$

where n_p is the number of pole pairs.

Substituting (3-33) into (3-35), the torque of DFIG can be written as

$$T_e = -n_p L_m \Big[\left(I_A I_a + I_B I_b + I_C I_c \right) \sin\theta_r + \left(I_A I_a + I_B I_b + I_C I_c \right) \sin\left(\theta_r + 120^\circ \right)$$

$$+ \left(I_A I_a + I_B I_b + I_C I_c \right) \sin\left(\theta_r - 120^\circ \right) \Big] \tag{3-36}$$

Although the DFIG model in the ABC frame is more complex than other models, it is the basis of other modelling methods and provides the straightforward information of the voltage and current of each phase. The nonlinearity of this model limits the analysis and controller design of the DFIG. A widely adopted method in DFIG analysis is to simplify the model with a coordinate transformation.

3.2.1.2 DFIG model in αβ reference frame

The ABC reference frame is a fixed frame. The stator and rotor current rotate in the frame according to the generator rotor movement. This leads to sinusoidal signals, which are inconvenient for analysis and control purposes. To simplify the analysis, the Clarke transformation is applied. The Clarke transformation used in this thesis is

I_S

explained in Appendix C.1. The Clarke transformation results in αβ coordinates, which rotate along with the rotor winding of DFIG. The stator current vector of the DFIG in the αβ reference frame is illustrated in Figure 3-21:

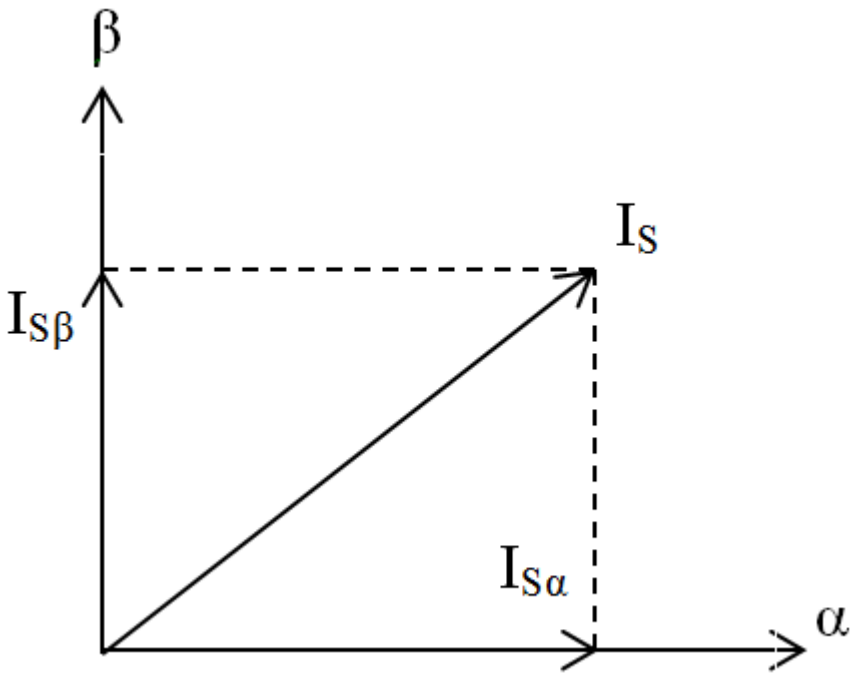

Figure 3-21: Vector diagram of DFIG stator current in αβ reference frame

Applying the Clarke transformation on (3-29), the stator voltage equation of the DFIG can be expressed in the αβ reference frame as in [59]

$$U_{s\alpha} = R_s I_{s\alpha} + \frac{d}{dt}\psi_{s\alpha} \tag{3-37}$$

$$U_{s\beta} = R_s I_{s\beta} + \frac{d}{dt}\psi_{s\beta} \tag{3-38}$$

where $\boldsymbol{U}_{s\alpha}$ and $\boldsymbol{U}_{s\beta}$ are the DFIG stator voltage components on the α and β axes. $\boldsymbol{\Psi}_{s\alpha}$ and $\boldsymbol{\Psi}_{s\beta}$ are the DFIG stator flux components on the α and β axes. It is assumed that three phases are balanced so that the more general αβγ transformation which is sometimes used can be simplified to the αβ transformation as $\boldsymbol{U}_{\gamma}$=0.

The rotor voltage equation of DFIG can be written in the αβ reference frame as

$$U_{r\alpha} = R_r I_{r\alpha} + \frac{d}{dt}\psi_{r\alpha} + \omega_r \psi_{r\beta} \tag{3-39}$$

$$U_{r\beta} = R_r I_{r\beta} + \frac{d}{dt}\psi_{r\beta} + \omega_r \psi_{r\alpha} \tag{3-40}$$

where $U_{r\alpha}$ and $U_{r\beta}$ are the DFIG rotor voltage components on the α and β axes. $\Psi_{r\alpha}$ and $\Psi_{r\beta}$ are the DFIG stator flux components on the α and β axes.

The DFIG flux equations in the αβ reference frame can be derived using same transformation[59]

$$\psi_{s\alpha} = L_s I_{s\alpha} + L_m I_{r\alpha} \tag{3-41}$$

$$\psi_{s\beta} = L_s I_{s\beta} + L_m I_{r\beta} \tag{3-42}$$

$$\psi_{r\beta} = L_m I_{s\beta} + L_r I_{r\beta} \tag{3-43}$$

$$\psi_{r\alpha} = L_m I_{s\alpha} + L_r I_{r\alpha} \tag{3-44}$$

where L_m is the mutual inductance between DFIG stator and rotor, $L_s = L_{ls} + L_m$ is the equivalent stator self-inductance in the αβ reference frame. $L_r = L_{lr} + L_m$ is the equivalent rotor self-inductance in the αβ reference frame.

Substituting flux equations into stator and rotor equations, the DFIG voltage equation in the αβ reference frame becomes:

$$U_{s\alpha} = R_s I_{s\alpha} + L_m \frac{d}{dt} I_{r\alpha} + L_s \frac{d}{dt} I_{s\alpha} \tag{3-45}$$

$$U_{s\beta} = R_s I_{s\beta} + L_m \frac{d}{dt} I_{r\beta} + L_s \frac{d}{dt} I_{s\beta} \tag{3-46}$$

$$U_{r\alpha} = R_r I_{r\alpha} + L_r \frac{d}{dt} I_{r\alpha} + L_m \frac{d}{dt} I_{s\alpha} + \omega_r (L_m I_{s\beta} + L_r I_{r\beta}) \tag{3-47}$$

$$U_{r\beta} = R_r I_{r\beta} + L_r \frac{d}{dt} I_{r\beta} + L_m \frac{d}{dt} I_{s\beta} - \omega_r (L_m I_{s\alpha} + L_r I_{r\alpha}) \tag{3-48}$$

Applying the αβ transformation on (3-35), the torque equation of the DFIG in αβ reference frame is

$$T_e = \frac{3}{2} n_p (\psi_{s\alpha} I_{s\beta} - \psi_{s\beta} I_{s\alpha}) \tag{3-49}$$

3.2.1.3 DFIG model in the dq reference frame

The DFIG variables can be expressed in DC form in the dq reference frame. The dq transformation is proposed in [60] to simplify the analysis of the three-phase electrical system. The dq transformation used in this thesis is explained in Appendix C.2. The relationship between the αβ reference frame and the dq reference frame is shown in Figure 3-22.

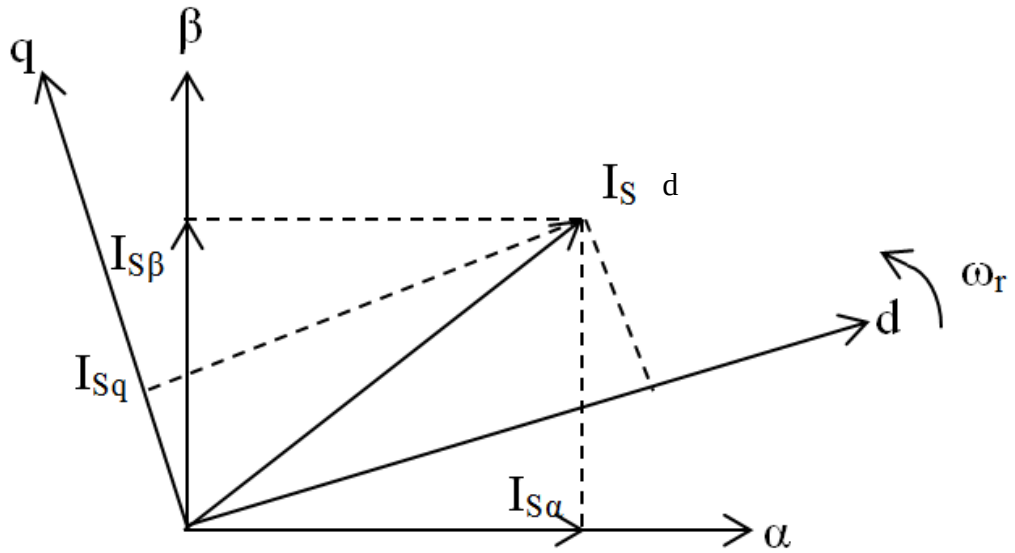

Figure 3-22: Relationship between dq and αβ reference frame

where ω_r is the synchronous speed of the dq reference frame.

The voltage equation in the dq reference frame is derived from (3-37) - (3-40) as

$$U_{sd} = R_s I_{sd} - \psi_{sq} + \frac{d}{dt}\psi_{sd} \tag{3-50}$$

$$U_{sq} = R_s I_{sq} + \psi_{sd} + \frac{d}{dt}\psi_{sq} \tag{3-51}$$

$$U_{rd} = R_r I_{rd} - s\psi_{rq} + \frac{d}{dt}\psi_{rd} \tag{3-52}$$

$$U_{rq} = R_r I_{rq} + s\psi_{rd} + \frac{d}{dt}\psi_{rq} \tag{3-53}$$

in which ω_s is the synchronous angular frequency and s is the slip of DFIG.

The flux equations in the dq reference frame are[61]

$$\psi_{sd} = L_s I_{sd} + L_m I_{rd} \tag{3-54}$$

$$\psi_{sq} = L_s I_{sq} + L_m I_{rq} \tag{3-55}$$

$$\psi_{rq} = L_m I_{sq} + L_r I_{rq} \tag{3-56}$$

$$\psi_{rd} = L_m I_{sd} + L_r I_{rd} \tag{3-57}$$

Combining the voltage equations and flux equations, the DFIG mathematical model is derived as[61]

$$U_{sq} = R_s I_{sq} + L_m \frac{d}{dt} I_{rq} + L_s \frac{d}{dt} I_{sq} + \omega_s (L_s I_{sd} + L_m I_{rd}) \tag{3-58}$$

$$U_{sd} = R_s I_{sd} + L_m \frac{d}{dt} I_{rd} + L_s \frac{d}{dt} I_{sd} - \omega_s (L_s I_{sq} + L_m I_{rq}) \tag{3-59}$$

$$U_{rd} = R_r I_{rd} + L_m \frac{d}{dt} I_{sd} + L_r \frac{d}{dt} I_{rd} - s(L_r I_{rq} + L_m I_{sq}) \tag{3-60}$$

$$U_{rq} = R_r I_{rq} + L_m \frac{d}{dt} I_{sq} + L_r \frac{d}{dt} I_{rq} + s(L_r I_{rd} + L_m I_{sd}) \tag{3-61}$$

Transforming (3-49) into the dq reference frame, we get the torque equation in dq reference frame as[59]

$$T_e = \frac{3}{2} n_p (\psi_{sd} I_{sq} - \psi_{sq} I_{sd}) \tag{3-62}$$

3.2.1.4 Simplified DFIG model

The above DFIG model is referred to as 5th order DFIG model. It is often simplified to a lower order model for the convenience of investigation and simulation such as in small-signal analysis [62]. A common representation of the DFIG model is to neglect stator transients by assuming $\frac{d\psi_{sd}}{dt} = 0$ and $\frac{d\psi_{sq}}{dt} = 0$ in (3-50) to (3-53). This

results in a 3rd order DFIG model. The validation of this simplification is based on the fact that during normal operation of the DFIG, the variation of grid voltage is relatively small. The stator voltage of the DFIG is assumed to be constant as the stator is connected to the grid directly. The transients of the DFIG stator flux are hence neglected. The 3rd order DFIG model can be expressed as[63]

$$U_{sd} = R_s I_{sd} - \omega_s \psi_{sq} \tag{3-63}$$

$$U_{sq} = R_s I_{sq} + \omega_s \psi_{sd} \tag{3-64}$$

$$U_{rd} = R_r I_{rd} - s\psi_{rq} + \frac{d}{dt}\psi_{rd} \tag{3-65}$$

$$U_{rq} = R_r I_{rq} + s\psi_{rd} + \frac{d}{dt}\psi_{rq} \tag{3-66}$$

The 3rd order model and 5th order model result in similar simulation results when grid voltage is stable. However, when grid voltage is subjected to amplitude drop or phase variation, neglecting of stator flux transients has significant influence on simulation results. The comparison of the simulation result of 3rd and 5th order DFIG model during grid voltage drop is shown in Figure 3-23.

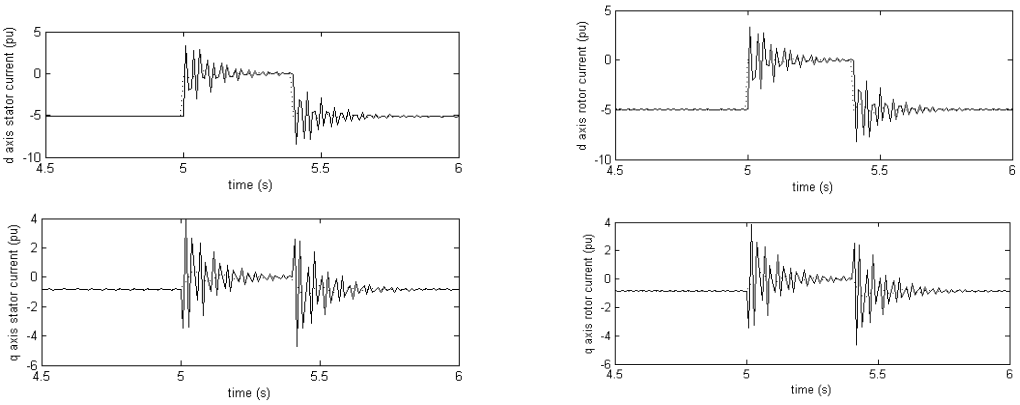

(a) (b)

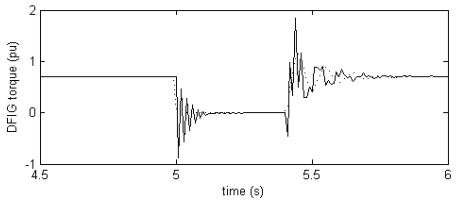

(c)

Figure 3-23: comparison of 3rd and 5th order DFIG model under grid voltage sag (a) stator d and q axis current (b) rotor d and q axis current (c) generator torque
Solid line: 5th order model. Dashed line: 3rd order model

It can be seen in the simulation results that the 5th order model contains evident electromagnetic oscillation while 3rd order model does not. However, the 3rd order model has the advantage of faster simulation speed which is very important in simulations that include a large number of models such as multi-machine power system simulations. It is noticed that stator flux transients are of synchronous frequency, which is high compared to wind turbine mechanical modes. It is therefore reasonable to use a 3rd order DFIG model in the study of wind turbine mechanical components fault ride-through to speed up simulations.

3.2.2 Converter system model

The power converter system is required in the DFIG concept. There are various converter topologies that can be applied to the DFIG. As dual-direction power transmission is required in the DFIG concept, the back-to-back converter topology has become the most popular converter system for the DFIG. The back-to-back converter consists of two voltage source converters (VSC) and a DC link. The converter is shown in Figure 3-24.

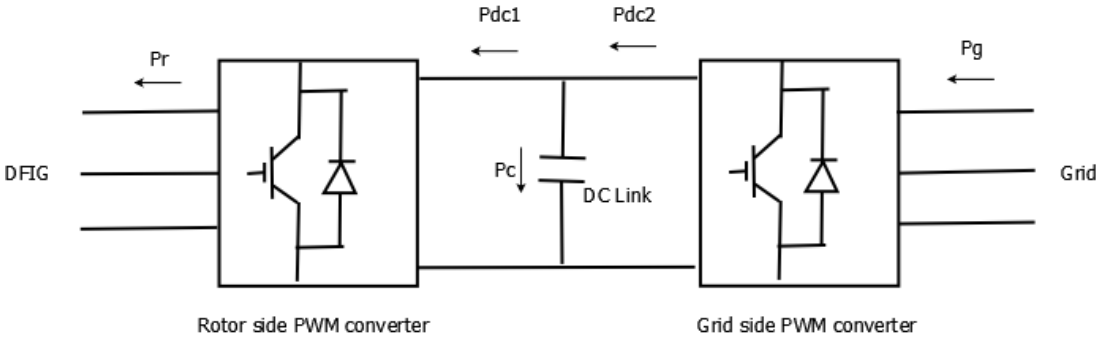

Figure 3-24: Back-to-back converter

where P_r is the active power absorbed by the DFIG rotor, P_g is the active power delivered by the grid. P_{dc1} and P_{dc2} are the DC power of the rotor and grid-side converters. P_c is the power stored in the DC link.

The DC link separates the rotor- and grid-side converters so that they can be controlled independently. The switching of the converter is assumed to be perfect, as it is not affected by the disturbance from either the generator side or the grid side. The rotor-side converter is normally integrated into the DFIG rotor and controller model. The grid-side converter and the DC link model are explained below.

3.2.2.1 Grid-side converter model

Given the assumption of perfect switching, the grid-side converter can be modelled simply by the losses associated with the resistance and inductance between the converter and the grid. Applying Kirchhoff's law on the converter model in the dq reference frame, the grid-side converter model is written as

$$V_{d1} - V_{d2} = RI_d - \omega_s LI_q + L\frac{d}{dt}I_d \tag{3-67}$$

$$V_{q1} - V_{q2} = RI_q + \omega_s LI_d + L\frac{d}{dt}I_q \tag{3-68}$$

Applying the Laplace transformation on (3-67) and (3-68), the grid-side converter is modelled as:

$$I_d = \frac{\omega}{Ls}\left(V_{d1} - V_{d2} - RI_d + L\,I_q\right) \tag{3-69}$$

$$I_q = \frac{\omega}{Ls}\left(V_{q1} - V_{q2} - RI_q - L\,I_d\right) \tag{3-70}$$

where I_d and I_q are d and q axis current in converter, V_{d1} and V_{q1} are AC side network voltages, V_{d2} and V_{q2} are DC inverter side voltages, R and L are the total resistance and inductance of the transformer and line connecting the grid and the grid-side converter.

3.2.2.2 DC link model

The capacitor in the DC link behaves as a temporary energy storage device. Assuming the loss in the DC link is neglected, the energy stored in the DC link is computed as

$$P_s - P_g = \frac{1}{2} C \frac{d}{dt} V_{dc}^2 \tag{3-71}$$

where P_s is the stator power, P_g is the grid power, C is the DC link capacitance, V_{dc} is the voltage across the DC link.

The DC link model contains the controlled variable V_{dc}^2, which is nonlinear. In practice this term is normally replaced by a new variable $u = V_{dc}^2$ for the convenience of the controller design. The DC link model is written as

$$P_s - P_g = \frac{1}{2} C \frac{d}{dt} u \tag{3-72}$$

3.2.3 DFIG controller model

The output of the DFIG is controlled by adjusting the rotor voltage via the rotor-side converter. Controlling the rotor voltage allows controlling the direction and magnitude of the rotor flux, so that the stator and rotor flux are oriented to produce the desired real and reactive power. As explained in Section 3.2.1, the reason for modelling the DFIG in the dq frame is for the purpose of control. The rotor voltage is divided into two components and aligned along two rotating axes. By decoupling these two rotor voltage vectors, the real power and reactive power of DFIG are controlled independently. This control scheme is referred to as vector control or current-mode control, which has been described in many publications.[54, 61, 63, 64].

There are two major types of vector control scheme for DFIG, namely stator flux oriented (SFO) control and stator voltage oriented (SVO) control. Both of them are able to provide real and reactive power control for DFIG. Aligning the reference frame along the stator flux is a more straightforward method as the angle between

stator flux and rotor voltage and the magnitude of the rotor voltage determines the output of DFIG. However, the following problems exist in this control scheme:

- The monitoring of the stator flux is affected by magnetic saturation. There will be a small difference between measured value and real value. Also, the stator flux cannot be directly measured. The stator flux is calculated from stator or rotor current [65]. The calculation requires accurate estimation of DFIG parameters such as stator resistance, reactance, mutual reactance and the measurement of rotor speed. All these parameter values add error to the magnitude and angle of the measured stator flux.

- Due to the existence of rotor resistance, the stator voltage is not strictly perpendicular to the stator flux. Although the biased angle is small, there will still be little coupling between d and q axis stator voltage. Therefore the decoupled control of real and reactive power cannot be realized.

- The rotor current on the d axis, which is set for reactive power control affects the stability of the generator system [66, 67]. The ability of the DFIG reactive power control is limited.

Considering the disadvantage of stator flux oriented control, an improved control scheme for DFIG is adopted which is stator voltage oriented control.

3.2.3.1 Rotor current control loop

In the stator voltage oriented dq reference frame, the q axis is aligned with the stator voltage vector. The stator voltage equations in the dq reference frame is

$$U_{sd} = 0 \tag{3-73}$$

$$U_{sq} = U_g \tag{3-74}$$

where U_{sd} and U_{sq} are the stator voltage d and q components, U_g is the amplitude of the grid voltage.

Ignoring the rotor resistance, the relationship between stator flux and voltage can be derived as follow:

$$U_s = \frac{d}{dt}\psi_s \tag{3-75}$$

Therefore the DFIG voltage equation in the new reference frame can be written as

$$0 = R_s I_{sd} - \omega_s \psi_{sq} + \frac{d}{dt}\psi_{sd} \tag{3-76}$$

$$U_{sq} = R_s I_{sq} + \omega_s \psi_{sd} \tag{3-77}$$

$$U_{rd} = R_r I_{rd} - s\psi_{rq} + \frac{d}{dt}\psi_{rd} \tag{3-78}$$

$$U_{rq} = R_r I_{rq} + s\psi_{rd} + \frac{d}{dt}\psi_{rq} \tag{3-79}$$

From the stator flux equations, the DFIG stator current can be derived:

$$I_{sq} = \frac{1}{L_s}\psi_{sq} - \frac{L_m}{L_s} I_{rq} \tag{3-80}$$

$$I_{sd} = \frac{1}{L_s}\psi_{sd} - \frac{L_m}{L_s} I_{rd} \tag{3-81}$$

Substituting (3-80) and (3-81) into DFIG rotor flux equations, the DFIG rotor flux in the dq reference frame is

$$\psi_{rq} = (L_r - \frac{L_m^2}{L_s})I_{rq} + \frac{L_m}{L_s}\psi_{sq} \tag{3-82}$$

$$\psi_{rd} = (L_r - \frac{L_m^2}{L_s})I_{rd} + \frac{L_m}{L_s}\psi_{sd} \tag{3-83}$$

With rotor flux equations given, the rotor voltage equations can be derived in terms of the rotor current as:

$$U_{rd} = \left(R_r + \frac{L_m^2}{L_s^2}R_s\right)I_{rd} - s\omega_s\left[\left(L_r - \frac{L_m^2}{L_s}\right)I_{qr}\right] + \left(L_r - \frac{L_m^2}{L_s}\right)\frac{d}{dt}I_{rd} - \frac{L_m R_s}{\omega_s L_s^2}\psi_{sd} \tag{3-84}$$

$$U_{rq} = \left(R_r + \frac{L_m^2}{L_s^2}R_s\right)I_{rq} + s\omega_s\left[\left(L_r - \frac{L_m^2}{L_s}\right)I_{rd}\right] + \left(L_r - \frac{L_m^2}{L_s}\right)\frac{d}{dt}I_{rq} - \frac{L_m R_s}{L_s^2}\psi_{sd} + \frac{L_m}{\omega_s L_s}\psi_{sq} \tag{3-85}$$

For big DFIG wind turbines, the stator resistance is small compared to the inductance and hence can be neglected [54]. Given that $\psi_{sq} \approx V_{sq}$, the rotor voltage equation for DFIG controller design can be shown as below,

$$U_{rd} = R_r I_{rd} - s\omega_s\left[\left(L_r - \frac{L_m^2}{L_s}\right)I_{qr}\right] + \left(L_r - \frac{L_m^2}{L_s}\right)\frac{d}{dt}I_{rd} \tag{3-86}$$

$$U_{rq} = R_r I_{rq} + s\omega_s\left[\left(L_r - \frac{L_m^2}{L_s}\right)I_{dr} + \frac{L_m V_s}{\omega_s L_s}\right] + \left(L_r - \frac{L_m^2}{L_s}\right)\frac{d}{dt}I_{rq} \tag{3-87}$$

It is noticed in equation (3-86) and (3-87) that the d and q axis voltage and current are not fully decoupled. The coupling components significantly increase the settling time of the controller. Feed-forward control is applied to decouple the d and q axis by eliminating coupling terms as shown in Figure 3-25. By applying the feed-forward control, the d and q axis rotor currents are directly controlled by the corresponding rotor voltage.

Using a PI controller to control the rotor current, the controller equations are

$$U_{rq\_ref} = (K_p + \frac{K_i}{s})(I_{rq\_ref} - I_{rq}) - U_{q\_comp} \tag{3-88}$$

$$U_{rd\_ref} = (K_p + \frac{K_i}{s})(I_{rd\_ref} - I_{rd}) - U_{d\_comp} \tag{3-89}$$

3.2.3.2 Torque control loop

The q-axis rotor current is adopted to regulate the torque of DFIG. Equation (3-62) is expressed in the stator voltage flux oriented frames as,

$$T_e = \frac{L_m U_{qs}}{L_s} I_{qr} \tag{3-90}$$

The wind turbine controller produces torque demand reference signal. Using (3-90) the rotor current reference of DFIG is calculated from the torque demand of the wind turbine.

$$I_{qr\_ref} = \frac{L_s}{L_m U_s} T_{ref} \tag{3-91}$$

The I_{qr_ref} is used as the reference signal of the DFIG torque control loop.

3.2.3.3 Reactive power control loop

Although wind turbine only requires active power control, the d-axis rotor current can be used to provide reactive power control for grid support. The reactive power produced by the DFIG is expressed as

$$Q = \frac{L_m U_s}{L_s} I_{dr} - \frac{U_s^2}{L_s} \tag{3-92}$$

where the term $\frac{U_s^2}{L_s}$ is the reactive power for the machine magnetization. Therefore I_{dr} is divided into two components, one to cancel the magnetization current and one for reactive power output control. The component for magnetization compensation is calculated as

$$I_{dr\_comp} = \frac{U_s}{L_s} \tag{3-93}$$

3.2.3.4 Simulation

The complete DFIG vector controller scheme is shown in Figure 3-25.

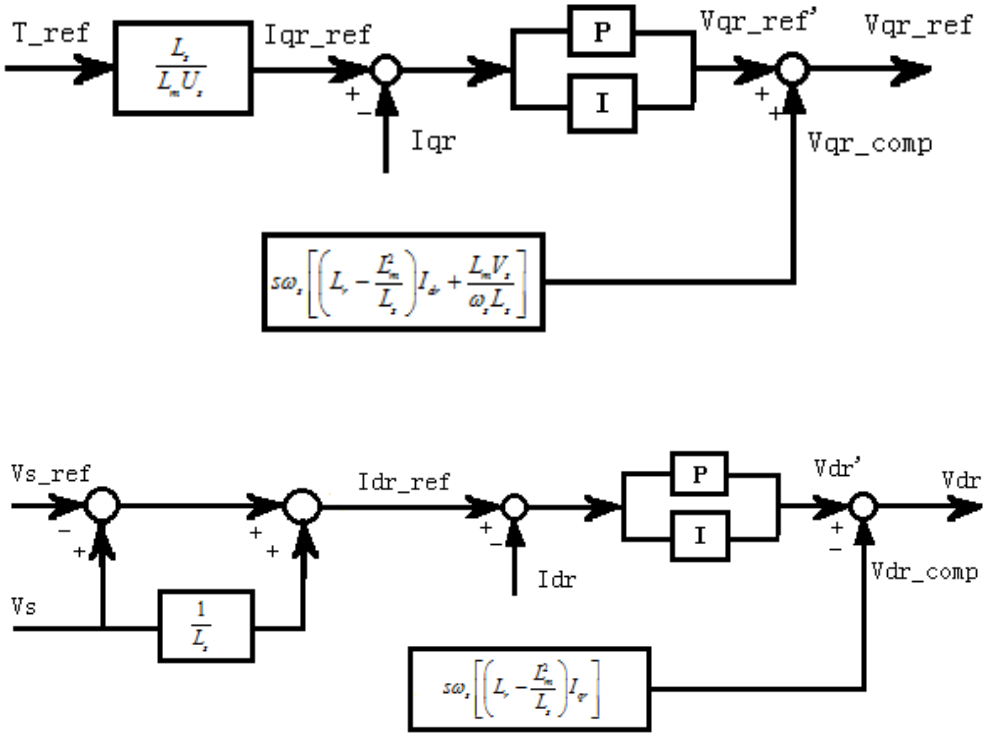

Figure 3-25: DFIG controller scheme

The DFIG model and control is implemented in Matlab/Simulink®. The simulation results of the step response of the system are shown in Figure 3-26. The transients of the electrical torque, stator and rotor current are observed and discussed. The controller performance between simple PI controller and PI controller with feed-forward compensation are compared in Figure 3-27.

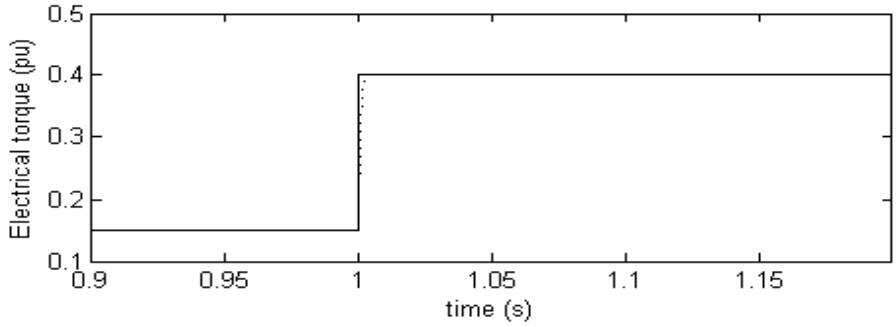

(a)

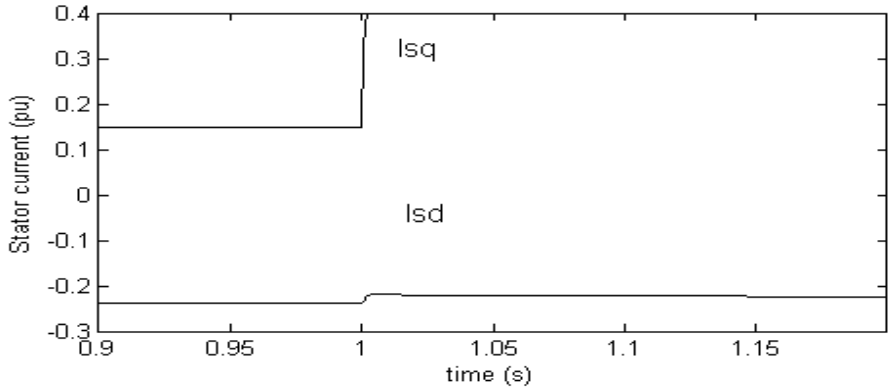

(b)

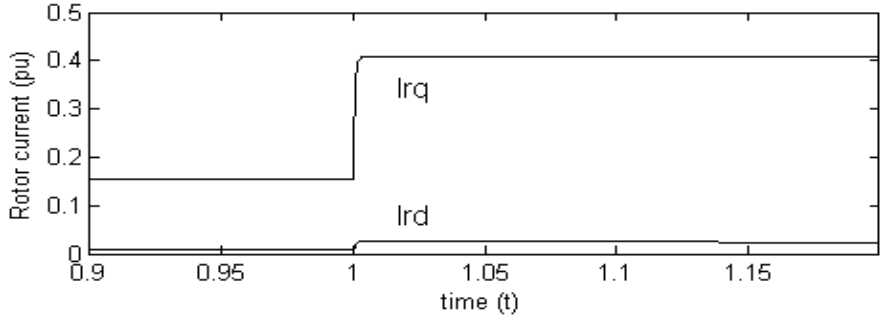

(c)

Figure 3-26: DFIG response to step input (a) Electrical torque. (b) Stator current. (c) Rotor current.

Solid line: Torque reference. Dashed line: Output torque.

The controller shows fast and accurate response to changes in the reference signal. It should be noticed that the rotor current reference signal is calculated based on machine parameters. In practice, there will be an error in the estimation of machine parameters.

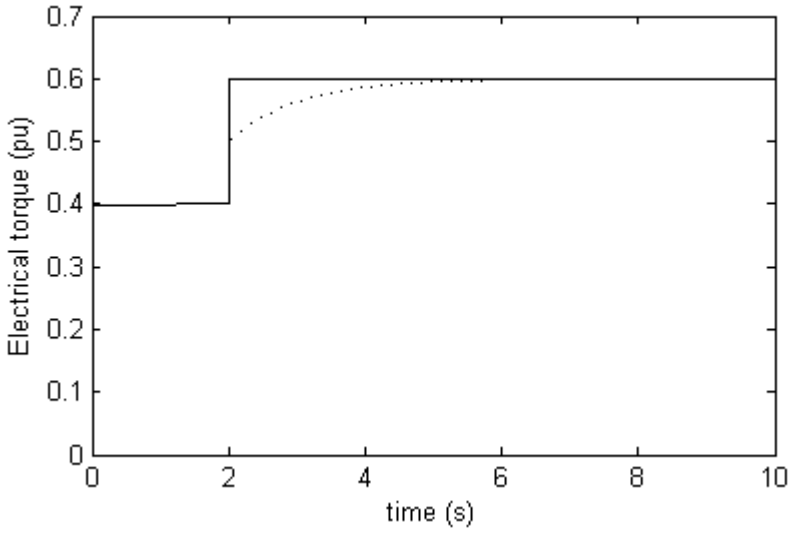

Figure 3-27: DFIG control with and without feed-forward control.
Solid line: DFIG control with feed-forward compensation
Dashed line: DFIG control without feed-forward compensation

Figure 3-27 shows the start-up of DFIG with and without the feed-forward compensation loop. The feed-forward control successfully reduced the settling time of the DFIG. With the compensation loop, the DFIG starts with reference rotor voltage and the controller only regulates torque ripples. The torque control loop is decoupled from the voltage control loop so the high start-up d-axis current variation for reactive power regulation does not affect the torque controller performance.

3.3 Power system modelling

In many publications on the integration of DFIG type wind turbine into power systems, the grid is normally modelled as an infinite bus [68, 69] or super grid [70].

With the increasing penetration level of wind energy, using a simplified grid model causes more misleading conclusions on wind farm dynamic performance analysis and may obscure significant dynamic characteristics [71]. The influence of power system components such as sources and the transmission network on wind turbine cannot be simply neglected in the wind farm compatibility study. Detailed modelling of grid components is needed for dynamic study of the interaction between wind turbine and power system.

3.3.1 Synchronous generator model

Conventional power plants adopt synchronous generator to produce power. The mathematical model of a 3rd order synchronous generator is given below [62]. To accommodate to the DFIG model, which is built in the dq reference frame, the synchronous generator model is transformed into dq reference frame too.

Considering a symmetrical three-phase synchronous generator with stator winding Y-connected, the stator voltage equations are:

$$E_A = \frac{d\psi_A}{dt} - R_S I_A \tag{3-94}$$

$$E_B = \frac{d\psi_B}{dt} - R_S I_B \tag{3-95}$$

$$E_C = \frac{d\psi_C}{dt} - R_S I_C \tag{3-96}$$

where E_A, E_B and E_C are the voltages of corresponding phases, I_A, I_B and I_C are the currents of corresponding phases, Ψ_A, Ψ_B and Ψ_C are the components of the stator flux on the three phases. R_S is the stator phase resistance.

Using the dq transformation the stator equations can be written as:

$$E_d = \frac{d\psi_d}{dt} - \omega_s \psi_q - R_a I_d \tag{3-97}$$

$$E_q = \frac{d\psi_q}{dt} + \omega_s \psi_d - R_a I_q \tag{3-98}$$

Where E_d and E_q are stator voltage on the d and q axes, Ψ_d and Ψ_q are d and q stator fluxes, R_a is the stator resistance in dq frame, I_d and I_q are the stator current components on the d and q axes.

The flux equations of the synchronous generator are given as

$$\psi_d = L_f I_f - L_d I_d + L_D I_D \tag{3-99}$$

$$\psi_q = -L_q I_q + L_Q I_Q \tag{3-100}$$

where L_d and L_q are the stator inductances in the d and q axes, L_f, L_D and L_Q are the mutual inductances between stator and excitation windings, d axis and q axis. I_D and I_Q are the induced currents in d and q axes.

In steady state, the stator voltage, current and flux are constant so the derivative terms in (3-97) and (3-98) are zero. Since the flux is constant, the induced current also equals to zero. The synchronous machine voltage and flux equations are simplified as

$$E_d = -\omega_s \psi_q - R_a I_d \tag{3-101}$$

$$E_q = \omega_s \psi_d - R_a I_q \tag{3-102}$$

$$\psi_d = L_f I_f - L_d I_d \tag{3-103}$$

$$\psi_q = -L_q I_q \tag{3-104}$$

Substituting (3-103) and (3-104) into (3-101) and (3-102) we get

$$E_d = L_q I_q - R_a I_d \tag{3-105}$$

$$E_q = L_f I_f - L_d I_d - R_a I_q \tag{3-106}$$

Equations (3-105) and (3-106) are used to represent the relationship between voltage and current of the synchronous generator in the d and q axes.

3.3.2 Excitation system

To accurately simulate the behaviour of synchronous generator during grid faults, the excitation system of synchronous generator has to be modelled in detail. The excitation system is in charge of controlling and producing the excitation current which determines the active and reactive power of the generator.

The excitation current for synchronous generator operation is provided to the generator field winding. The basic function of the excitation current is to generate the electromagnetic field for the operation of the synchronous generator. The excitation system can be controlled to improve the contribution of synchronous generators to power system stability by incorporating an auxiliary loop like a power system stabilizer (PSS) or an automatic voltage regulator (AVR) [62].

A functional block diagram of the excitation system employed in this thesis is shown in Figure 3-28. These include the exciter, stabiliser (PSS) and regulator.

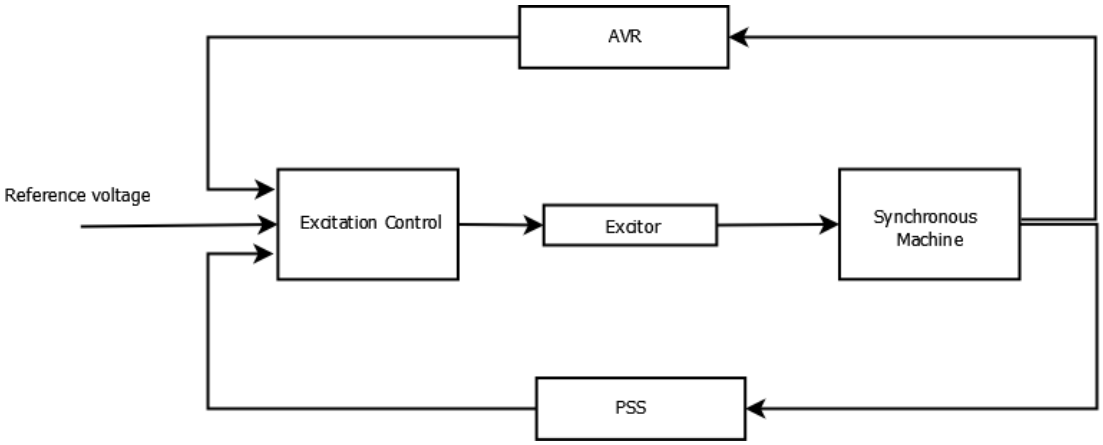

Figure 3-28: Block diagram of synchronous generator excitation system

3.3.2.1 Excitation control system

There are many forms that a generator excitation system can take. The excitation system can be categorized as:

- DC excitation system
- AC excitation system
- Static excitation system

based on the sources used to drive the system or:

- Stationary excitation system
- Rotating excitation system

depending on the rectifier arrangement.

The AC4A type excitation system model [64, 72] is employed as the excitation system for the synchronous generator model. The block diagram of the AC4A excitation system is shown in Figure 3-29. The major aim of this type of excitation

system is regulating the terminal voltage of the machine to which it is attached. The AC4A excitation system provides high gain and fast response AVR function. The frequency domain analysis is adopted when designing such excitation system. A lead-lag compensation block is designed so that the internal excitation voltage of the generator response to the terminal voltage error of certain frequency. The thyristor is modelled by a gain with time delay.

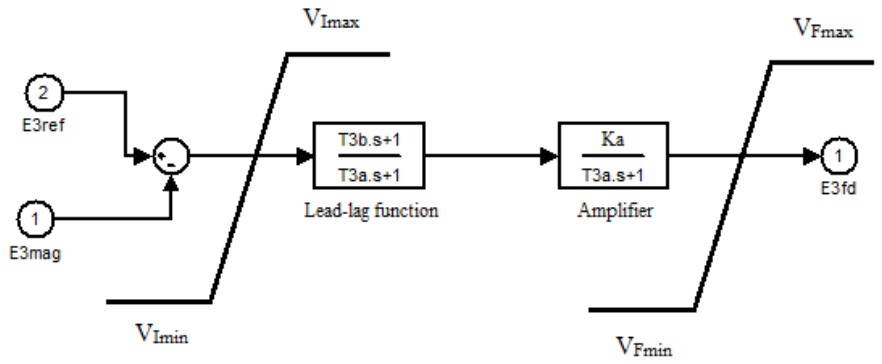

Figure 3-29: IEEE type AC4A excitation system model

The voltage regulation performance of the modelled excitation system is illustrated in Figure 3-30. A network disturbance occurs at time=30 seconds resulting in a voltage surge. Figure 3-31 shows that the excitation system generates an inverse current against the voltage variation and successfully damps out the voltage change in 3 seconds.

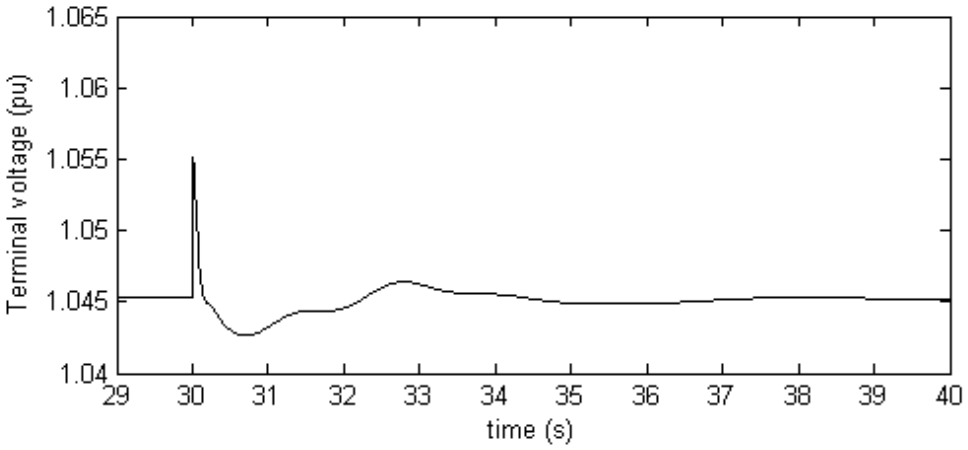

Figure 3-30: Stator voltage of synchronous generator.

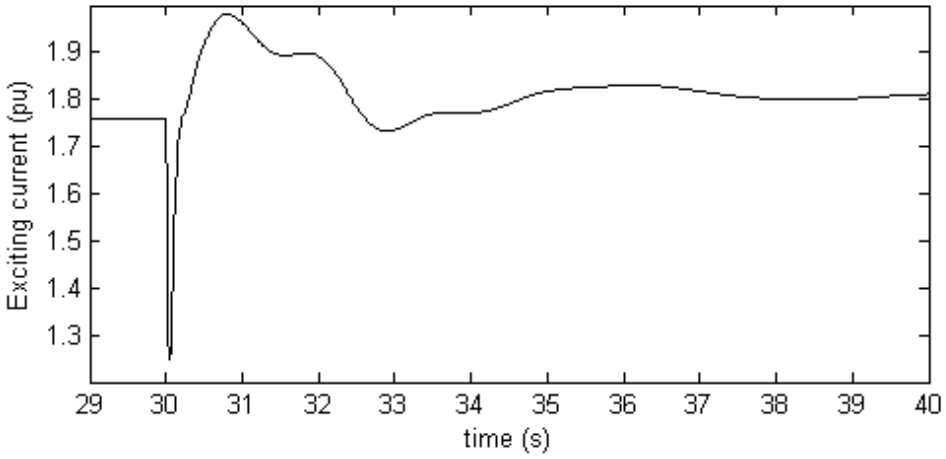

Figure 3-31: excitation current during network disturbance.

3.3.2.2 Power system stabilizer model

As the classic mechanism to improve the dynamic performance of a power system, a PSS is included in the model to accurately simulate the power system behaviour during a disturbance. A PSS adds an auxiliary control signal to the excitation system to increase the damping provided by the synchronous generator (hence enhancing system stability). Typical reference signals that can be used as input for a PSS are

shaft speed, terminal frequency and power. The PSS modelled here is an IEEE type PSS1A power system stabiliser model. The diagram of the PSS model is illustrated in Figure 3-32. The PSS representation consists of the transducer model, signal washout block, and a series-connected lead-lag phase compensation section. By adjusting the phase difference of the exciter and generator system, the PSS allows the generation of a torque component that is in phase with the of rotor speed oscillations so that they can be effectively damped.

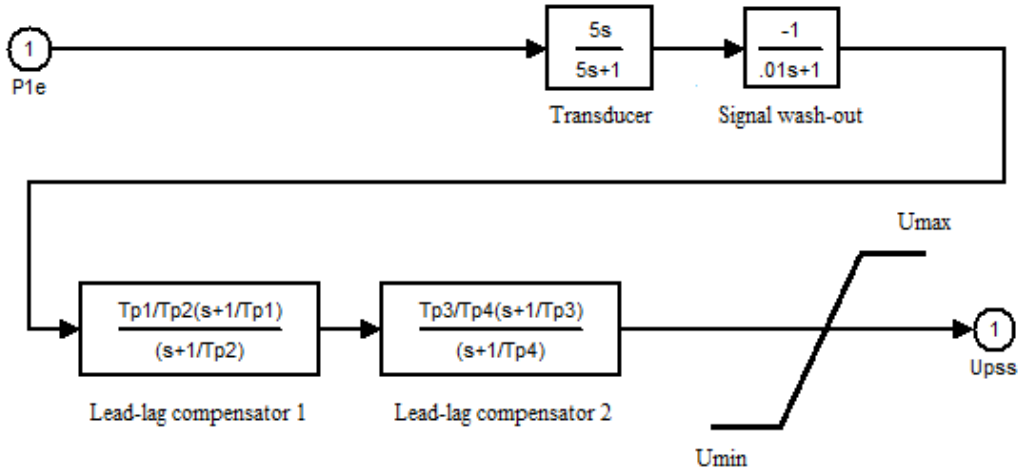

Figure 3-32: PSS model block diagram

The PSS is tested in a case study where a remote grid fault happens and causes a sudden increase of the synchronous generator terminal power. The PSS produces an auxiliary control signal in phase with the power oscillation to suppress the power oscillation hence maintaining the power output and system frequency as shown in Figure 3-34.

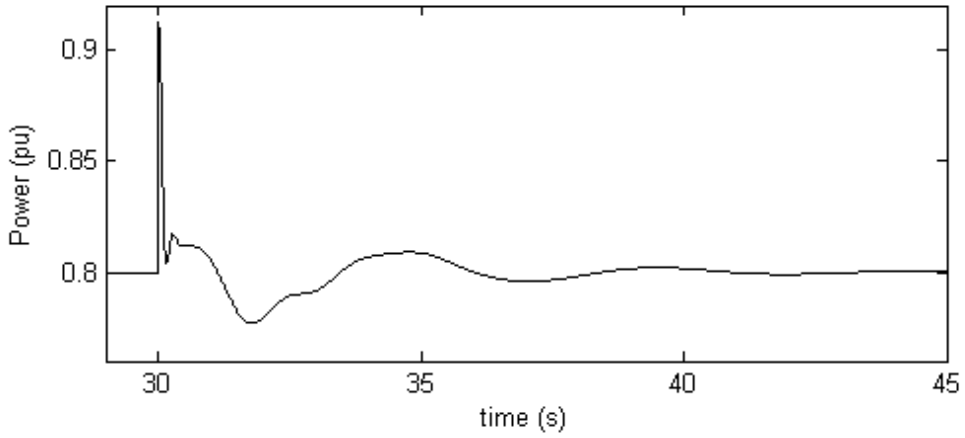

Figure 3-33: Power output of synchronous generator

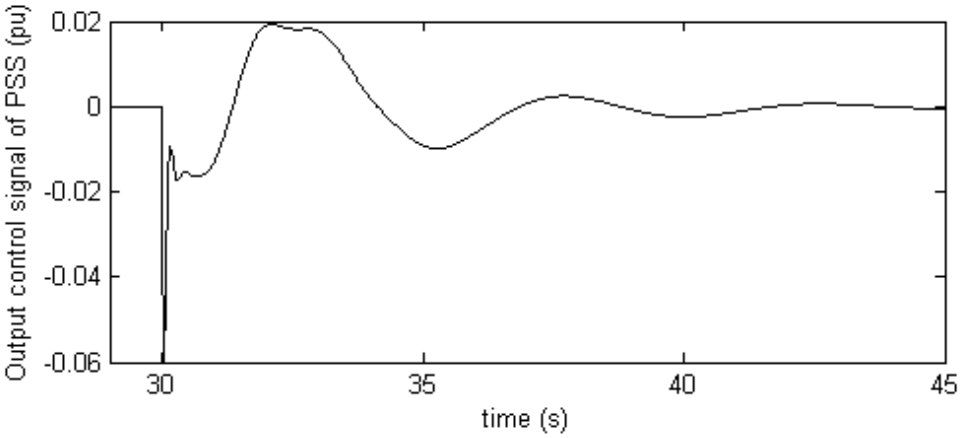

Figure 3-34: output signal of the PSS

3.3.3 Grid model

Many publications on the DFIG system are based on the assumption that the stator voltage of the DFIG is constant. The assumption can be understood as the DFIG being connected to an infinite bus. However, with the increase in wind power penetration, the grid model needs to be sufficiently detailed to represent the influence of wind power on network dynamics as accurate as possible.

Most wind farms are located far from customers and loads, e.g. offshore wind farms. Therefore, wind farms require long-distance transmission line and large-scale transformers for wind power transmission. The output voltage of wind turbine is first boosted at the site and transmitted through long transmission cables. This section presents the mathematical model of transmission line and transformer. Following the model of components, the generic grid model used in this thesis to represent the dynamic response of power system is given.

3.3.3.1 Transmission line model

Power is transmitted via transmission lines in the form of electromagnetic waves. When the size of an electrical device is much smaller compared to the wavelength of the electromagnetic wave it carries, the device can be considered as a lumped component [29]. The parameters such as reactance and resistance can be considered as evenly distributed on the components. In case of transmission line, when the length is less than 250km, the lumped parameter approach can be applied [73]. The conceptual plot of transmission line with lumped parameters is shown in Figure 3-35.

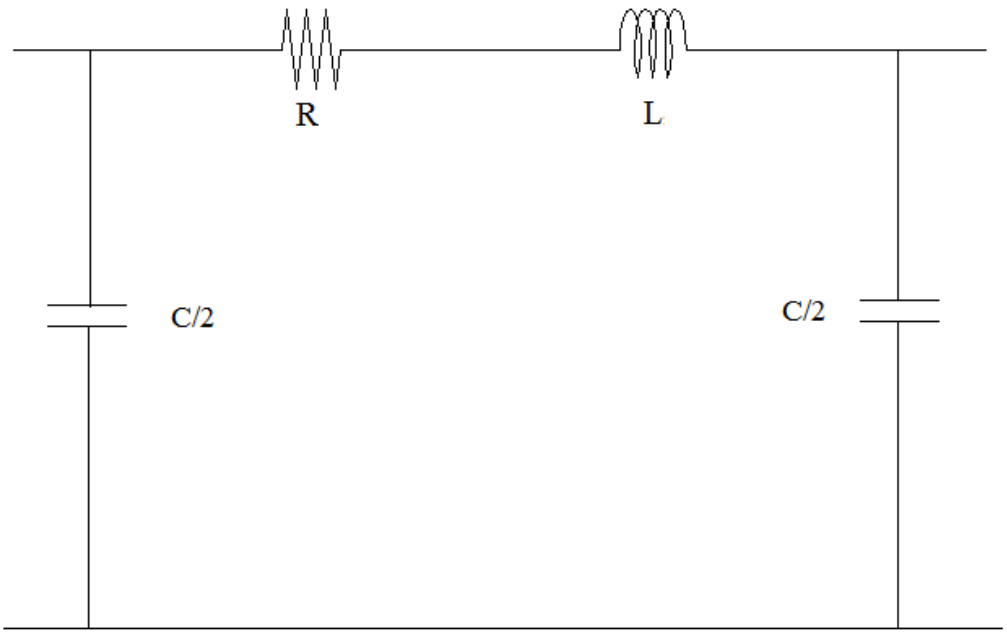

Figure 3-35: Transmission line with lumped parameters

R represents the total resistance of the transmission line. As the current flows through the transmission line, the induced magnetic field causes the voltage to drop which is represented by the inductance L. The leakage inductance between transmission lines is represented by C.

Applying Kirchhoff's voltage law (KVL) to the circuit shown in Figure 3-35 and transforming into the dq reference frame leads to the voltage equation:

$$U_d = RI_d + L\frac{d}{dt}I_d - \omega LI_q \tag{3-107}$$

$$U_q = RI_q + L\frac{d}{dt}I_q + \omega LI_d \tag{3-108}$$

where ΔU_d and ΔU_q are the d and q axis voltage across the line. I_d and I_q are the line current.

Similarly, applying Kirchhoff's current law (KCL) and we can get

$$I_{dc} = C\frac{d}{dt}V_d - \omega C V_q \tag{3-109}$$

$$I_{qc} = C\frac{d}{dt}V_q + \omega C V_d \tag{3-110}$$

where I_{dc} and I_{qc} are the dq currents across the capacitance of the transmission line.

3.3.3.2 Transformer model

The transformer is an electrical device that transfers energy between its windings. A typical equivalent circuit representation of a transformer is shown in Figure 3-36. The modelled transformer is chosen to be of the two-winding type.

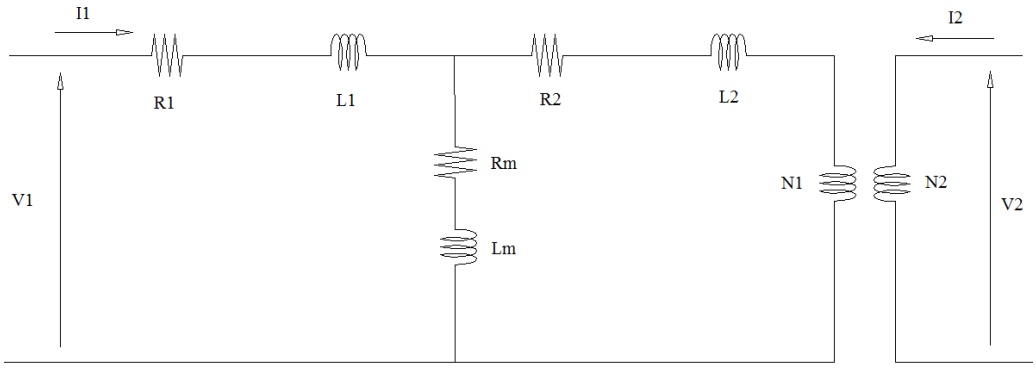

Figure 3-36: Transformer equivalent circuit model

The voltage equation is give as,

$$U_1 = R_1 i_1 + L_1 \frac{d}{dt} i_1 + R_m i_2 + L_m \frac{d}{dt} i_2 \quad (3\text{-}111)$$

$$U_2 = R_2 i_2 + L_2 \frac{d}{dt} i_2 + R_m i_1 + L_m \frac{d}{dt} i_1 \quad (3\text{-}112)$$

where U_1, R_1, L_1, I_1 are the terminal voltage, resistance, inductance and current of the primary winding; U_2, R_2, L_2, I_2 are the terminal voltage, resistance, inductance and current of the secondary winding; R_m and Lm are the mutual resistance and inductance.

As the mutual resistance and inductance are relatively small, the model can be further simplified by neglecting the coupling between primary and secondary winding. The transformer model is thus derived as

$$U_1 = R_1 i_1 + L_1 \frac{d}{dt} i_1 \quad (3\text{-}113)$$

$$U_2 = R_2 i_2 + L_2 \frac{d}{dt} i_2 \quad (3\text{-}114)$$

3.3.3.3 Multi-machine grid model

The power system model used to examine the dynamic characteristic of the grid has a similar layout as the generic network described in [71]. It is essentially a three-area power system. The diagram of the generic network model is presented in Figure 3-37.

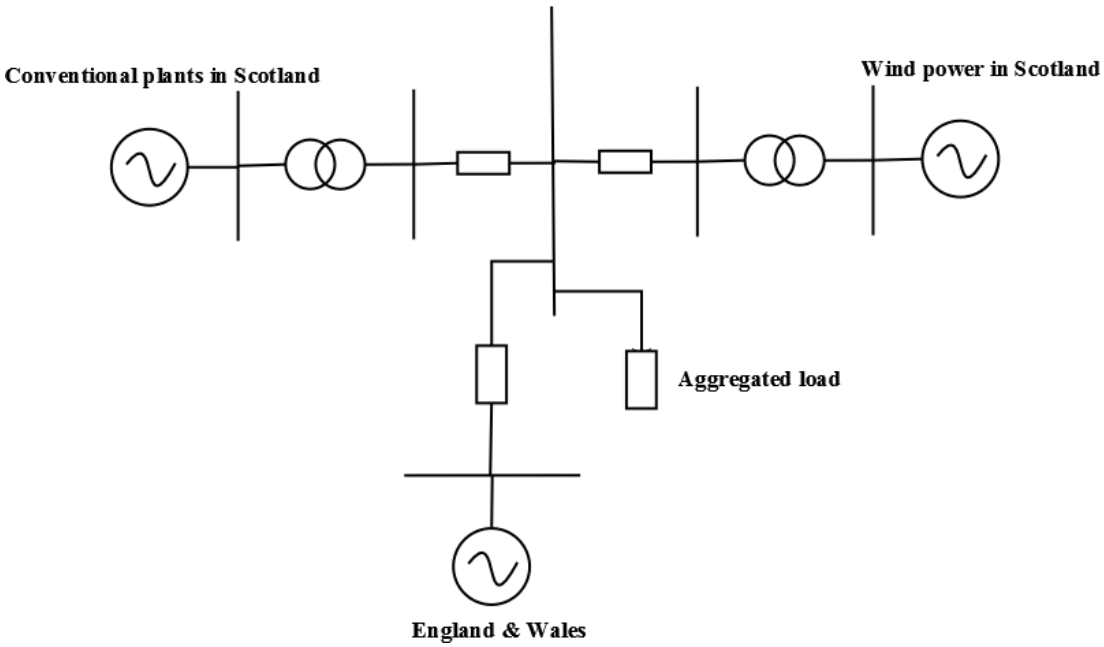

Figure 3-37: Generic network model

The network data used are collected from the GB network operator [74]. The model aims to simulate a much simplified version of the GB power system in the context of fast growth of wind power in Scotland. The England-Wales power system is modelled by a 6th order synchronous generator and associated excitation and turbine-governor controls. This area is considered to have a large capacity and to be relatively strong compared to the other areas. The conventional power stations in Scotland are aggregated and represented by a synchronous generator model with AVR and PSS control. The synchronous generator model with power system support capability is included in the model to provide a reference for the assessment of the ability of wind turbine to contribute to grid stability. The wind turbine model includes both the mechanical and the electrical subsystems. The holistic model of wind turbine adopted in this research enabled the investigation of the interaction between the generic network and wind turbine structural components.

The model is simple in form but contains sufficient detail to represent the GB power system. As the simulations in this research include a detailed model of wind turbine structural and electrical systems, the complete model is complex and the simulation speed is of great importance. The infinite bus model absorbs the current and power oscillation in the system so that the characteristic of a large power system is represented. The generator equivalent model provides a more realistic oscillatory response to the grid fault in addition to the response of the local system. This generic network model, which contains three machines, was sufficient as a first pass to represent the power system dynamics during various types of fault.

3.4 Integrated simulation platform

The wind turbine mechanical and electrical component models are implemented in Simulink as illustrated in Figure 3-38. The wind turbine dynamic model comprises the mechanical model, aerodynamic model, wind model, control model and electrical model including induction machine model and power converter model. The grid model includes synchronous generator model AVR, PSS and network models.

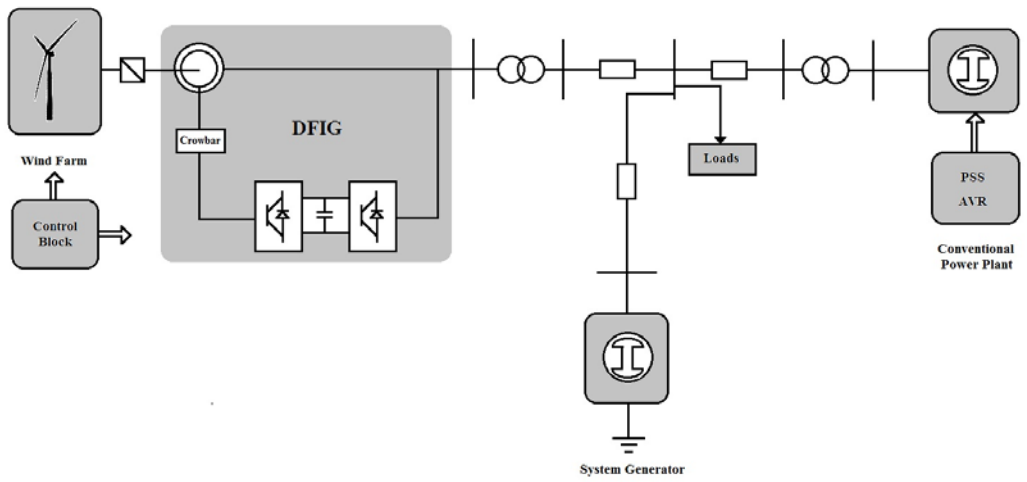

Figure 3-38: Integrated simulation platform

The integrated simulation platform enabled the analysis of the interaction between the mechanical structures of the wind turbine and the electrical network both during normal operation and during transient grid fault. The necessary study of the integration of the wind turbine into grid can be carried out using the platform. The platform can be used to identify potential issues of connecting wind turbines into grid and develop corresponding solutions thus provide valuable information and facilitate the integration of wind turbine into grid.

3.5 Summary

Detailed modelling of wind turbine and power system is required for the study of the large-scale integration of wind power into power systems. The mathematical model of the wind energy generation system was developed in this chapter. The model can be categorized as a combined mechanical model and electrical model.

In the mechanical model section, the wind speed model was described first. The aerodynamics of the wind turbine is then introduced to present the relationship between the wind speed model and the wind turbine mechanical torque. The two-mass wind turbine drive-train model was also presented.

In the electrical model section, the DFIG model and its control system used in this thesis were introduced. The relevant electrical system component model including synchronous generator model, excitation system control and grid model were developed to represent the power system.

CHAPTER 4: SYMMETRICAL FAULT RIDE-THROUGH OF DFIG-BASED WIND TURBINE

This chapter deals with the symmetrical fault ride-through problem of the wind turbine. The challenge of the fault ride-through (FRT) and the low-voltage ride-through (LVRT) issue for wind turbine is briefly explained first. The classification of various fault types is introduced. The dynamic response of the DFIG during grid faults is studied mathematically followed by the analysis of the FRT and LVRT of the DFIG. Possible solutions to these problems are given and discussed taking into account the wind turbine structural loads. A variable-rotor resistance control scheme is proposed by the author to improve the FRT ability of the DFIG while minimising the drive-train oscillations therefore reducing the loads on the wind turbine. Few other modifications on the wind turbine control system are proposed to reduce the structural loads that the wind turbine experiences during a grid fault.

4.1 Introduction

The FRT and LVRT problems of the wind turbine have drawn significant attention by wind turbine manufactures in recent years as the TSOs have been increasing the requirements on this issue. Wind turbines equipped with fully-rated converter are not heavily influenced by grid faults as the wind turbine is completely decoupled from the grid by the converter. The FRT performance mainly depends on the grid-side converter. The major application of the fully-rated converter is on wind turbine with permanent magnetic generator (PMG). The deployment of this type of wind turbine is limited by high price. The dominant wind turbine generator type is still the DFIG with partially-rated converter.

As the stator of the DFIG is directly connected to the grid, only a portion of the output of the DFIG is controlled by the converter system. During a grid fault, the

disturbance in the stator winding causes large electrical transients in the DFIG. In a serious grid fault case, the rotor winding of DFIG may experience over current and over voltage, which activates the protection system and potentially leads to the emergency shut-down of the DFIG.

In the past, the wind turbines could be disconnected from the grid during faults without influencing significantly the stability of the whole power system as the capacity of wind power was small compared to conventional generation. With more wind farms connected to the power system, the effect of the wind turbine protection system operation on the power system stability cannot be neglected. Wind turbines are required to stay connected during grid faults as conventional power stations do. Some TSOs even require wind farms to provide frequency and reactive power control to power system during grid fault.

Driven by the requirements from TSOs, there has been extensive research on the FRT and LVRT of the DFIG. To study this problem, the voltage profile during grid fault has to be presented first.

During a grid fault, the wind turbine and the DFIG experience voltage sags of different levels. Equipment with modern power electronics are especially vulnerable to voltage drops [75]. Many researches are carried out to study how different types of voltage sag affects the electrical equipment and how the fault ride-through capability of this equipment can be improved [76, 77]. A method for voltage sag characterization is given in [78]. The typical voltage sags are categorized as follows:

- Fault related sags (FRS)
- Large motor starting related sags (MSRS)
- Motor re-acceleration related sags (MRRS)

As shown in Figure 4-1:

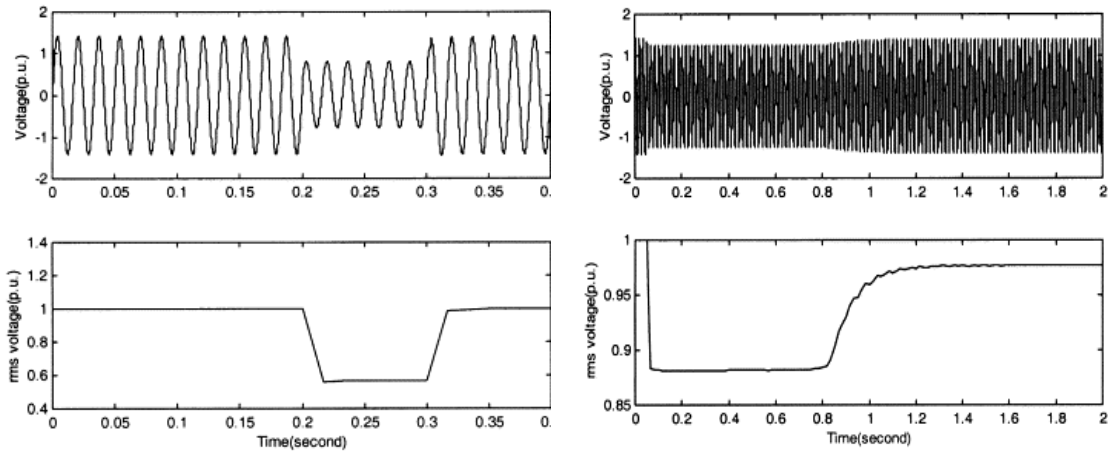

(a) (b)

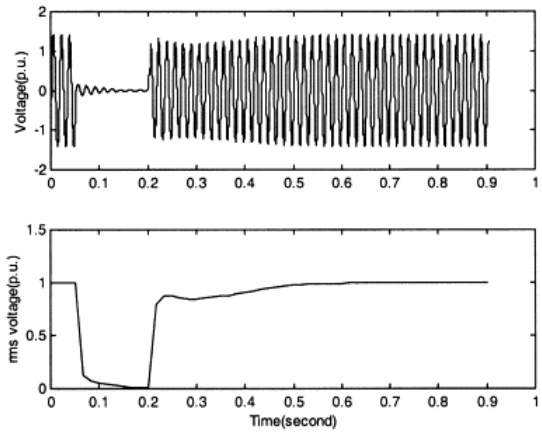

(c)

Figure 4-1: Voltage sag classification [78]. (a) Fault related sags (FRS) (b) Large motor starting related sags (MSRS) (c) Motor re-acceleration related sags (MRRS)

It is observed in Figure 4-1(b) that MSRS results in fast initial voltage drop and slow voltage recovery. The MRRS has long voltage drop and recovery period as the motor acts as a damper during its reacceleration. Figure 4-1(a) shows that FRS normally

lasts for a shorter time than other types of fault. Moreover, FRS could come up with the unbalance between three-phase voltages due to asymmetrical faults.

4.2 Dynamics of DFIG during symmetrical fault

This section presents the analysis of the dynamics of the DFIG under a symmetrical grid fault condition. An equivalent circuit analysis approach is adopted to investigate the relationship between DFIG parameters and grid fault behaviour. It is calculated in Chapter 3 that the DFIG flux and voltage equations in αβ reference frame are

$$\psi_{s\alpha\beta} = L_s I_{s\alpha\beta} + L_m I_{r\alpha\beta} \tag{4-1}$$

$$\psi_{r\alpha\beta} = L_r I_{s\alpha\beta} + L_m I_{s\alpha\beta} \tag{4-2}$$

$$U_{s\alpha\beta} = R_s I_{s\alpha\beta} + \frac{d}{dt}\psi_{s\alpha\beta} \tag{4-3}$$

$$U_{r\alpha\beta} = R_r I_{r\alpha\beta} + \frac{d}{dt}\psi_{r\alpha\beta} - j\omega_r \psi_{r\alpha\beta} \tag{4-4}$$

It can be derived from (4-2) that

$$L_{r\alpha\beta} = \frac{1}{L_r}\psi_{r\alpha\beta} - \frac{L_m}{L_r} I_{s\alpha\beta} \tag{4-5}$$

Substituting (4-5) into (4-1)

$$\psi_{s\alpha\beta} = \psi_{r\alpha\beta} - L_r I_{r\alpha\beta} + L_s I_{s\alpha\beta} \tag{4-6}$$

Combining (4-3) and (4-6) gives

$$U_{s\alpha\beta} = R_s I_{s\alpha\beta} + L_s \frac{d}{dt} I_{s\alpha\beta} + \frac{d}{dt}\psi_{r\alpha\beta} - L_r \frac{d}{dt} I_{r\alpha\beta} \tag{4-7}$$

Using a similar method, the rotor voltage equation is calculated as

$$U_{r\alpha\beta} = R_r I_{r\alpha\beta} + L_r \frac{d}{dt} I_{r\alpha\beta} + \frac{d}{dt}\psi_{s\alpha\beta} - L_s \frac{d}{dt} I_{s\alpha\beta} \tag{4-8}$$

Based on (4-7) and (4-8), the equivalent circuit of the DFIG stator and rotor circuit can be drawn as

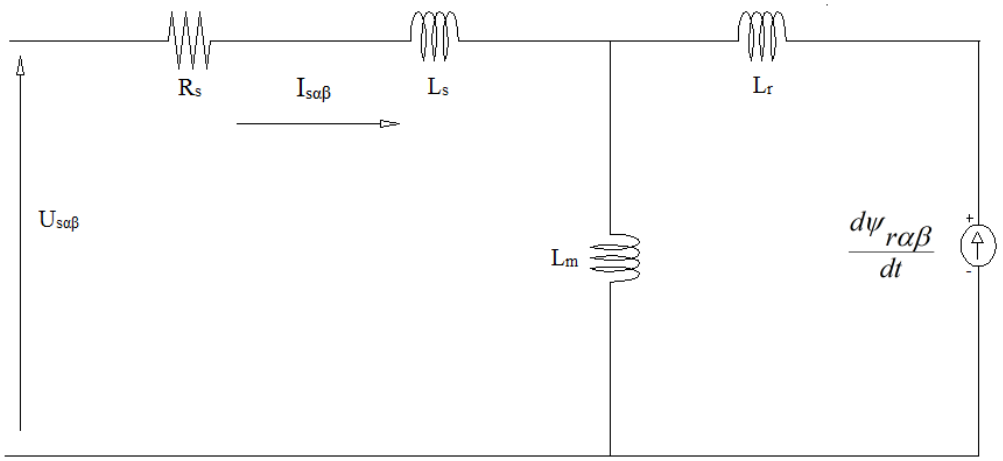

Figure 4-2: Equivalent circuit of DFIG stator winding

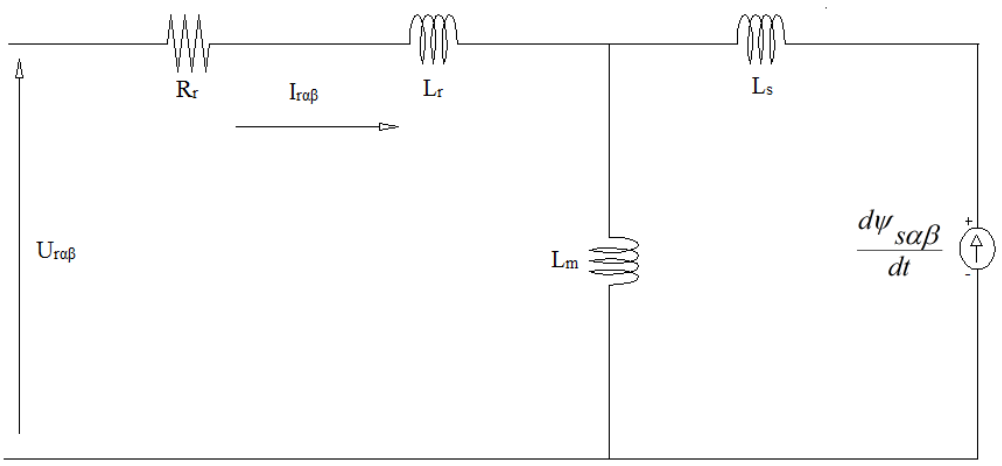

Figure 4-3: Equivalent circuit of DFIG rotor winding

In Figure 4-2, it can be observed that the stator current is affected by two factors, namely stator voltage and rotor flux. The stator current can hence be divided into a stator voltage induced component and a rotor voltage induced component. During a grid fault, the rotor converter is normally disconnected from the rotor winding. The rotor voltage can be assumed to be zero during the steady-state analysis of the FRT. Meanwhile, the stator winding is subjected to a large voltage drop so the rotor voltage induced current is much smaller than the current variation caused by stator voltage sag. The DFIG equivalent circuit can be further simplified by neglecting the coupling between the stator and rotor winding. The simplified equivalent circuit is illustrated in Figure 4-4.

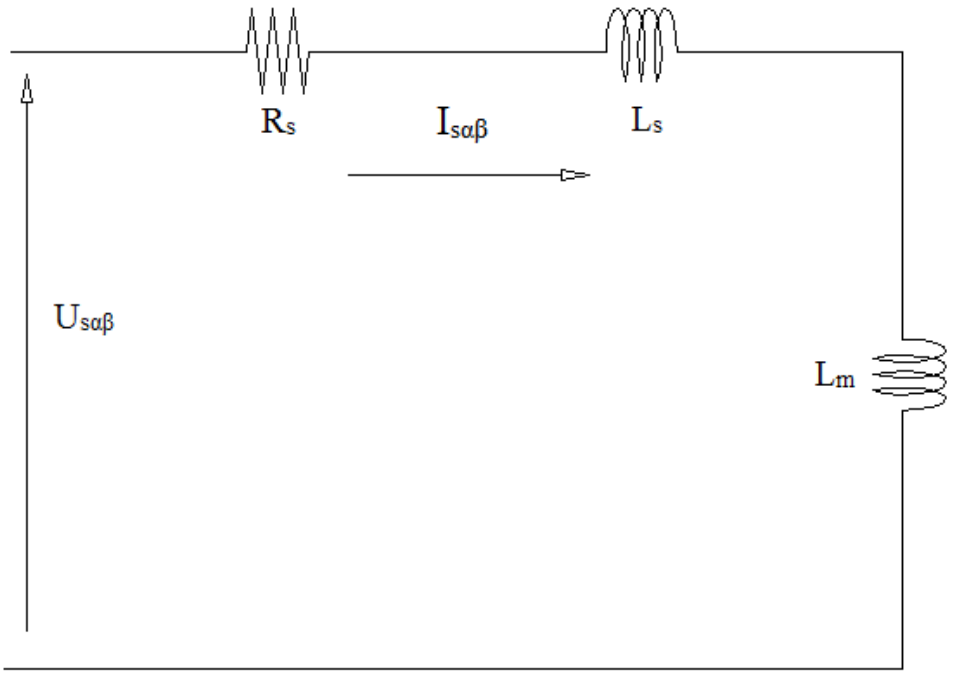

Figure 4-4: DFIG stator equivalent circuit neglecting rotor voltage transients

The DFIG stator winding is approximated by a first-order series RL circuit. From basic circuit theory it can be concluded that the time constant of DFIG stator is $\frac{L_s}{R_s}$. The same result is obtained using time-domain analysis in [79]. When a step input is applied on the RL circuit, a DC component with the attenuating time constant of $\frac{L_s}{R_s}$ can be predicted.

The DFIG rotor circuit is disconnected from the converter therefore no control can be applied and the rotor voltage is zero. The equivalent rotor circuit diagram can be redrawn as shown in Figure 4-5.

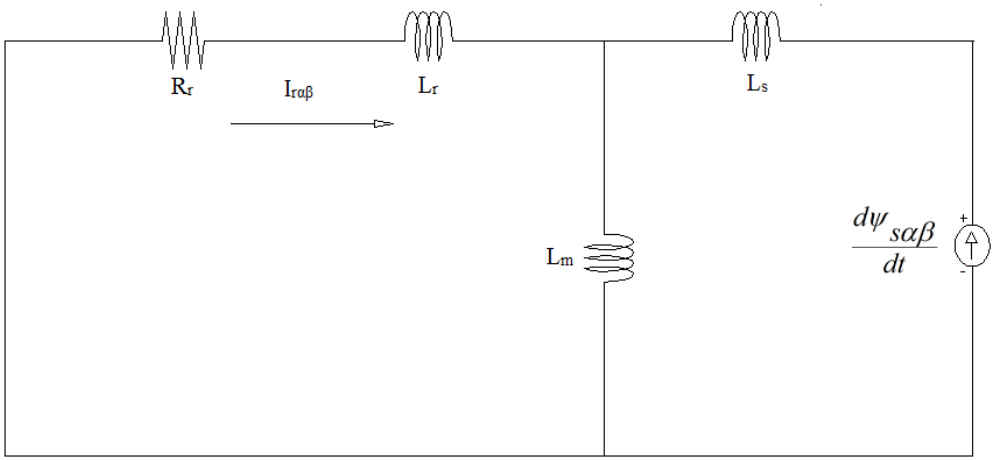

Figure 4-5: Rotor circuit with zero rotor voltage

Defining the stator current time constant $\tau_s = \frac{L_s}{R_s}$, the induced stator flux also contains a component with time constant τ_s. As the rotor circuit is short circuited during fault, the stator flux becomes the only source of the rotor current variation. The impedance of the DFIG rotor circuit during the grid fault can be calculated from Figure 4-5 as

$$Z_r = \frac{s^2(L_s L_r - L_m^2) + sR_r L_s}{sL_s + R_r} \tag{4-9}$$

The rotor circuit resistance is relatively small without a protection system such as crowbar. Equation (4-9) can be approximated as

$$Z_r = \frac{s(L_s L_r - L_m^2)}{L_s} + R_r \tag{4-10}$$

The time constant of the rotor circuit is hence derived as

$$\tau_r = \frac{(L_s L_r - L_m^2)}{L_s R_r} \tag{4-11}$$

Equation (4-11) shows the relationship between the transient current that grid fault causes and DFIG parameters. The circuit analysis implies the possibility of manipulating DFIG parameters to increase the temporary damping of the DFIG during grid fault.

4.3 Technology review of the FRT strategy of the DFIG

During grid faults, the DFIG is subjected to a terminal voltage dip. According to previous research, the voltage dip induces large transient rotor voltage and rotor current. The transient over voltage and over current can lead to the activation of the protection system of power electronic devices. The control of DFIG is thus lost during the fault. The loading and rotating speed of DFIG also influences the FRT capability of the wind turbine. The operating speed of DFIG is larger under high wind speeds. The torque that the wind turbine drive-train experiences is also larger. If the DFIG is not able to ride-through the fault and thus cut off by the protection system, the wind turbine rotational speed will increase rapidly and lead to the extra load on the drive-train system and over speed of wind turbine. Not only during a fault, but also the post-fault operation of the wind turbine may be prevented by the failure of DFIG fault ride-through. The FRT of DFIG is a crucial problem limiting the large-scale integration of the wind turbine.

There has been considerable research on the FRT of the DFIG-based wind turbines in recent years. The solutions to this problem can be divided into three categories

i. Modification of conventional controller
ii. Active crowbar control

iii. The application of dynamic braking resistors

To realize the wind turbine FRT by means of modified controller design has been reported in many publications [9, 80-82],[83]. A rotor current controller is proposed in [80]. A second-order band pass filter is employed to reduce the rotor current oscillation. A similar result is achieved in [82] by using a feed-forward controller. A method to calculate the rotor current reference in the time domain to improve the damping during a symmetrical fault is given in [81]. However, the implementation of the controller is not given and detailed discussion on results is missing. A vector-based controller is proposed to operate during grid faults to increase the damping of the DFIG in [83]. A common problem for the above methods is they all require stator flux estimation for the controller to generate the correct reference signal. Some require flux decomposition during the grid fault. The flux estimation is based on machine parameters and the procedure introduces considerable time delay. Also, the modified controller only takes care of the oscillating fault current in DFIG rotor circuit. The protection system of the DFIG still activates under deep voltage sags. The modified controller approach is only suitable for low-voltage sags level conditions.

The use of the active crowbar or similar technology can be widely observed in publications [40, 70, 84, 85]. An active crowbar system switching strategy is introduced in [84] to help the DFIG to ride-through faults by limiting the rotor voltage. A crowbar system which monitors both the rotor winding and the dc-link is explained in [40] but detailed analysis is missing. References [85] and [70] present the application of a dynamic resistor in the rotor and stator circuit of the DFIG. However, the value of the resistor is fixed so the effect of the protection is not controllable. An active crowbar is proved to be capable of successfully reducing the rotor over-current during grid fault. The damping of the DFIG can be significantly

improved by the introduced resistor. However, the fixed value resistor limits the controllability of the crowbar system.

The inclusion of the crowbar with variable resistance or the DFIG with variable rotor resistance is investigated and reported in publications [59, 86-88]. The concept of the wind turbine generator with variable rotor resistance has been commercialized by Vestas. Some variable-speed wind turbine models produced by Vestas such as the V80 are with variable rotor resistance control which is referred to as the Opti-slip technique. There is no detailed literature on how the control system is designed. It is briefly explained in [59] that a simple PI controller is employed to control the rotor resistance value. The simulation result shows that the reaction torque of the induction generator can be regulated to follow the reference value using a PI control. However, the speed of the PI controller is relatively slow. The use of PI controller limits the variable speed range of the wind turbine. As shown in Figure 4-7, only within a small slip range the torque-slip curve of the DFIG can be considered linear. The variable rotor resistance based wind turbine with PI controller can vary rotor speed from -5% to 5% of the nominal speed.

The control of the rotor resistance can be developed to improve the damping of the wind turbine during grid fault. As shown in Chapter 2, the grid fault normally lasts significantly less than 1 second. The speed of the rotor resistance controller must be improved to cope with FRT requirements. The variable speed range is to be extended to accommodate to modern wind turbines that have larger variable speed range.

Most of the existing FRT research focuses on the electrical side solutions. To the author’s knowledge, the structural loads of the wind turbine during grid faults are taken into consideration only in [41, 89]. The controller proposed in these papers neglects the voltage and current limit of the converter system. The FRT strategy

proposed in [41] is able to reduce the wind turbine structural loads when converter system can keep connected. The strategy is no longer valid during severe grid faults.

The author proposes a fault ride-through strategy based on variable rotor resistance control. The controller focuses on reducing the wind turbine drive-train load caused by grid faults while limiting the rotor voltage and current. The theoretical analysis and the implementation of the FRT strategy are presented below.

4.4 Conventional crowbar protection

Crowbar-based protection is currently the major protection scheme for the DFIG during grid faults. The crowbar system aims to protect the converter of the DFIG from damage due to over current and over voltage induced by grid fault. The early crowbar systems are mostly a simple thyristor-based passive crowbar. When over current is detected, the thyristor short circuits the rotor circuit with a set of resistors and disconnects the converter from the rotor winding during the entire duration of grid fault. This type of crowbar only aims to protect the power electronic devices. No active support is provided during fault. The crowbar automatically reconnects when the rotor current dies out [90]. This means even if the grid fault is cleared, the DFIG will not be switched back on immediately if there is still transient current in the rotor winding. The FRT period may actually be much longer than actually needed.

Many crowbar control strategies have been proposed to improve the performance of the crowbar [91-93]. The crowbar is able to actively connect or disconnect with an applied control strategy to optimize the FRT performance of the DFIG. The choice of the crowbar resistance influences both the mechanical and electrical characteristic of the DFIG. There are many papers proposing different optimal crowbar resistance calculations in order to achieve different goals [94-96]. The influence of the crowbar

resistance on DFIG operation is shown below. The effect of the crowbar with different stator voltages is also presented.

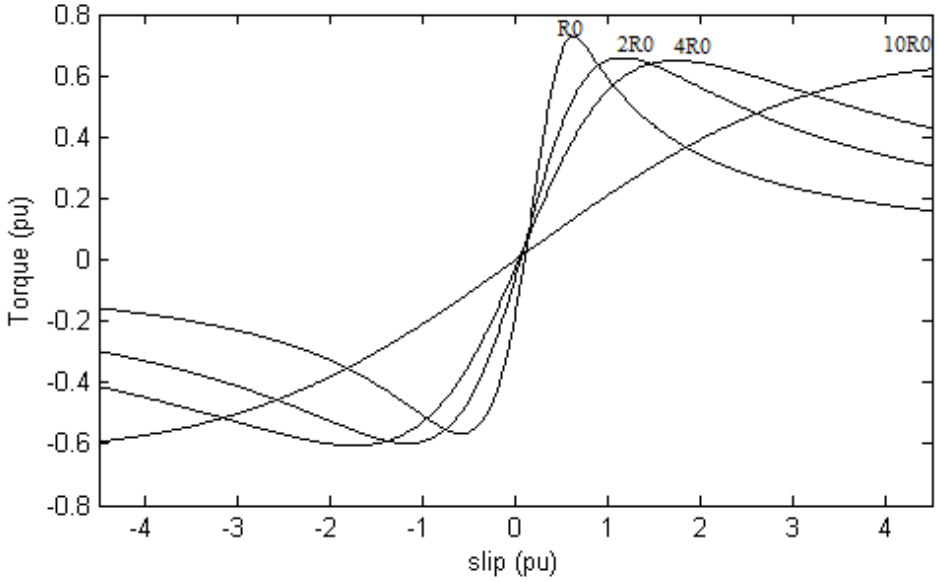

Figure 4-6: DFIG torque-slip curve under different rotor resistance

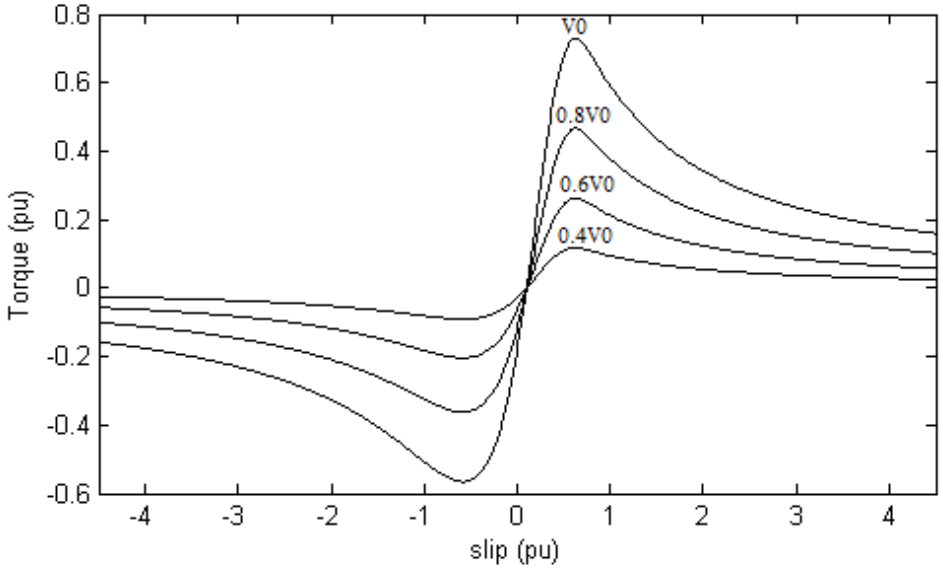

Figure 4-7: DFIG torque-slip curve under different stator voltage

Figure 4-6 shows the DFIG torque variation with rotor resistance increasing from 1 to 10 times of the original value. With the increase of the rotor resistance, the slip value where the DFIG reaches maximum torque reduces. Assuming the rotor speed does not change, the larger the rotor resistance, the smaller the magnitude of the torque output is.

Figure 4-7 shows how stator voltage affects the DFIG output when the converter is disconnected. It is shown that the stator voltage significantly limits the maximum output torque that the DFIG can provide. The DFIG torque reduces dramatically with the stator voltage.

The DFIG rotor winding is short circuited by the crowbar resistance regardless of the crowbar type. The DFIG runs in squirrel-cage induction machine mode with an extra rotor resistance during faults. The difference between active and basic crowbar protection is that when grid fault is cleared, an active crowbar can follow a predefined control strategy so that various benefits including fast reconnection, avoiding false reactivation of protection and improving stability contribution to fault recovery, can be gained. The switch between crowbar protection mode and normal operation mode raises the problem of the rotor acceleration and the reactive power extraction. The reactive power needed for the fault ride-through can be compensated by stator side converter with power factor control or voltage control [97, 98]. However, there is very limited research on how to improve the rotor acceleration of the DFIG and wind turbine rotor. During a grid voltage sag, the inrush current activates the crowbar and the generator reaction torque is reduced because of both the dropped voltage and the increased rotor resistance as shown in Figure 4-6 and Figure 4-7. In the meantime, the mechanical torque that the wind turbine experiences does not vary because the wind remains unchanged. The difference between electrical torque and mechanical torque results in rotor speed-up. On the wind turbine

mechanical side, the speed variation introduces extra mechanical load on wind turbine components and power extraction loss; on the DFIG side, the increased slip causes large transient magnetisation current when the DFIG is reconnected. The grid voltage recovery is deteriorated due to the reactive power absorption. An emergent pitch control strategy is proposed in [99] as a solution to this problem. The pitch angle of the wind turbine is set to change with the maximum rate during grid faults to balance the mechanical torque and electrical reaction torque. However, detailed modelling of the wind turbine and simulation is missing.

The effect that pitch control has on wind turbine damping is tested using the wind turbine mechanical model defined in [43], and the result is shown in Figure 4-8. It is clear that the pitch control is not able to regulate the high frequency drive-train oscillation induced by a grid fault.

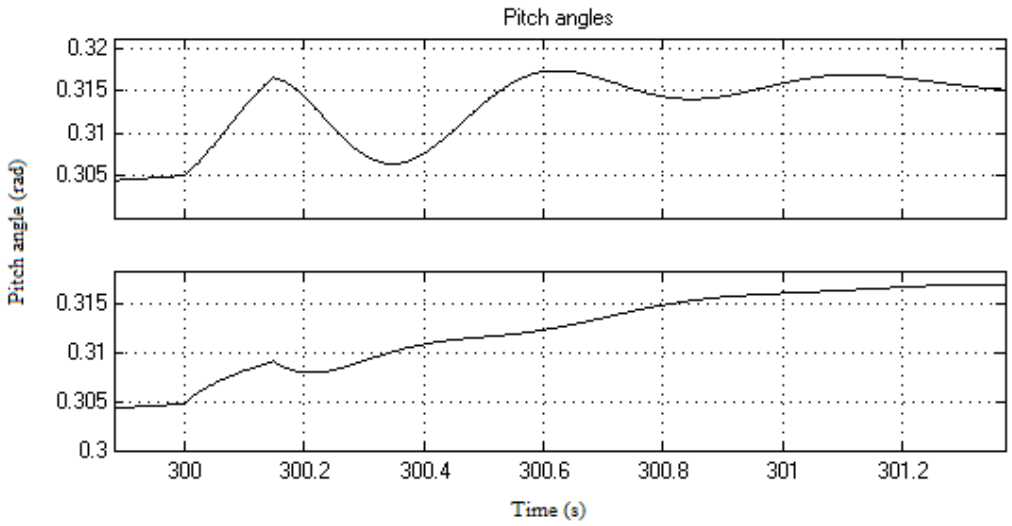

(a)

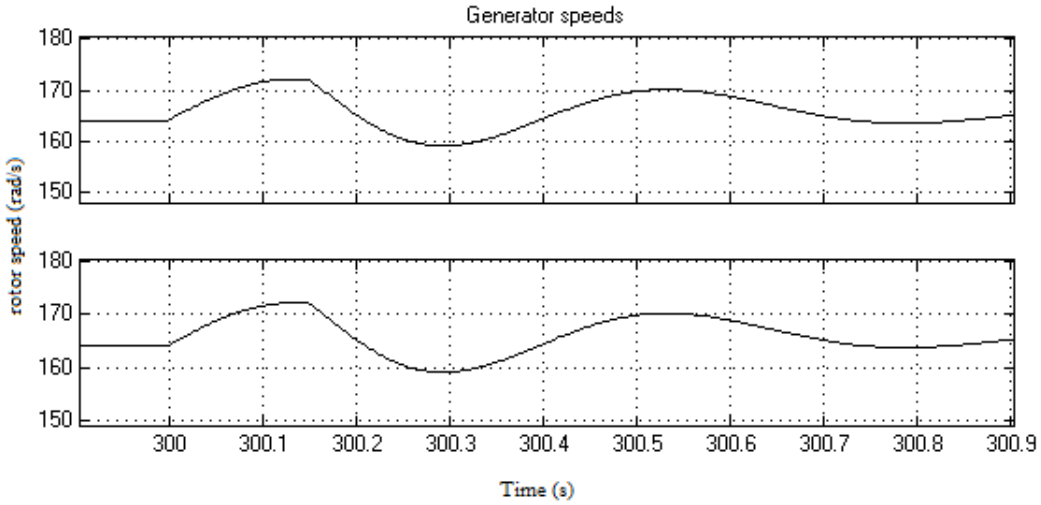

(b)

Figure 4-8: Pitch angle and generator speed during disturbance. (a) Pitch angle. (b) Generator rotating speed.

Top: Pitch control activated. Bottom: Pitch control blocked

Due to the large time constant of the wind turbine structure, the pitch control is not able to regulate the high frequency rotor speed variation caused by grid fault. As shown in Figure 4-8, although the pitch angle changes fast according to the rotor speed variation, the rotor speed is barely affected. The torque regulation via wind turbine pitch control is proved to be ineffective because the large inertia of the wind turbine. The grid fault lasts up to a few hundred milliseconds. It is evident that wind turbine cannot vary the generated mechanical torque fast enough within this timeframe. Torque control of the DFIG during the time when rotor converter is temporarily lost is needed in order to solve the rotor acceleration problem.

The author proposes a crowbar resistance control strategy to regulate the DFIG torque without the need of the converter control.

4.5 Variable rotor resistance control for DFIG torque regulation during fault

4.5.1 Steady-state analysis

Under grid fault, the converter systems are short circuited due to the initial over-current. The DFIG can be considered simply as an induction machine. The steady-state analysis of such machine can be carried out using the equivalent circuit shown in Figure 4-9.

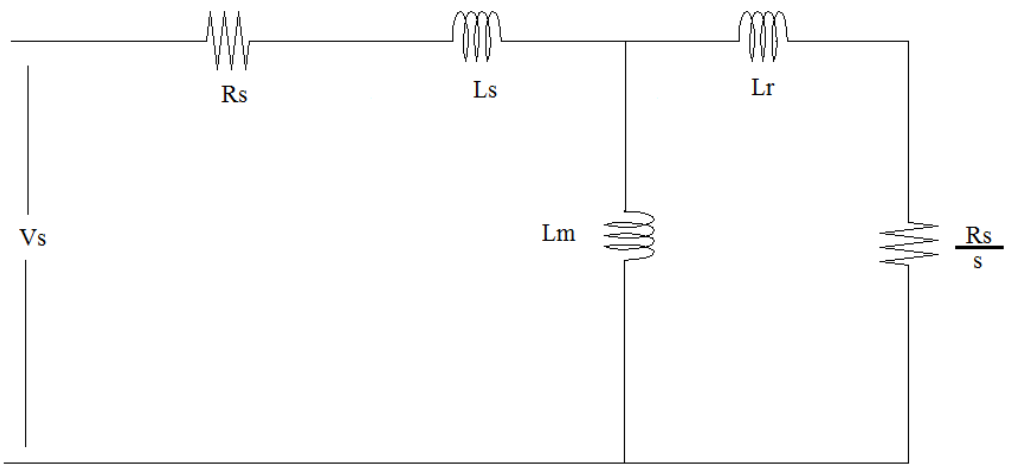

Figure 4-9: Induction generator equivalent circuit

Using this equivalent circuit of DFIG with rotor short circuited, the output torque can be calculated as [100]:

$$T = \frac{3}{2}\frac{p_f R_r I_r^2}{s\omega_s} \tag{4-12}$$

where T is the generator torque, p_f is the number of poles, R_r is the rotor resistance, I_r is the rotor current, $s = \frac{\omega_s - \omega_r}{\omega_s}$ which is the slip, ω_s is the synchronous speed and ω_r is the rotor rotating speed.

The impedance of the circuit in Figure 4-9 is:

$$Z = R_s + \frac{R_r}{s} + j*(L_s + L_r) \tag{4-13}$$

Using Kirchhoff's current law, the rotor current is calculated as

$$I_r = \frac{V_s}{R_s + \frac{R_r}{s} + j*(L_s + L_r)} \tag{4-14}$$

where V_s is the stator voltage, R_s is the stator resistance, L_s is the stator reactance and L_r is the rotor reactance.

Substituting (4-14) into (4-12) gives the following relationship

$$T = \frac{3}{2} \frac{p_f R_r V_s^2}{s\omega_s \left[\left(R_s + \frac{R_r}{s} \right)^2 + (L_s + L_r)^2 \right]} \tag{4-15}$$

Equation (4-15) is the design basis for using dynamic rotor resistance to control the induction generator torque.

The characteristic of an induction generator can be demonstrated by plotting the torque versus slip curve as shown in Figure 4-6. From equation (4-15) it is clear that the output torque for a given induction generator only depends on the rotating speed and the terminal voltage.

From the plot we can see that by varying the rotor resistance, the generator torque-slip characteristic can be modified and hence control the torque for a given value of slip. It is also noticed that the maximum torque available does not change with rotor resistance variation. In fact, from equation (4-15) we can see that the maximum torque is proportional to the value of V_s^2.

4.5.2 Stability assessment of wind turbine operating in SCIG mode

As explained before, the DFIG normally works in SCIG mode during grid fault. Without successful fault clearance, the crowbar or other equivalent protection

schemes stay connected due to the fault current thus the wind turbine operates with SCIG for a relatively long time after fault occurrence. Knowing which factor affects the stability of the wind turbine with closed crowbar helps to design the FRT strategy to improve the stability of the DFIG-based wind turbine during and possibly after the grid fault.

The torque versus slip curve can be used to define the stability limit of the induction machine or the DFIG during a fault [101]. Several methods have been developed based on the torque-slip curve to determine the stability of the induction machine during a grid fault [86, 102]. The conventional technique compares the decelerating electrical torque and the accelerating mechanical torque. The wind turbine is considered to be unstable when it operates at the condition where the maximum electrical reaction torque is less than the mechanical input torque. This method is mainly used to assess the influence that the reduced grid voltage has on the wind turbine stability. Both dynamic stability [86] and steady-state stability [102] of the wind turbine can be assessed using this approach. However, this research does not take parameter changes into consideration. The generator torque-speed curve is assumed to be unchanged throughout the fault period. The author of this thesis extends the technique so that the effect of the change of the torque-slip curve has on the wind turbine stability can be assessed. The improvement on the wind turbine steady-state stability by varying rotor resistance is then demonstrated.

The torque versus slip curve of the same DFIG for a different grid voltage is shown in Figure 4-10.

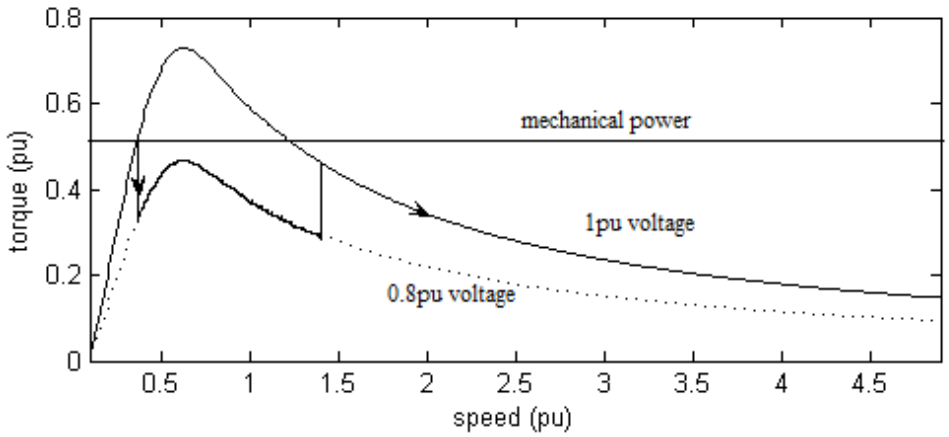

Figure 4-10: Failed fault ride-through shown by generator torque-speed curve
Solid line: 100% grid voltage. Dotted line: 80% grid voltage.

The fault ride-through procedure of a SCIG without any crowbar protection under 20% voltage dip (80% retained voltage) is shown in Figure 4-10. The mechanical torque is assumed to be constant during the whole period of the fault as the fault duration is too short for wind turbine mechanical torque to have large variation. The SCIG torque dropped immediately at the occurrence of the fault. During the fault the SCIG operates in the new torque-slip curve of 80% voltage. It can be observed that the electrical torque is smaller than the mechanical torque so the wind turbine has been speeding up when the grid fault happens. After the fault clearance the SCIG torque jumps back to the 100% voltage trajectory. As shown on the plot, the electrical torque is still smaller than the mechanical torque at the time when fault is cleared. The wind turbine rotor speed will keep increasing. However, the torque-slip curve in Figure 4-10 shows the fact that the electrical torque will continue to drop with the increased rotating speed. The wind turbine is forced to shut-down eventually because of the over-speed.

The same fault is applied again with increased generator rotor resistance during the fault. The result is explained in Figure 4-11.

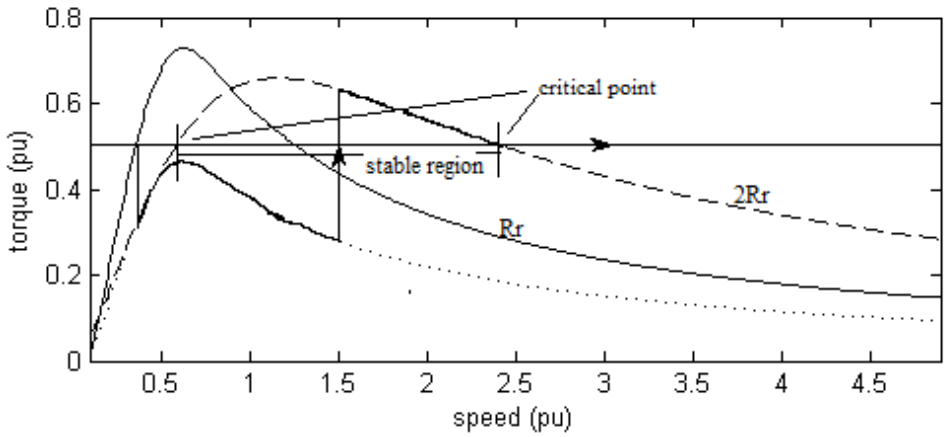

Figure 4-11: Successful FRT with increased rotor resistance

Solid line: 1pu rotor resistance. Dashed line: 2 pu rotor resistance

Dotted line: 1pu rotor resistance under 80% voltage

Figure 4-11 shows the fault ride-through of the SCIG when an external rotor resistance is added. A fault, which has exactly same level and duration as in Figure 4-10 is applied. The only difference is that the rotor resistance is increased when the fault is cleared. The result shows how the wind turbine successfully rides-through the fault with the injected resistance. Because the external rotor resistance changes the torque-slip characteristic of the generator, the electrical torque exceeds the mechanical torque at the point when grid fault is cleared and the voltage is recovered. The electrical torque eventually decreases to the same level as the mechanical torque. The new torque balance is achieved and the wind turbine speed-up is prevented. The result shows that a wind turbine can operate safely with an appropriate rotor resistance value even if the rotor side circuit of the DFIG is disconnected from the grid.

It can be summarized from the above analysis that the two points where electrical torque and mechanical torque have the same value determines at what the speed range over which the wind turbine can operate safely without entering the area where

the electrical torque can never reach the mechanical torque value. These two points are defined as critical points and the curve between these two points is the stable region. It is clear that the generator with larger rotor resistance has a wider stable region.

The result also shows how the torque-slip characteristic can be modified by the rotor resistance value. It is possible to keep the wind turbine electrical torque at a constant value, e.g. mechanical torque, during a grid fault with a controllable rotor resistance.

4.5.3 Variable crowbar resistance control theory

First, the theory behind variable crowbar resistance control is explained. The controller is based on the fact that during a grid fault the DFIG rotor winding is short circuited and the wind turbine generator turns into a squirrel-cage induction generator. The rotor current, which determines the magnetizing flux, cannot be controlled by the DFIG controller. An auxiliary controller is hence needed in case of a grid fault.

There are several eligible parameters to control the output of induction generator, namely rotor resistance, rotor inductance, stator inductance and slip. Due to the large time constant of the wind turbine drive-train, the generator rotating speed is not suitable as the controlled variable. Resistances and inductance are both available as controlled variable. Resistors have an advantage in price compared to inductors. Also the existing crowbar technology can be adopted for such control with just a little modification. Hence, the rotor resistance is chosen to be the controlled variable.

In past research on variable rotor resistance control [103, 104], either PI controllers are used to regulate the rotor resistance or simply a constant resistor is connected to increase the damping of the generator. The controller performance is acceptable considering the task was just over-current protection. However, the control method

needs to be carefully examined when the task is maintaining demanded generation during a grid fault. The electrical transients experienced during the fault are normally very fast. The grid faults duration is about tens or hundreds of milliseconds. The controller must be fast enough but without too much overshoot to avoid the damage due to by overcurrent. It has been discovered by simulation that the PI controller does not give satisfactory performance.

However, it is noticeable that all the parameters of the controlled system are measurable and the relationship between the reaction torque and rotor resistance is given. Therefore, the desired rotor resistance to produce the reference torque can be calculated from generator parameters directly. The demanded resistance is then injected to the rotor circuit in series through power electronic switches. The configuration is shown in Figure 4-12.

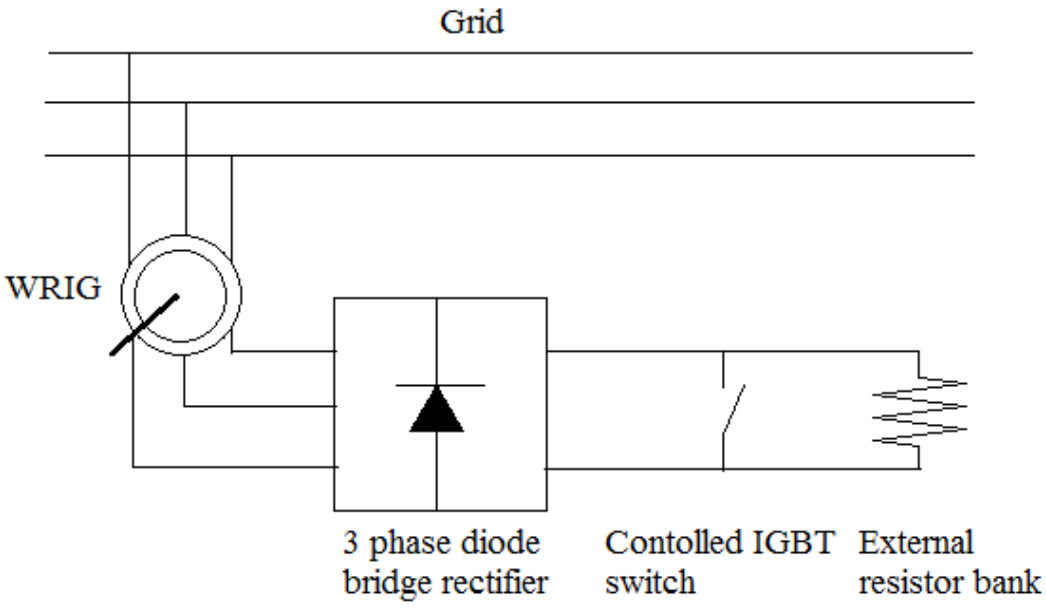

Figure 4-12: DFIG with variable crowbar resistance scheme

In normal operation the DFIG controller is activated with the crowbar bypassed. When grid voltage falls below a certain level, depending on the Grid Code requirement, the fault detection unit sends signals both to the wind turbine converter to shut it down and to the crowbar rectifier and IGBT switch to connect the resistor bank. The basic chopper control is applied to IGBT switches to achieve the control over DFIG rotor resistance.

4.5.4 Proposed controller – design considerations

To enhance efficiency, some considerations need to be taken into account during the design of the proposed controller. The grid voltage level at the PCC is a major limitation on the controller performance. From equation (4-15) it can be easily derived that the maximum generator torque, which is also called pull-out torque, is proportional to V_s^2. The stable region of the induction generator shrinks rapidly with the grid voltage drop. There is a critical grid voltage for each wind speed. If the voltage drops below the critical voltage, the generator reference torque cannot be produced and the generator will be running in the unstable region. The lower the grid voltage is, the smaller the maximum torque will be. The proposed rotor resistance control strategy is designed to produce the maximum torque under such condition. The detailed operation will be explained in the next section.

The success of the control strategy also depends on the rotor speed, which is determined by the wind speed. The induction machine is capable of operating either as generator or motor. The uncontrolled induction generator runs in generator mode when the rotor speed is above the synchronous speed and in motor mode when the rotor speed is below the synchronous speed. The proposed control strategy can only be applied when the wind turbine generator is operating in super-synchronous mode. When the rotor speed is too low the best choice is to increase the generator damping

to reduce the absorbed torque. The FRT issue under low wind speed is not as serious as under high wind speed because the aerodynamic torque is relatively small when wind speed is low. The loads on wind turbine components are small as well. Figure 4-13 shows a typical DFIG tracking curve

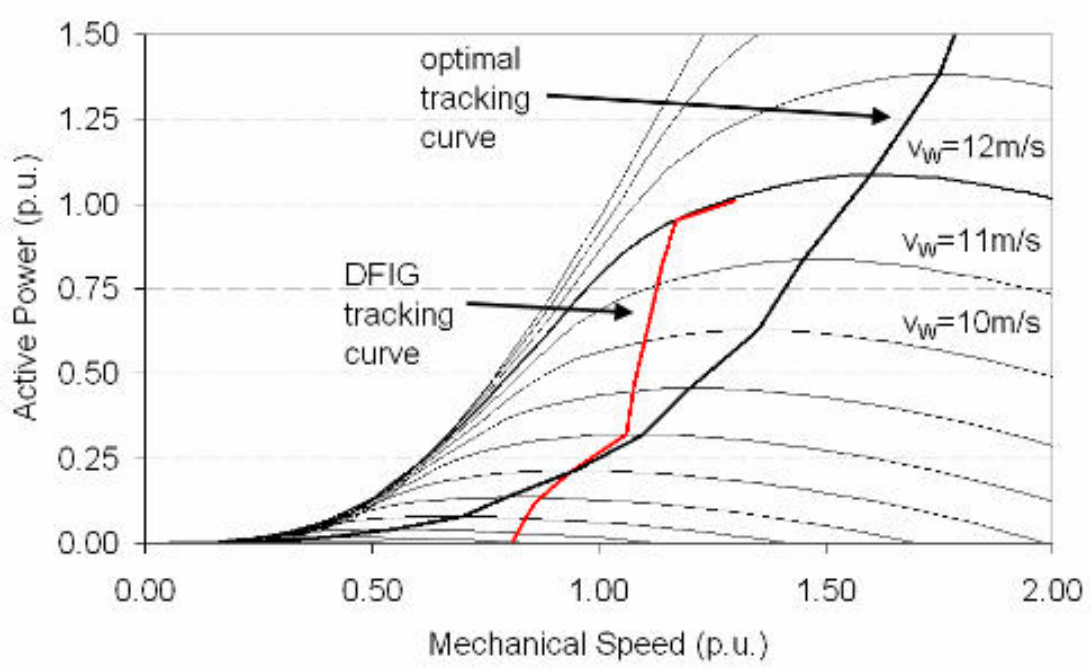

Figure 4-13: DFIG maximum power tracking curve [105]

The synchronous speed is 1pu. The DFIG rated speed is normally chosen to be the mid-point of the wind turbine variable speed range to allow minimizing the rating of the power electronic devices [105]. In this case the wind turbine varies its rotor speed when wind increases from 4m/s to 12m/s and the rotor speed changes from 0.8pu to 1.2pu roughly. From Figure 4-13 it can be seen that the wind speed is about 7m/s when the generator reaches its rated speed. The analysis of the wind turbine model used in this project gives the same result. The cut-in wind speed is 4m/s while the cut-out wind speed is 24m/s. The wind speed range in which the variable crowbar resistance control can be applied is from 7m/s to 24m/s. By analysing the wind speed profile across UK, it is discovered that the time wind speed lies within this range is

above 85% of total wind turbine operation time. It can be concluded that the FRT control strategy can be applied in most occasions.

4.5.5 Controller scheme

The controller requires the monitoring of several variables to account for the voltage level influence discussed above. Both the grid voltage and wind turbine high-speed shaft rotating speed are measured. The FRT controller takes over the control of the wind turbine generator when the DFIG protection system is triggered by the grid fault

When grid fault occurs, the generator speed is compared with the synchronous speed first. If the generator speed is greater, the controller will calculate the optimal resistance of the crowbar. Otherwise the crowbar of a fixed resistance will be injected to increase generator damping.

The first step is to determine if the generator is able to produce the demanded torque. The calculation is described in Chapter 4.5.6 Maximum torque determination. The reference signal is set to the maximum torque available according to the grid voltage and the post fault damping system (see Section 4.6 Active drive-train damping strategy) is activated if the result shows that the demanded torque cannot be achieved. If the demanded torque can be achieved, the crowbar with the optimal resistance is connected. The grid voltage is continuously measured during the fault. The DFIG controller is switched on and the crowbar is disconnected when the fault is cleared and the grid voltage returns to the acceptable value. The flow chart of the FRT control strategy is shown in Figure 4-14.

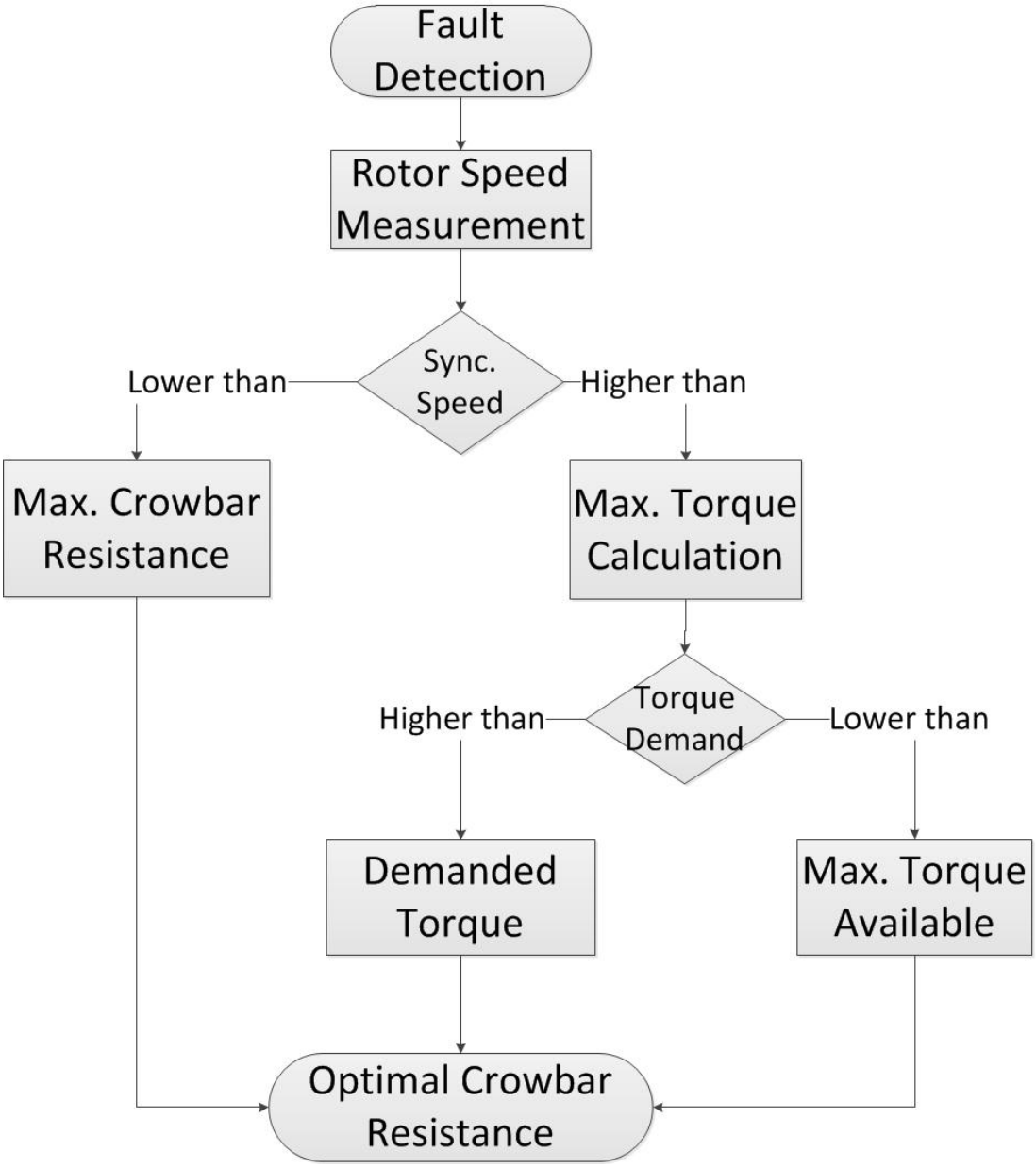

Figure 4-14: FRT strategy flow chart

4.5.6 Maximum torque determination

Determination of the maximum torque is based on equation (4-15). With the grid voltage and rotor resistance given, the maximum torque can be calculated. This maximum torque is the largest torque that can be generated under the given voltage

since the rotor resistance only shifts the torque-speed curve horizontally without changing the maximum value.

The procedure to get the maximum torque is to calculate first the derivative of equation (4-15). Thus the slip at which the maximum torque is achieved can be obtained. Then the slip is substituted back into equation (4-15) to get the maximum torque.

4.5.7 Simulation results

The controller is tested with two different wind speeds, 8m/s and 14m/s, respectively, representing above rated and below rated operation. The fault scenario is chosen to be 0.7 seconds with 50% voltage drop according to NGC requirement. The selection of the fault scenario is made according to the FRT requirement in National Grid's Grid Code (NGC). The performance of the variable rotor resistance FRT controller under different voltage sag levels is also tested. The response of the wind turbine with variable rotor resistance control under less severe but longer duration fault is shown. The case aims to simulate the influence of a remote fault. A fault happens in the main system causes a 20% voltage dip at the PCC of wind farm. According to NGC, The successful FRT time when grid voltage drops by 20% is 1.2 seconds. The voltage and current of DFIG are monitored to show how the FRT strategy limits the over-voltage and over-current, which normally lead to DFIG shut-down. On the wind turbine side, the drive-train and tower behaviour during fault are investigated and shown. The results are shown below.

4.5.7.1 Influence of wind speed on controller performance

The behaviour of wind turbine under below rated (8m/s) and above rated (14m/s) wind speed during a 50% voltage dip is shown in Figure 4-15 and Figure 4-16. The

wind turbine mechanical and electrical transients with and without variable rotor resistance protection scheme are compared.

The protection system identifies the rotor over-current immediately when the grid fault happens. The rotor converter is disconnected following the protection signal. Crowbar fixed and controllable resistances are injected to two wind turbines with the same configuration and parameters. Large torque oscillation is observed at the DFIG with fixed crowbar resistance. The initial torque impulse caused by the short circuiting of rotor winding reached 4 times of the reference value. The oscillation is slowly damped out in the next two seconds. As a result, the rotor speed of wind turbine and generator suffers from large fluctuation. The amplitude of the rotor speed change is about 10% of nominal value under 8m/s wind speed. Since the drive-train is connected with wind turbine rotor and mounted on the tower, the wind turbine structure also experiences extra loads. Tower oscillations can be observed from the simulation result.

The transients that wind turbines suffer in 14m/s wind speed are worse than at lower wind speed. The high wind speed contributes to the extra loads. However, the major reason is related to the DFIG operating in very high rotating speed. The DFIG operates near the pull-out torque point therefore the generated torque reduces with increased wind speed. The torque is rapidly reduced to about 0. The extreme low torque leads to wind turbine rotor acceleration. Although the fault duration is short and the wind turbine inertia is big, the rotor speed still increased about 5% by average. The maximum rotor speed exceeds the rated value by 10%. The rotor speed excursion is high enough to trigger wind turbine supervisory control to shut-down the wind turbine. Even if the protection system of wind turbine is not activated, the rotor speed oscillation, which lasts about 5 seconds with high frequency, can cause a lot of damage to wind turbine drive-train.

The employment of variable rotor resistance control completely suppressed the torque oscillation as shown in Figure 4-15 in below rated wind speed. The generator is able to produce torque of the reference value with appropriate rotor resistance. The wind turbine rotor speed is smooth during the fault as the demanded torque is supplied. The variable rotor resistance control provides similar performance during fault as conventional DFIG control in normal operation. It should be noted that the torque control is achieved with extra rotor heating. As the rotor resistance is increased during fault, the power consumed in rotor winding is also increased. The increase of the rotor power is small except at the occurrence of the fault. The initial inrush current leads to the large initial power as seen in Figure 4-15. Since the converter is already disconnected at the time and the high current only lasts less than 100ms, the cost is small considering the successful torque control during fault.

In 14m/s wind speed, it can be seen that the rotor resistance does not vary according to the reference torque change. This is because the maximum torque that can be produced is achieved. The rotor resistance is set so the maximum torque that is generated. A small rotor speed variation can be observed. However, the difference between reference torque and maximum torque is not big for the given wind turbine. There is only 0.05pu difference between the demanded and the actual electrical torque. The improvement of variable rotor resistance control is still significant. The variable rotor resistance protection will be less effective for severe grid fault such as 90% or complete voltage dip.

To summarize, it can be concluded that the variable crowbar resistance control strategy successfully sustained the power generation in both below and above rated wind speed given that the available torque in the generator is greater than the aerodynamic torque produced by wind turbine. The controller switching takes about 20ms, which is acceptable. The drive-train oscillation is completely eliminated

during the fault under below rated wind speed and significantly suppressed under above rated wind speed. The rotor current remains at about the same level. It is noticed that the power dissipated in the rotor circuit is significantly increased due to the increase in the rotor resistance. However, the power loss is still acceptable as the fault ride-through time is relatively short.

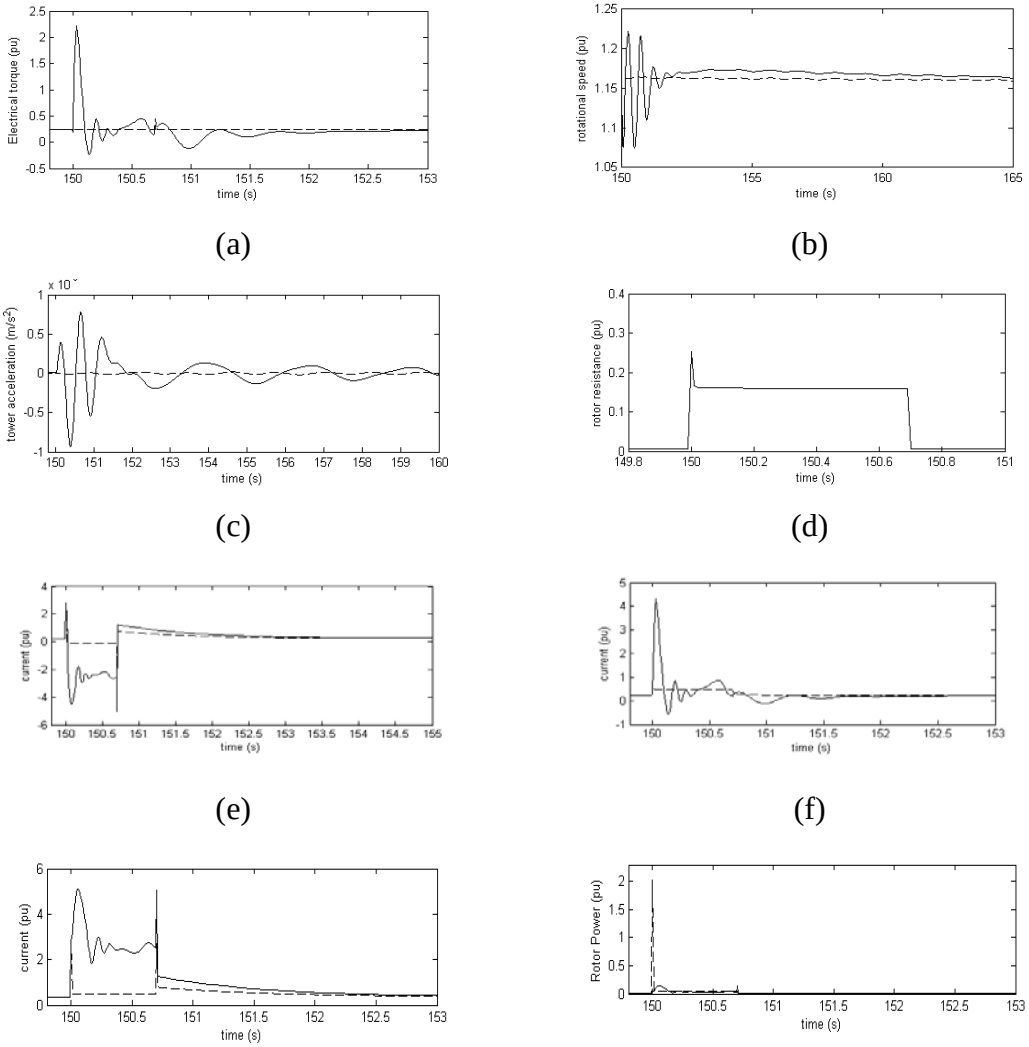

Figure 4-15: wind turbine under 8m/s wind speed with and without variable rotor resistance control: (a) electrical torque; (b) generator speed; (c) tower acceleration; (d) rotor resistance; (e) d-axis rotor current; (f) q-axis rotor current; (g) magnitude of rotor current; (h) rotor power.

Solid line: wind turbine with conventional crowbar; Dashed line: wind turbine with variable rotor resistance control.

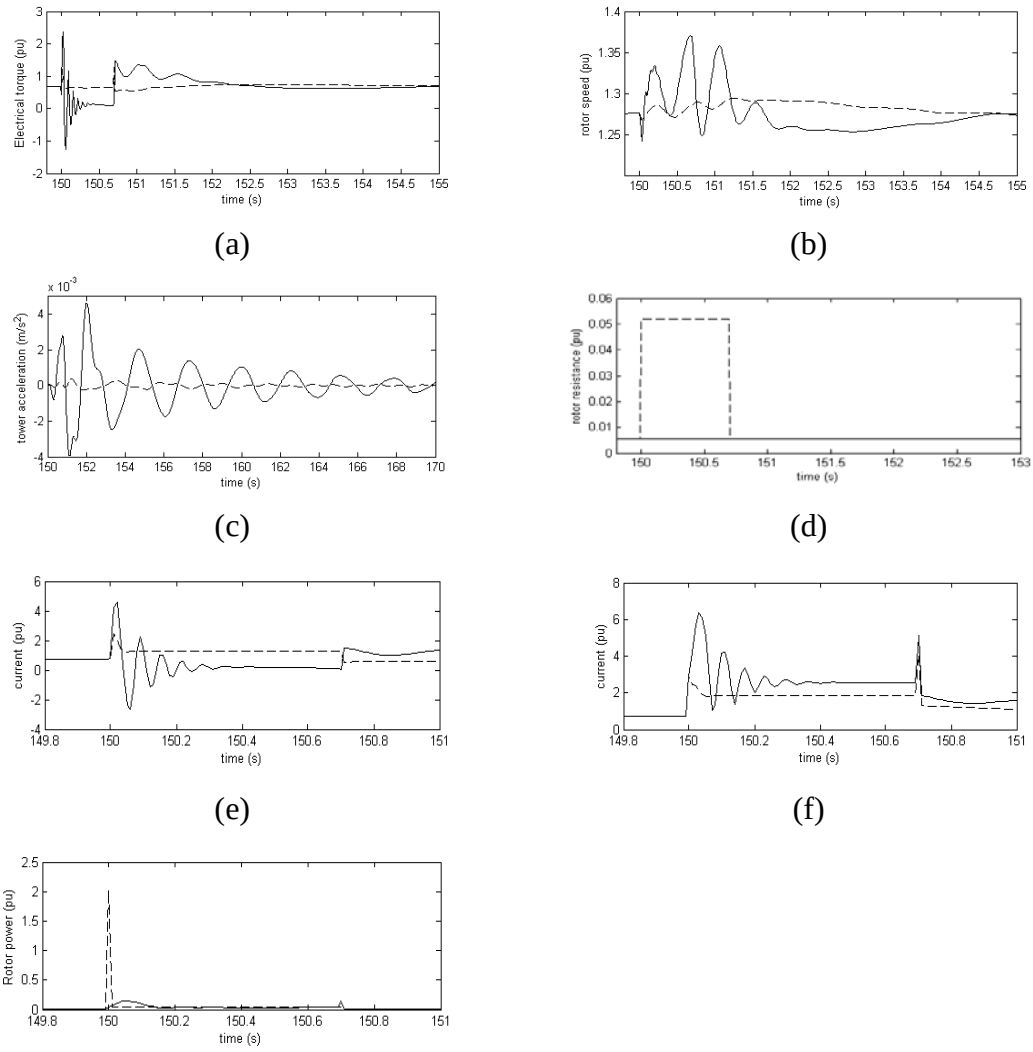

Figure 4-16: wind turbine under 14m/s wind speed with and without variable rotor resistance control: (a) electrical torque; (b) generator speed; (c) tower acceleration; (d) rotor resistance; (e) d-axis rotor current; (f) q-axis rotor current; (g) magnitude of rotor current.

Solid line: wind turbine with conventional crowbar; Dashed line: wind turbine with variable rotor resistance control.

4.5.7.2 Influence of voltage sag level on controller performance

A fault which is less severe but with longer duration is applied to investigate the long-term performance of the variable rotor resistance control. The wind speed variation is taken into consideration as the wind speed can no longer be considered as constant when the grid fault lasts for long time. National Grid requires the wind turbine to withstand an 80% grid voltage level for 2.5 seconds. The fault scenario is set up accordingly. Without appropriate control of rotor resistance, the torque oscillation is more detrimental than a short duration fault. The rotor speed oscillation is damped out faster as the torque oscillation amplitude is smaller. However, the continuous loss of the torque control results in significant rotor speed deviation. It takes more than 10 seconds for the wind turbine to return to the maximum power extraction curve. The production of wind turbine is reduced and moreover, it is possible that the rotor speed deviation leads the wind turbine into the stall region where control over the wind turbine is lost.

The variable rotor resistance is shown to be able to maintain the torque control within the fault duration. The rotor resistance changes according to the wind speed and grid voltage as illustrated in Figure 4-17. As the grid voltage is relatively high, it is not likely that the DFIG reaches the torque cap. According to the calculation based on the maximum torque determination procedure, the wind turbine torque can be controlled over all wind speeds with a 20% grid voltage sag. The variable rotor resistance control has better performance during remote or light faults.

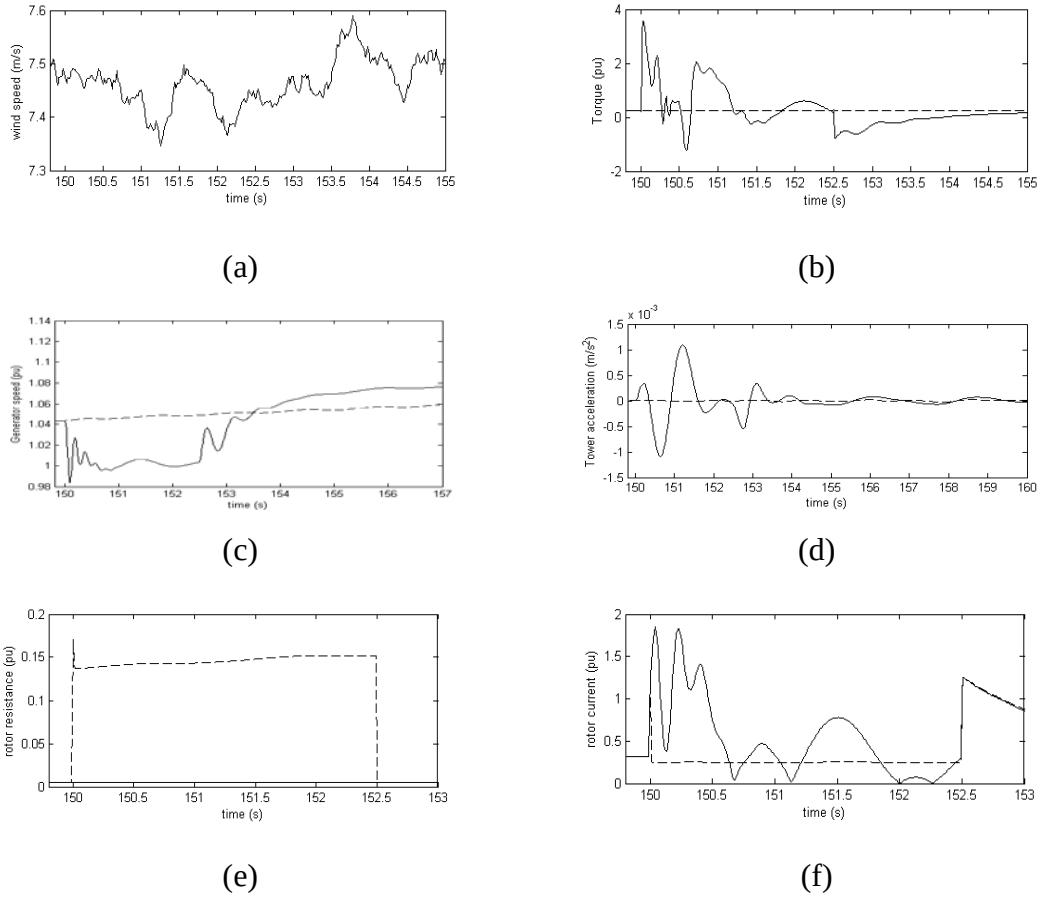

Figure 4-17: wind turbine under 80% voltage dip for 2.5 seconds with and without variable rotor resistance control: (a) wind speed (b) electrical torque; (c) generator speed; (d) tower acceleration; (e) rotor resistance; (f) rotor current.
Solid line: wind turbine with conventional crowbar; Dashed line: wind turbine with variable rotor resistance control.

4.5.7.3 Contribution to power system stability

The proposed full wind turbine FRT control strategy is tested on the generic grid model described in Chapter 3. The influence of the successful wind turbine FRT on the local grid is shown in Figure 4-18 and Figure 4-19. It can be seen from the results that the FRT of wind farm is able to reduce the fault current in the wind farm hence reducing the voltage fluctuations at a nearby conventional power plant.

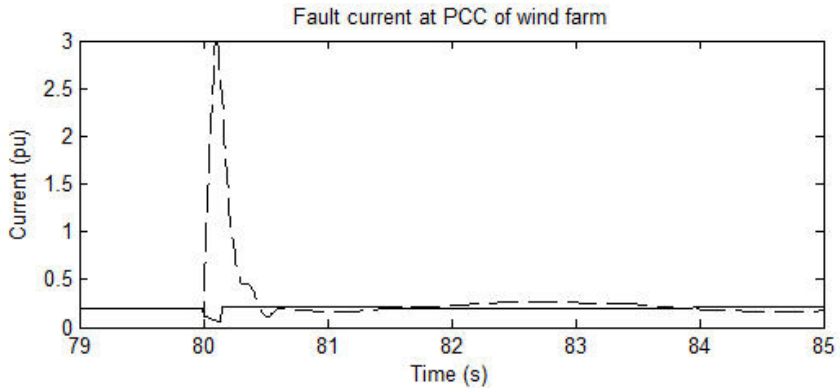

Figure 4-18: The fault current at the PCC of the wind farm during a nearby grid fault with/without FRT control

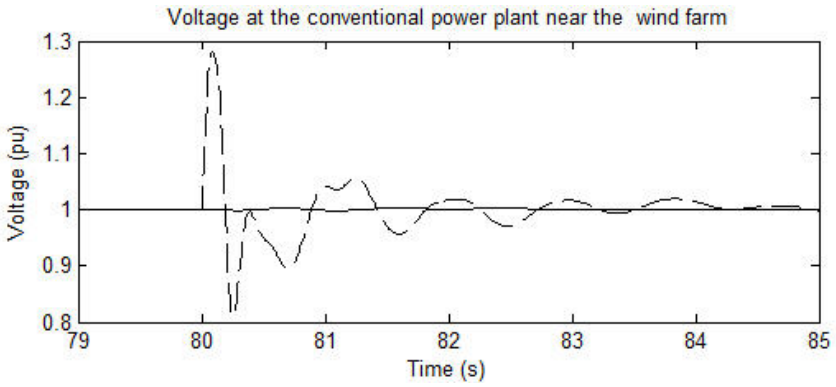

Figure 4-19: The voltage at the PCC of the conventional power plant during a fault near the wind farm with/without FRT control

4.6 Active drive-train damping strategy

As described before, the wind turbine generator operates as an induction generator during the grid fault. The induction generator provides large damping to the wind turbine drive-train because the generator torque increases rapidly with the generator speed. The generator switches back to DFIG mode after fault clearance. The damping under this mode is much smaller since the generator torque is controlled by the DFIG controller rather than regulated by the torque-slip curve. The generator experiences large torque variation at the time when fault is cleared and crowbar is disconnected.

This torque variation, plus the possible torque imbalance during the fault, creates large torsional oscillation on the drive-train after grid fault recovery. The oscillation is to be damped to avoid structural loads on the wind turbine and rotor speed excursion.

In [104] a PI controller is developed to reduce the post fault oscillation. The controller uses generator speed as input and varies generator torque to damp the oscillation of the generator rotor shaft. Only generator control is considered in this paper. Most modern wind turbines include the control loop of drive-train damping filter, which manipulates the same variable to increase the damping of the drive-train. The collaboration of these two controllers is not considered in the paper. In this thesis, the modification on the existing wind turbine drive-train damping filter is investigated to achieve the increased damping in post-fault phase.

A drive-train damping filter is a widely used method to reduce the loads on the drive-train. The wind turbine drive-train oscillating frequency can be obtained with its mechanical parameters known or from experiment. The drive-train filter is basically a band pass filter sitting on the drive-train vibration frequency. The wind turbine torque demand is slightly modified to increase the drive-train damping.

The drive-train damping filter is normally tuned for the normal operation of the wind turbine. The vibration induced by a grid fault is much larger than the vibration induced by the wind speed variation. The damping filter is not able to cope with the drive-train oscillation of such level. Therefore, the grid fault level is integrated into the conventional drive-train damping filter design.

Combining equation (3-11) and (4-15), a relationship can be derived such that the rotor speed variation caused by grid fault is proportional to V_s^2. The post fault active drive-train damper is developed based on this relationship. Assuming the drive-train

damper during normal operation is perfectly tuned, the gain of the damper is multiplied by the reverse of the voltage dip level so during and after fault the drive-train damping is temporally boosted according to the fault severity.

The filter for wind turbine normal operation is not changed. When grid fault is detected, an auxiliary filter with its coefficient tuned according to the value of V_s^2 is added.

The effectiveness of the auxiliary filter is tested and the result is shown below:

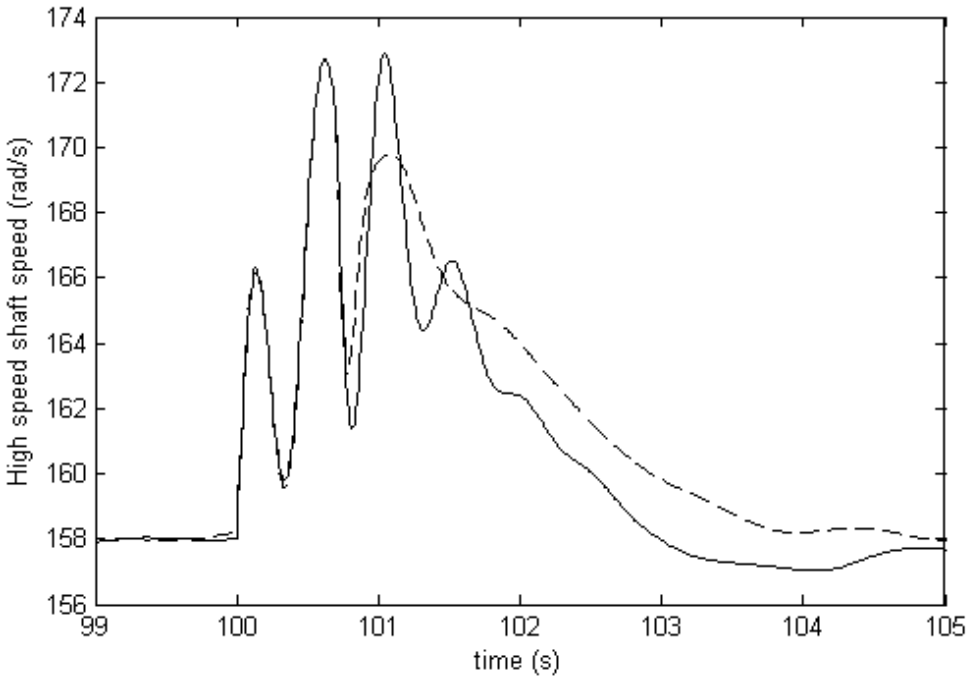

Figure 4-20: Generator speed with/without active drive-train damping
Solid line: without active drive-train damping. Dashed line: with active drive-train damping

It is clear that the drive-train damping is increased with the tuning based on grid voltage. The oscillation takes less than 1 second with active damping while about 5 seconds with original drive-train damping filter.

4.7 Pitch load alleviation filter design

Blade pitching is an effective method to regulate wind turbine rotating speed. The blade pitch angle is determined by the measured generator speed. Grid faults cause significant generator speed oscillation, which also has impact on the pitch control system. Due to the disturbance from the grid side, the rotor speed is no longer on the optimal operational curve of the wind turbine. Wind turbine blades change their angles to counter the speed variation. However, the pitching does not improve the post-fault oscillation because the wind turbine has a large time constant while grid transients are within the scale of milliseconds. The grid fault impact on wind turbine pitch control is then removed by adding a filter so that the wind turbine pitches on slow transients which indicate wind speed variation rather than fast transients caused by grid disturbance. The filter is added to wind turbine control loop as shown in Figure 4-21.

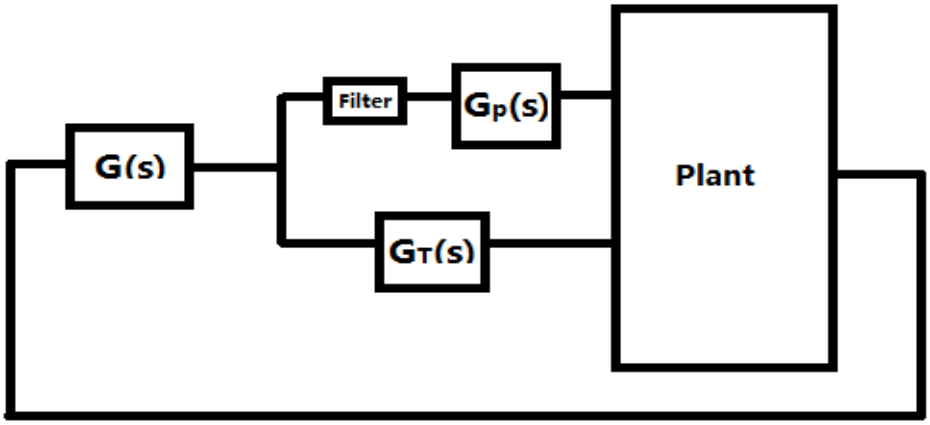

Figure 4-21: Pitch fatigue alleviation filter

The torque control works normally trying to reduce the fault transients while the pitch control only regulates the input power.

Similarly to the active drive-train damping control, the filter is only switched on when grid fault is detected and switched off when rotor oscillation stops. The filter is essentially a band-pass filter centred at the rotor oscillation frequency with a large gain and relatively narrow peak. The reason is the torque variation only induces drive-train modes and pitch action on another frequency should not be influenced. The transfer function is

$$\frac{s^2 + 0.3142s + 157.9}{s^2 + 31.42s + 157.9} \tag{4-16}$$

The Bode plot of the filter is shown below

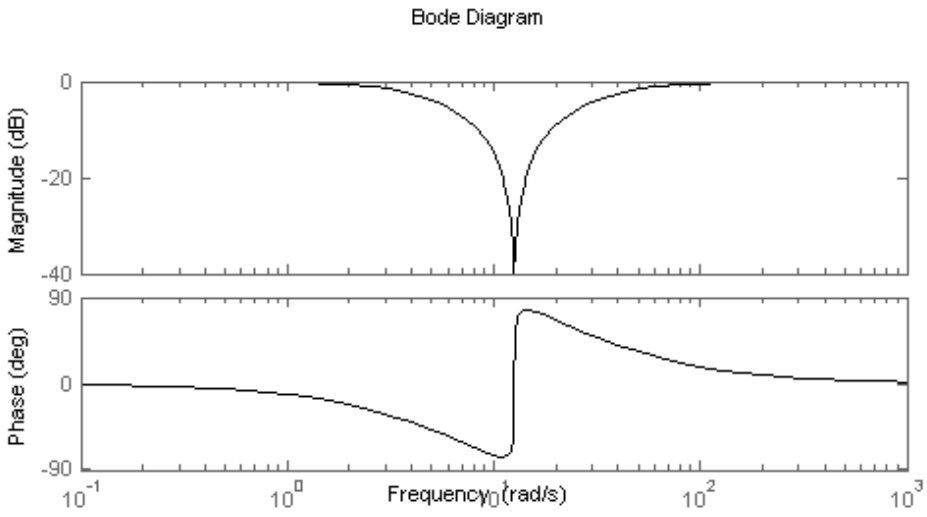

Figure 4-22: Bode plot of the filter

The filter is tested by simulation and result is illustrated in Figure 4-23

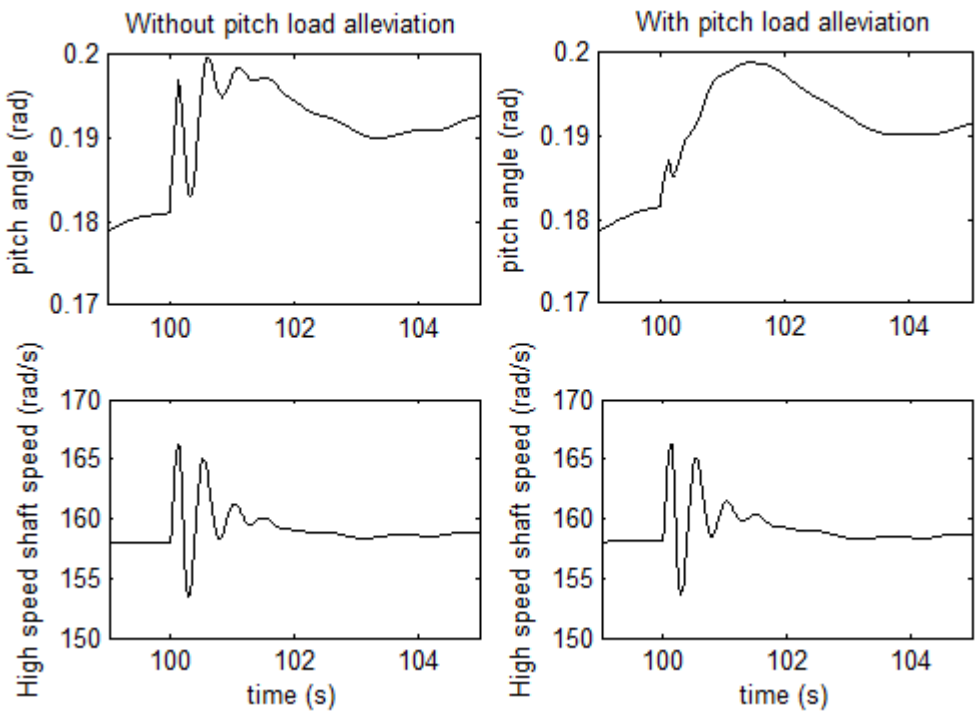

Figure 4-23: Pitch angles and generator speeds during fault with/without pitch load alleviation

The left-side results in Figure 4-23 are obtained without the filter and the right-side results are with the filter. The pitch angle and generator speed are compared. It is shown that the pitch angle does not affect the generator speed in wind turbine FRT. Without the filter the wind turbine blades pitch much more frequently than with the filter. The filter successfully reduces the blades vibration during grid fault.

4.8 Summary

This chapter presented a symmetrical FRT strategy for DFIG-based wind turbines. To the author's knowledge most wind turbine FRT strategies only focus on wind turbine protection rather than sustained operation and grid support. The method introduced in this chapter attempts to allow the wind turbine to maintain its generation during grid fault as same as in normal operation. The FRT problems from both mechanical

and electrical side are considered in the research. Not only sustained generation, but also wind turbine structural loads during grid fault are improved. With large amounts of wind power generation, it is important to take the grid integration issue into consideration when developing wind turbine controllers in the future.

CHAPTER 5: ASYMMETRICAL FAULT RIDE-THROUGH OF DFIG BASED WIND TURBINE

In Chapter 3 and Chapter 4 it was assumed that the DFIG operates in a 3-phase balanced power system. Most of the existing research on the FRT of DFIG only considers the case of symmetrical faults. The zero and negative sequence currents are neglected. However, asymmetrical faults happen more frequently than symmetrical faults in real power systems. Most of faults are single-line-to-ground or line-to-line faults. The unbalance of the stator voltage and current will cause highly unbalanced DFIG rotor current, high frequency pulsation of generator torque, high drive-train load and generator heating etc. For a DFIG, which employs poor control, the asymmetrical fault will also result in malfunction of the controller. The asymmetrical fault could cause wind turbine disconnection if not controlled properly [106]. Most existing wind turbines can only stand a voltage unbalance level of 2% which means most of wind turbines will disconnect from the grid when an asymmetrical fault happens near the location [107]. The Fixed-speed wind turbine (FSWT) with SCIG is not able to ride-through an asymmetrical fault due to lack of control capability. As the stator is directly connected to the grid, a VSWT with DFIG is also affected by asymmetrical fault in the grid. However, the control of the rotor converter can be designed to minimize the damage caused by the asymmetrical fault.

There are several publications on the operation of the DFIG under unbalanced 3-phase voltage conditions. The use of an additional series connected converter to reduce the effect of voltage unbalance is proposed in [90]. The grid side converter is controlled to operate as a STATCOM under unbalanced grid voltage to compensate the stator voltage unbalance [108]. These publications focus on using the stator converter to compensate the grid voltage imbalance. The control of DFIG rotor current is not considered. A dual current control scheme which can be employed to

regulate the positive and negative rotor current of the DFIG separately is introduced in [109]. A more detailed control strategy which sets various reference signals for the DFIG under unbalanced grid voltage based on dual current control is explained in [107]. The dual current control can effectively regulate the positive and negative sequence current of DFIG but requires real-time decomposition of variables. The measurement of positive and negative variables is highly dependent on the filtering technique. The complexity of the control system is significantly increased as the variables to be controlled are doubled. The measurement and decomposition of voltage and current in dual reference frame (DRF) also introduces extra error in to the control system.

The major advantage of using dual current control is that the control target can be chosen with high flexibility. The DFIG can be controlled to realize the following control target under asymmetrical grid fault: (i) Balanced stator current. (ii) Constant output power. (iii) Constant electrical torque. (iv) No rotor current oscillation [110]. Although all the above control strategies can be designed, only one control target can be achieved at a time. It is clear that from the wind turbine perspective that the elimination of electrical torque ripple is desired. The dual-current control can be simplified to single current control for the specific control target.

The control of DFIG in single reference frame(SRF) during asymmetrical voltage dip is reported in [111]. A simple band-pass filter is used to reduce the electrical torque oscillation but no theoretical analysis is given. In this chapter, the mathematical analysis of DFIG under asymmetrical grid voltage is presented first. A PI controller to eliminate the high frequency torque oscillation caused by asymmetrical grid voltage is then proposed by the author. It is noticed that both the PI controller and the band-pass filter methods introduce coupling between the rotor voltage control loop and the rotor current control loop. A method to decouple the outer and inner loop

controller to further improve the DFIG control during asymmetrical voltage is described.

5.1 Analysis of asymmetrical electrical system

The method to analyse a symmetrical fault is no longer applicable to asymmetrical system as the three phases can no longer be represented by a one-phase single line diagram. In the case of asymmetrical electrical system, the power system is represented by the superposition of three components: positive sequence, negative sequence and zero sequence components. These three components are symmetrical respectively but with different phases.

A DFIG employs three-phase three-wire system where the zero-sequence component is zero. Only the positive and negative sequences are considered in this chapter. The three phase asymmetrical components can be decomposed into the sum of three symmetrical positive and negative components [112]. Define U as the voltage vector in asymmetrical system. U_a, U_b, U_c are the components of U on each phase. The following relationship can be derived.

$$\boldsymbol{U}_a = \boldsymbol{U}_a^+ + \boldsymbol{U}_a^- \tag{5-1}$$

$$\boldsymbol{U}_b = \boldsymbol{U}_b^+ + \boldsymbol{U}_b^- \tag{5-2}$$

$$\boldsymbol{U}_c = \boldsymbol{U}_c^+ + \boldsymbol{U}_c^- \tag{5-3}$$

where U^+ represents the vector rotating in the positive direction and U^- represents the vector rotating in the negative direction. The positive components are expressed as

$$U_a^+ = U_m^+ \cos\left(\omega t + \varphi_+\right) \tag{5-4}$$

$$U_b^+ = U_m^+ \cos\left(\omega t - \frac{3\pi}{2} + \varphi_+\right) \tag{5-5}$$

$$U_c^+ = U_m^+ \cos\left(\omega t + \frac{3\pi}{2} + \varphi_+\right) \tag{5-6}$$

where U_m^+ is the amplitude of the positive sequence voltage vector and φ_+ is the phase of the positive sequence voltage vector.

Similarly, the negative components are expressed as

$$U_a^+ = U_m^+ \cos\left(\omega t + \varphi_+\right) \tag{5-7}$$

$$U_b^+ = U_m^+ \cos\left(\omega t - \frac{3\pi}{2} + \varphi_+\right) \tag{5-8}$$

$$U_c^+ = U_m^+ \cos\left(\omega t + \frac{3\pi}{2} + \varphi_+\right) \tag{5-9}$$

where U_m^- and φ_- are the amplitude and phase of the negative sequence voltage vector.

Applying Clarke's transformation on above equations, the positive and negative sequence voltage of DFIG in stationary rotating reference frame can be derived.

$$\boldsymbol{U}_\alpha = \boldsymbol{U}_\alpha^+ + \boldsymbol{U}_\alpha^- \tag{5-10}$$

$$\boldsymbol{U}_{\beta} = \boldsymbol{U}_{\beta}^{+} + \boldsymbol{U}_{\beta}^{-} \tag{5-11}$$

Assuming α-axis represents the real part and β-axis represents the imaginary part of the voltage vector, by applying Euler's formula the voltage can be written as

$$U_{\alpha\beta}^{+} = U_{\alpha}^{+} + jU_{\beta}^{+} = U_{m}^{+} e^{j(\omega t + \varphi_{+})} \tag{5-12}$$

$$U_{\alpha\beta}^{-} = U_{\alpha}^{-} + jU_{\beta}^{-} = U_{m}^{+} e^{j(\omega t + \varphi_{-})} \tag{5-13}$$

Assuming the positive sequence voltage rotates with the phase sequence ABC and negative sequence voltage rotates with the phase sequence ACB, which in the dq reference frame is in effect that positive sequence voltage rotates anti-clockwise and negative sequence rotates clockwise, the positive and negative sequence voltage in rotating reference frame can be derived

$$U_{dq}^{+} = U_{\alpha\beta}^{+} e^{-j\theta} \tag{5-14}$$

$$U_{dq}^{-} = U_{\alpha\beta}^{-} e^{j\theta} \tag{5-15}$$

Two reference frames are created for positive and negative voltage respectively. The positive reference frame is assumed to rotate anticlockwise with synchronous speed ω_0 and negative reference frame clockwise with the speed $-\omega_0$. The voltage vector in positive frame can be written as

$$\boldsymbol{U}_{\boldsymbol{dq}} = \boldsymbol{U}_{\boldsymbol{dq}}^{+} + \boldsymbol{U}_{\boldsymbol{dq}}^{-} = U_{dq+}^{+} + U_{dq+}^{-} e^{-j2\omega t} \tag{5-16}$$

A similar relationship can be derived in the negative reference frame

$$\boldsymbol{U}_{\boldsymbol{dq}} = \boldsymbol{U}_{\boldsymbol{dq}}^{-} + \boldsymbol{U}_{\boldsymbol{dq}}^{+} = U_{dq-}^{-} + U_{dq-}^{+} e^{j2\omega t} \tag{5-17}$$

It is shown in equation (5-16) and (5-17) that the asymmetrical (negative sequence) component appears in the positive reference frames as a vector with twice the synchronous frequency. The positive sequence component remains as a constant value. The asymmetrical grid voltage is plotted in positive reference frame in Figure 5-1.

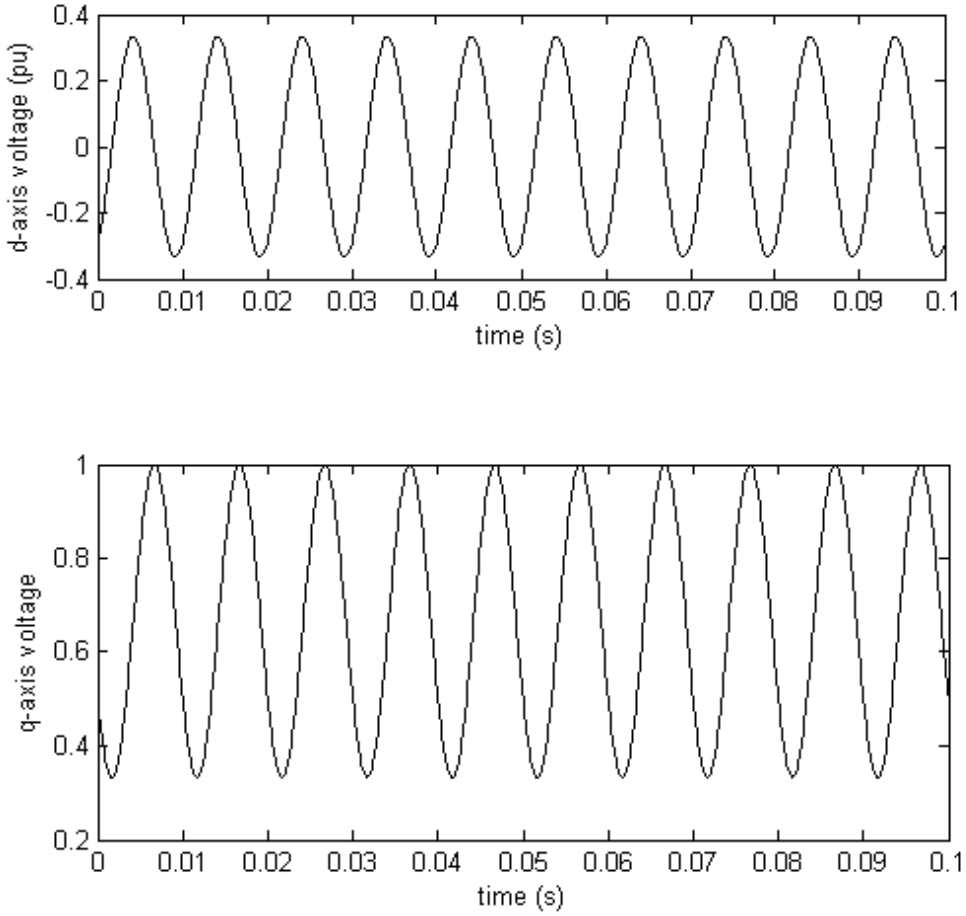

Figure 5-1: Stator voltage in positive dq reference frame under single-phase fault

It is shown in Figure 5-1 that the DC component of the asymmetrical grid voltage is still oriented by voltage. The DC component of q-axis is 0.66 which is due to the loss of one phase voltage and d-axis is 0. The AC component of the asymmetrical grid

voltage exists in the positive reference frame as a sinusoidal wave with twice the grid frequency, which is 100Hz.

5.2 DFIG under asymmetrical voltage

In this section the DFIG is modelled in both the positive and negative reference frame. The positive sequence stator voltage creates positive sequence stator current, which induces positive sequence flux and the negative sequence stator voltage generates negative sequence flux.

In the positive reference frame, the DFIG is modelled as [107, 113]:

$$\psi_{sdq}^{+} = L_s I_{sdq}^{+} + L_m I_{rdq}^{+} \tag{5-18}$$

$$\psi_{rdq}^{+} = L_r I_{rdq}^{+} + L_m I_{sdq}^{+} \tag{5-19}$$

$$U_{sdq}^{+} = R_s I_{sdq}^{+} + \frac{d}{dt}\psi_{sdq}^{+} + j\omega_0 \psi_{sdq}^{+} \tag{5-20}$$

$$U_{rdq}^{+} = R_r I_{rdq}^{+} + \frac{d}{dt}\psi_{rdq}^{+} + j\left(\omega_0 - \omega_r\right)\psi_{rdq}^{+} \tag{5-21}$$

In the negative reference frame, the DFIG model is defined as

$$\psi_{sdq}^{-} = L_s I_{sdq}^{-} + L_m I_{rdq}^{-} \tag{5-22}$$

$$\psi_{rdq}^{-} = L_r I_{rdq}^{-} + L_m I_{sdq}^{-} \tag{5-23}$$

$$U_{sdq}^{-} = R_s I_{sdq}^{-} + \frac{d}{dt}\psi_{sdq}^{-} + j\omega_0 \psi_{sdq}^{-} \tag{5-24}$$

$$U_{rdq}^{-} = R_r I_{rdq}^{-} + \frac{d}{dt}\psi_{rdq}^{-} + j\left(\omega_0 - \omega_r\right)\psi_{rdq}^{-} \tag{5-25}$$

The positive sequence stator current can be derived from (5-18) as

$$I_{sdq}^{+} = \frac{1}{L_s}\left(\psi_{sdq}^{+} + \psi_{sdq-}^{-} e^{-j2\omega_0 t}\right) - \frac{L_m}{L_s}\left(I_{rdq}^{+} + I_{rdq-}^{-} e^{-j2\omega_0 t}\right) \tag{5-26}$$

The stator active and reactive power are given by

$$P_s + jQ_s = \frac{3}{2} U_{sdq}^{+} I_{sdq}^{+} \tag{5-27}$$

Substituting (5-20) and (5-26) into (5-27), the real and reactive power can be written in different oscillating components

$$P_s = P_{s0} + P_{s\sin 2}\sin\left(2\omega_0 t\right) + P_{s\cos 2}\cos\left(2\omega_0 t\right) \tag{5-28}$$

$$Q_s = Q_{s0} + Q_{s\sin 2}\sin\left(2\omega_0 t\right) + Q_{s\cos 2}\cos\left(2\omega_0 t\right) \tag{5-29}$$

where P_{s0} and Q_{s0} are the DC terms of real and reactive power, $P_{s\sin 2}$, $P_{s\cos 2}$, $Q_{s\sin 2}$, $Q_{s\cos 2}$ are the double frequency components of real and reactive power. The frequency is $2\omega_0$.

The oscillating terms in real and reactive power are written in matrix form as

$$\begin{bmatrix} P_{s\sin 2} \\ P_{s\cos 2} \\ Q_{s\sin 2} \\ Q_{s\cos 2} \end{bmatrix} = \begin{bmatrix} U_{sq}^{-} & U_{sd}^{-} & U_{sq}^{+} & U_{sd}^{+} \\ -U_{sd}^{-} & U_{sq}^{-} & U_{sd}^{+} & -U_{sq}^{+} \\ -U_{sd}^{-} & U_{sq}^{-} & -U_{sd}^{+} & U_{sq}^{+} \\ -U_{sq}^{-} & -U_{sd}^{-} & U_{sq}^{+} & U_{sd}^{+} \end{bmatrix} \begin{bmatrix} I_{sq}^{+} \\ I_{sd}^{+} \\ I_{sq}^{-} \\ I_{sd}^{-} \end{bmatrix} = A \begin{bmatrix} I_{sq}^{+} \\ I_{sd}^{+} \\ I_{sq}^{-} \\ I_{sd}^{-} \end{bmatrix} \tag{5-30}$$

Using Leibniz formula, the determinant of matrix A is calculated as

$$\det(A) = -16\left[\left(U_{sd}^{-}U_{sq}^{+}\right)^2 + \left(U_{sd}^{-}U_{sd}^{+}\right)^2 + \left(U_{sq}^{-}U_{sq}^{+}\right)^2 + \left(U_{sq}^{-}U_{sd}^{+}\right)^2\right] \qquad (5\text{-}31)$$

det(A) is nonzero when negative voltage component exists which means A is invertible. Therefore, the formula $\begin{bmatrix} P_{s\sin 2} \\ P_{s\cos 2} \\ Q_{s\sin 2} \\ Q_{s\cos 2} \end{bmatrix} = 0$ has no solution. The double frequency components of real and reactive power cannot be eliminated at the same time.

It can be concluded from (5-28) that without control over $P_{s\sin 2}$ and $P_{s\cos 2}$, the DFIG output power contains component of twice the grid frequency as shown in Figure 5-2.

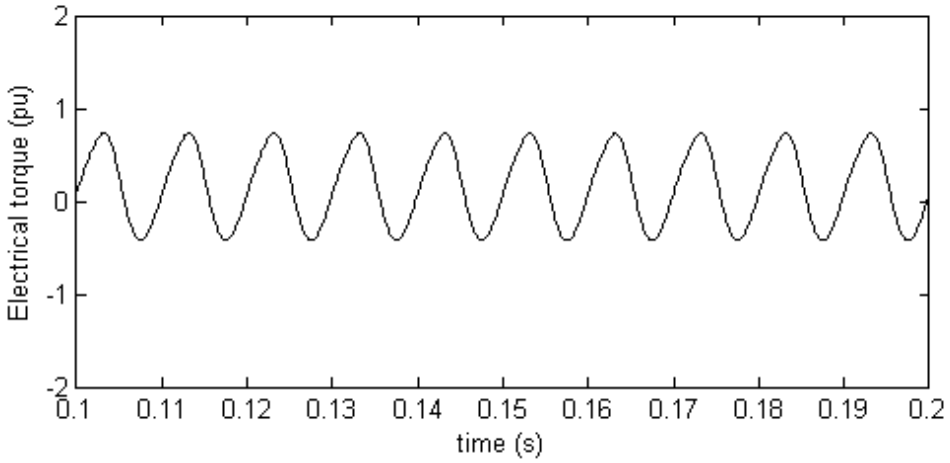

Figure 5-2: DFIG torque control under asymmetrical stator voltage

The rotor real and reactive power of DFIG is calculated by

$$P_r + jQ_r = \frac{3}{2} U_{rdq}^{+} I_{rdq}^{+} \tag{5-32}$$

By substituting equation (5-19) and (5-21) into (5-32) we can get

$$P_r = P_{r0} + P_{r\sin 2} \sin\left(2\omega_0 t\right) + P_{r\cos 2} \cos\left(2\omega_0 t\right) \tag{5-33}$$

$$Q_r = Q_{r0} + Q_{r\sin 2} \sin\left(2\omega_0 t\right) + Q_{r\cos 2} \cos\left(2\omega_0 t\right) \tag{5-34}$$

The torque of the DFIG is given as

$$T_e = \frac{1}{\omega_r}\left(P_s + P_r\right) \tag{5-35}$$

Substituting (5-28) and (5-33) into (5-35)

$$T_e = \frac{1}{\omega_r}\left(P_{r0} + P_{r\sin 2} \sin\left(2\omega_0 t\right) + P_{r\cos 2} \cos\left(2\omega_0 t\right) + P_{s0} + P_{s\sin 2} \sin\left(2\omega_0 t\right) + P_{s\cos 2} \cos\left(2\omega_0 t\right)\right) \tag{5-36}$$

It is possible to control the rotor voltage so that

$$P_{r\cos 2} \cos\left(2\omega_0 t\right) = -P_{s\cos 2} \cos\left(2\omega_0 t\right) \tag{5-37}$$

and

$$P_{r\sin 2} \cos\left(2\omega_0 t\right) = -P_{s\sin 2} \cos\left(2\omega_0 t\right) \tag{5-38}$$

So that equation (5-36) becomes

$$T_e = \frac{1}{\omega_r}\left(P_{r0} + P_{s0}\right) \tag{5-39}$$

Equations (5-37) and (5-38) show that by properly placing the rotor voltage vector, the rotor torque can be controlled to cancel the double frequency oscillation in stator torque.

5.3 Wind turbine asymmetrical fault ride-through controller

An asymmetrical fault is typically characterized by frequent occurrence and long duration compared to a symmetrical fault. Modern wind turbines must be capable to ride-though an asymmetrical fault as well as a symmetrical fault. A DFIG can be controlled to achieve various goals during an asymmetrical fault [107]. Among all the control targets, the ability to generate desired torque is the most crucial requirement for the wind turbine to stay connected during the fault. Compared to dual-current control which is employed in most publications on the asymmetrical FRT of wind turbines, single current control based on existing DFIG controllers has the advantage of reduced complexity and similar performance when the priority is considered to be successful ride-through for the wind turbine. A FRT controller is proposed by the author to minimize the effect of asymmetrical grid voltage on the wind turbine. In this chapter the theoretical basis of the FRT controller is derived first. The controller is described and the simulation results presented. The author discovered that the control of asymmetrical grid voltage would influence the rotor current control loop. Lastly an improved current control loop based on conventional DFIG rotor current controller is explained.

5.3.1 Theoretical analysis

It is derived in Chapter 3 that in a voltage oriented DFIG, the generated electrical torque is

$$T_e = \frac{L_m U_{qs}}{L_s} I_{qr} \tag{5-40}$$

given that $U_{ds} = 0$. To analyse the influence of the varying stator voltage and rotor current, the differential of electrical torque is calculated.

$$\frac{d}{dt} T_e = \frac{L_m}{L_s} \left(I_{qr} \frac{d}{dt} U_{qs} + U_{qs} \frac{d}{dt} I_{qr} \right) \tag{5-41}$$

The simplified DFIG model is introduced in Chapter 3. Substituting (3-47) and (3-48) into (3-56) and (3-57), the following relationship can be derived

$$U_{rd} = R_r I_{rd} + \left(L_r - \frac{L_m^2}{L_s} \right) \frac{d}{dt} I_{rd} - s \left(L_r - \frac{L_m^2}{L_s} \right) I_{rq} \tag{5-42}$$

$$U_{rq} = R_r I_{rq} + \left(L_r - \frac{L_m^2}{L_s} \right) \frac{d}{dt} I_{rq} + s \left[\left(L_r - \frac{L_m^2}{L_s} \right) I_{rd} + \frac{L_m}{L_s} U_{sq}^2 \right] \tag{5-43}$$

The differentiation of rotor current can be separated from (5-42) and (5-43) as

$$\frac{d}{dt} I_{rd} = \frac{1}{\left(L_r - \frac{L_m^2}{L_s} \right)} \left(-R_r I_{rd} + U_{rd} \right) - s I_{rq} \tag{5-44}$$

$$\frac{d}{dt}I_{rq} = \frac{1}{\left(L_r - \frac{L_m^2}{L_s}\right)}\left(-R_r I_{rq} + U_{rq}\right) - s\left(I_{rd} + \frac{L_m}{L_s L_r - L_m^2}U_{sq}\right) \quad (5\text{-}45)$$

Substituting (5-45) into (5-41) we can get

$$\frac{d}{dt}T_e = \frac{L_m}{L_s}\left(I_{rq}\frac{d}{dt}U_{sq} - \frac{R_r I_{qr} U_{sq}}{\left(L_r - \frac{L_m^2}{L_s}\right)} + \frac{U_{sq}\left(U_{rq} - s\left(I_{rd} + \frac{L_m}{L_s L_r - L_m^2}U_{sq}\right)\right)}{\left(L_r - \frac{L_m^2}{L_s}\right)}\right) \quad (5\text{-}46)$$

The torque of DFIG under asymmetrical stator voltage can be written as

$$T_e = T_{e0} + T_{e2} \quad (5\text{-}47)$$

Defining T_{e0} as the DC term in electrical torque and T_{e2} as the AC term in electrical torque, we get $\frac{d}{dt}T_{e0} = 0$. Substituting (5-46) into (5-47)

$$\frac{d}{dt}T_{e2} = \frac{L_m}{L_s}\left(I_{rq}\frac{d}{dt}U_{sq} - \frac{R_r I_{rq} U_{sq}}{\left(L_r - \frac{L_m^2}{L_s}\right)} + \frac{U_{sq}\left(U_{rq} - s\left(I_{rd} + \frac{L_m}{L_s L_r - L_m^2}U_{sq}\right)\right)}{\left(L_r - \frac{L_m^2}{L_s}\right)}\right) \quad (5\text{-}48)$$

Equation (5-48) expresses the torque oscillation caused by asymmetrical grid fault in terms of DFIG stator and rotor current and voltage.

In equation (5-48), U_{sq} is the stator voltage, which is uncontrollable. I_{rq} and I_{rd} are controlled by U_{rq} and U_{rd} respectively to follow the torque and reactive power reference. Therefore, the oscillating term in the electrical torque of the DFIG can be controlled to the desired value by manipulating the rotor voltage U_{rq} and U_{rd}. The d-axis rotor current exists in (5-48) due to the coupling between d and q axis rotor

current. The term, which contains I_{rd} is very small compared to the overall torque. The double frequency torque can be controlled using only q-axis rotor voltage by neglecting the coupling of rotor winding.

5.3.2 Controller design

The controller to eliminate the double frequency torque of the DFIG under asymmetrical voltage is shown in Figure 5-3. The controller works as an auxiliary loop attached to the original DFIG torque controller. G (ω) is a band-pass filter centred on the double frequency of synchronous speed. The filter has the form of

$$G(\omega) = \frac{s^2 + 2\frac{d}{c}\omega_0 s + \omega_0^2}{s^2 + 2\frac{1}{c}\omega_0 s + \omega_0^2} \tag{5-49}$$

where ω_0 is the doubled frequency, d and c are adjusted to limit the gain and bandwidth of the filter.

The double frequency component is separated from the original torque first. A PI controller is employed to regulate the double frequency torque oscillation to reference value, which is 0. The PI controller produces a compensation signal, which is added to the rotor voltage which is controlled to produce desired torque.

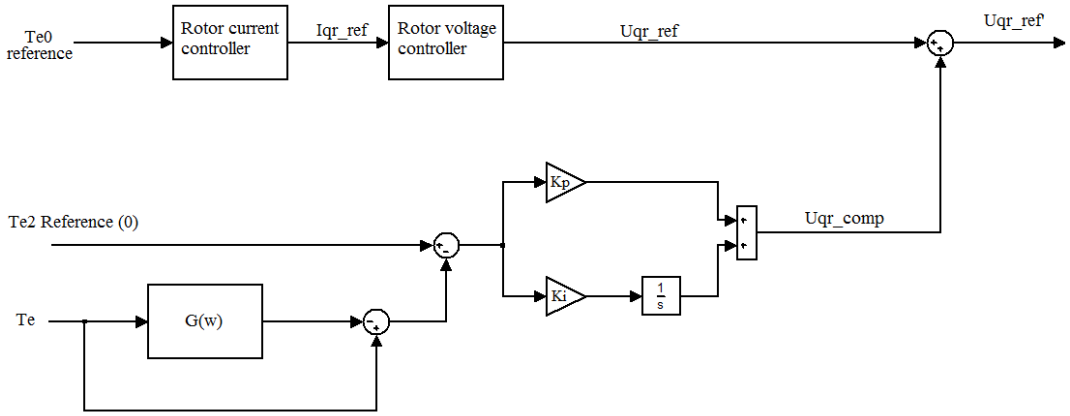

Figure 5-3: DFIG control under asymmetrical stator voltage

The DFIG torque under unbalanced grid voltage is shown in Figure 5-4. The grid is experiencing a single-phase-to-ground fault as illustrated in Figure 5-1. The result shows that with the proposed asymmetrical fault ride-through controller, the DFIG torque is controlled to reference value. The double frequency torque oscillation is almost completely eliminated.

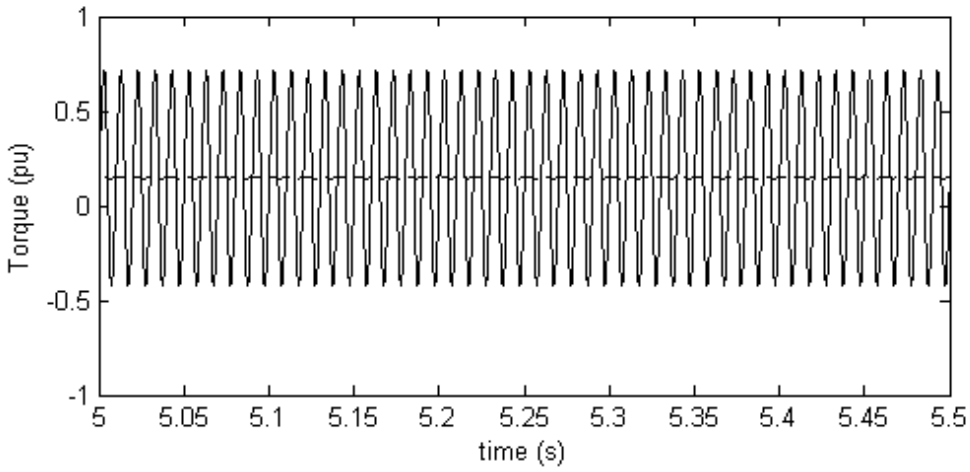

Figure 5-4: DFIG torque with and without asymmetrical fault ride-through control Solid line: DFIG with conventional controller. Dashed line: DFIG with proposed controller

5.3.3 Decoupling between current control loop and double frequency disturbance

The asymmetrical FRT controller employs the rotor voltage to damp the oscillation caused by grid voltage imbalance. It is clear that the original DFIG torque control is influenced by the additional control signal. Assuming the DFIG rotor voltage changed caused by FRT controller is ΔU_r, the rotor current change is

$$\Delta I_r = \frac{1}{R_r + \left(L_r - \frac{L_m^2}{L_r} \right) s} \Delta U_r \tag{5-50}$$

The gain between rotor current and rotor voltage is

$$K_r = \frac{\Delta I_r}{\Delta U_r} = \frac{1}{\sqrt{R_r^2 + \left[\left(L_r - \frac{L_m^2}{L_r} \right) \omega \right]^2}} \tag{5-51}$$

The DFIG current controller sees the damping torque induced by ΔU_r as a disturbance. To regulate the damping torque, the reference rotor voltage is changed from U_{r_ref} to $U_{r\_ref} + \Delta U_{r\_ref}$. Defining the current control loop gain as K_{ic}, the rotor voltage deviation caused by FRT controller can be calculated as

$$\Delta U_{r\_ref} = \Delta I_r * K_{ic} \tag{5-52}$$

Combining (5-50) to (5-52) we can get

$$\Delta U_{r\_ref} = \Delta U \left(1 - K_r K_{ic} \right) \tag{5-53}$$

Equation (5-53) shows the coupling effect between the proposed FRT controller and the original DFIG torque control loop. It can be seen that the DFIG controller weakened the effect of FRT controller and the FRT controller affects the DFIG torque controller when in action.

The negative influences that original the DFIG controller and FRT controller have on each other can be removed by decoupling these two controllers. It is noticed that the torque variation has a fixed frequency, which is twice the synchronous frequency. The control signal generated to reduce the torque oscillation is also fixed to the double grid frequency as a consequence. The double-frequency rotor voltage disturbance causes rotor current oscillation at the same frequency. The oscillating component in the rotor current is removed before feeding back to the rotor current controller to eliminate the influence that the oscillating rotor current has on rotor the current controller. A notch filter is added to the rotor current feedback loop. The filter passes all frequencies except the signal near double the grid frequency. As the grid frequency is rather high compared to the wind turbine torque variation, the wind turbine torque control is not influenced. The modified controller is plotted in Figure 5-5.

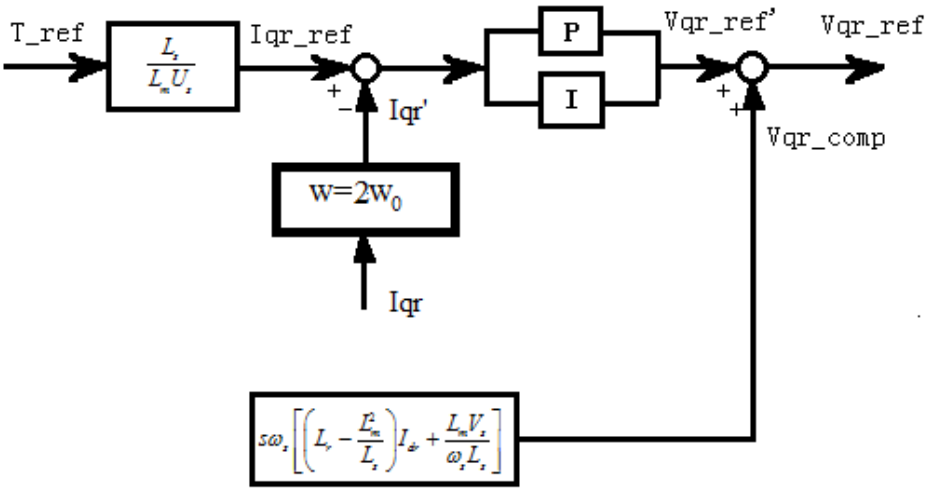

Figure 5-5: Decoupled torque controller for DFIG asymmetrical FRT as described in Section 4.3.3

The filtered q-axis current does not contain the high frequency oscillation which means K_{ic}=0. The rotor voltage reference deviation is $\Delta U_{r\_ref} = 0$ according to (5-53). The simulation of the DFIG torque with and without decoupled control is compared in Figure 5-6. A single phase fault occurs at 2 second at the end of the generator stator and the resulted electrical torque is illustrated.

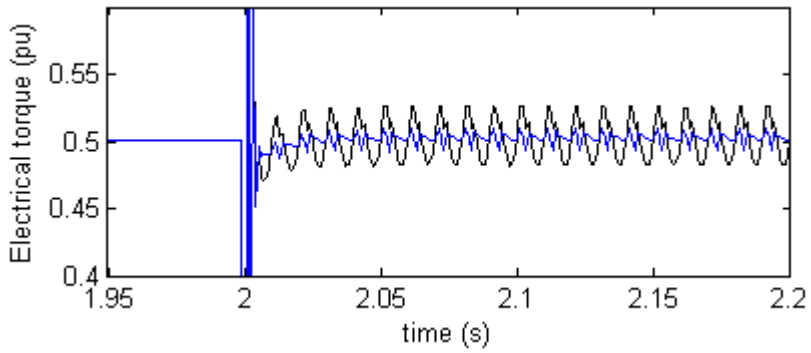

Figure 5-6: Comparison of DFIG torque with and without decoupled rotor current Black line: without decoupled rotor current. Blue line: with decoupled current

It is shown in Figure 5-6 that the removal of the high frequency rotor current oscillation from the torque control loop can suppress the electrical torque variation. The double frequency torque oscillation is further reduced compared to a DFIG without the decoupling of the FRT controller and original controller.

5.4 Summary

The wind turbine is subjected to torque oscillation of double the grid frequency when experiencing asymmetrical grid voltage. The life-time of the wind turbine, especially drive-train, is significantly influenced without appropriate control on the asymmetrical voltage. In this chapter, the effect of asymmetrical grid voltage on the DFIG was discussed first. The existing control of asymmetrical grid voltage on the DFIG was reviewed. It is discovered that both SRF and DRF control can successfully reduce the torque oscillation induced by asymmetrical grid voltage. The SRF is easier to implement on current DFIG controller.

It is noticed that the SRF asymmetrical voltage control is coupled to the existing DFIG controller. The DFIG controller is affected by the asymmetrical voltage controller, while the effect of asymmetrical voltage controller is weakened by the DFIG controller. The author presents a decoupled asymmetrical voltage controller, which is decoupled from the original DFIG control loop. The performance of this controller is shown to be improved from the original SRF asymmetrical voltage controller for DFIG.

CHAPTER 6: A MULTIBAND POWER SYSTEM STABILIZER FOR DFIG-BASED WIND FARM

6.1 Introduction

The tendency of the modern power system to exhibit oscillatory instability is increasing. The use of high performance exciters is effective in improving the transient stability of the power system. At the meantime, negative damping is introduced by the action of exciters which affects the small-signal stability associated with local plant modes of oscillation [62]. The conventional method to solve such problem is by incorporating a power system stabilizer on large conventional synchronous generation plant.

Accompanying the increase of wind power penetration, the proportion of conventional plant in the power system is reducing continuously. Current commercial wind turbine design does not include the function of providing damping to the power system. Power system stability strongly depends on the damping provided by the PSS. To further increase the penetration of wind power, the wind turbine design must be modified so that it is able to provide damping against power system oscillation.

A PSS for DFIG-based wind turbine is proposed in [74]. The basic PSS function is realized by adding an auxiliary loop in the DFIG rotor voltage control loop. The comparison of different types of PSS with different input signals for wind energy generation is introduced in [114] and [115]. A minor control loop is proposed as a simplified PSS in [116]. Some publications focus on the inter-area oscillation mode damping rather than local oscillation [117-119]. The tuning of a PSS for wind turbine is also well discussed in [120-122].

Almost all the above publications only consider the interaction between a DFIG and the power system. The PSS is set for local power system oscillation modes or inter-area oscillation modes so that the electromechanical oscillation of all frequencies in the power system can be suppressed. The interaction between the DFIG and the mechanical system of the wind turbine is not examined. The oscillatory mode of wind turbine structure is also ignored. To the author's knowledge, the effect of a PSS on wind turbine drive-train and blade damping is only discussed in [123]. However, the paper focuses more on the parameter selection rather than the design of PSS. Several high-pass and band-pass filters are combined to act as a PSS.

This chapter proposes a multi-band PSS based on PSS4b type in IEEE PSS family [124]. The multiband PSS has two channels, one providing damping to power system oscillation and one increasing wind turbine structural damping. Firstly, the conventional PSS is introduced. Then the concept of multi-band PSS is introduced and the characteristic of the proposed PSS is investigated by frequency domain analysis. The proposed PSS for a DFIG-based wind turbine is then tested by a case study. The damping improvement provided by the proposed PSS to both the wind turbine and the power system is shown in this section.

6.2 Basic PSS concept

A PSS is an automatic control device on synchronous generator excitation system. The action of a PSS is to improve the stability of synchronous generator by providing supplementary damping to the rotor oscillation of synchronous machine. The synchronous generator excitation system is normally designed to have a high gain and fast response characteristic. The transient stability is improved by the fast excitation control but the small signal stability is decreased at the same time. A PSS positively contributes to the small signal stability of the synchronous generator by

generating an electrical torque, which is in phase with the rotor speed variation. The swing of rotor angle is limited by the torque, which provides additional damping to the generator system. In a power system, the rotor angle swing can occur within a wide frequency range [125]. The typical frequency range desired for a PSS is 0.2 to 2.5Hz [126].

Most PSS concepts are based on phase-lead and phase-lag compensation. The goal of a PSS is to behave as a pure gain between electrical torque and rotor speed variation. As the excitation system and synchronous generator systems are not linear, there is a phase difference between generator torque and speed. As a result, adjusting phase compensation to eliminate this phase difference is the main task for PSS. Active voltage regulation also introduces considerable phase-lag to the system. The PSS is normally tuned to compensate such phase-lag as well.

The input signal for a PSS can take various forms including rotor speed, grid frequency, active power and accelerating power. There is no essential difference in using a different input for the PSS. The choice of PSS input signal is made considering the transducer performance available.

A typical phase lead-lag type PSS is illustrated in Figure 6-1. There are 3 blocks in the diagram: Gain, wash-out and lead-lag compensation.

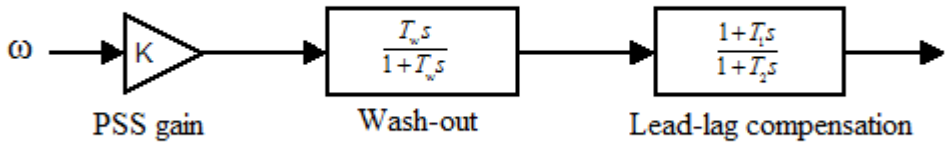

Figure 6-1: Basic PSS structure

The gain block determines how much damping is introduced by the PSS. The gain is limited by the generator parameters. It is commonly set to achieve the maximum damping. However, there is usually an output limit on the PSS to prevent the action of PSS from interfering with the transient response of the excitation system. The PSS damping level is further limited.

The wash-out block is to limit the extreme low frequency variation. The block is essentially a high-pass filter. The steady-state change of the rotor speed is removed and the rotor oscillation in the frequency of interest is passed.

The lead-lag compensation block employs different time constants to adjust the frequency characteristic of the PSS. The phase compensation amount is tuned according to the frequency response of the target power system. Large power systems normally contain several oscillation modes so compromises must be made in practice. More than one lead-lag compensation block can be employed to increase the flexibility of the tuning of the PSS.

6.3 Multi-band PSS for wind turbine

6.3.1 Influence of single-band PSS on wind turbine

The PSS design for power system stability improvement has been well discussed and developed. Various implementation guidelines and tuning methods are reported for a PSS to achieve the best damping against power system oscillation [121, 127, 128]. Implementation of a PSS with different forms such as a PI controller and adaptive control can be found in the literature [129-131]. It is proposed in many publications to implement conventional PSS concepts directly on a wind turbine with DFIG or PMG systems [74, 132, 133]. The damping on power system oscillation modes is as good as the PSS on a synchronous generator. However, the difference between a

wind turbine and steam turbine is that a wind turbine is more expensive and fragile to fatigue loads. Since the PSS manipulates generated torque to provide grid service, wind turbine structural loads result. It is controversial if increasing power system damping at the cost of increased wind turbine loads is worthwhile.

The classic PSS concept is not able to provide accurate damping over a wide range of frequencies. When conventional a PSS is implemented on a wind turbine, the dynamics from the wind turbine rotor speed to torque is modified, especially at the frequency of the PSS. The steady-state operation is influenced. The start-up of the wind turbine with and without PSS is illustrated in Figure 6-2. The PSS has the same structure and tuning as described in [74]. Clearly the wind turbine dynamics are changed by the PSS. The phase difference introduced by the PSS caused the wind turbine torque not to change according to the rotor speed in the manner that the wind turbine controller is designed for. The wind turbine deviates from the optimum operation curve and the maximum power extraction is affected. The transient response of wind turbine during disturbances such as wind gusts or grid faults may also be affected when the frequency is within the PSS frequency range.

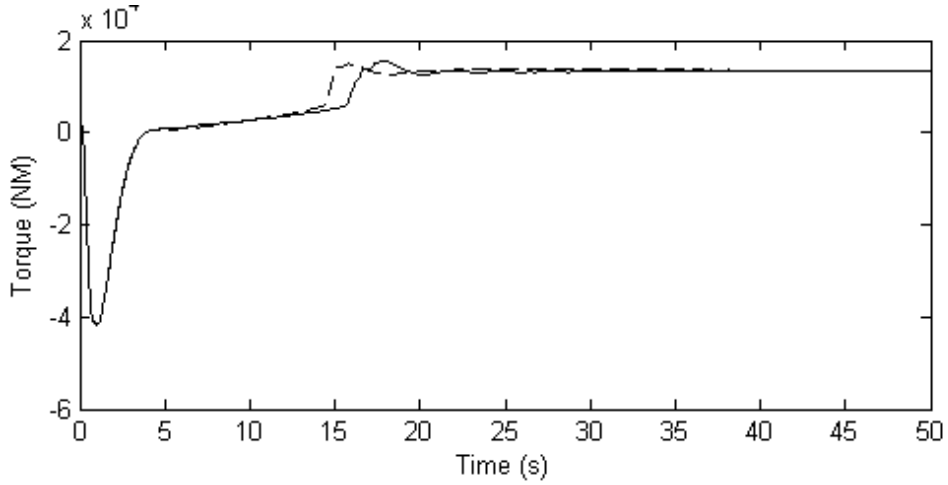

(a)

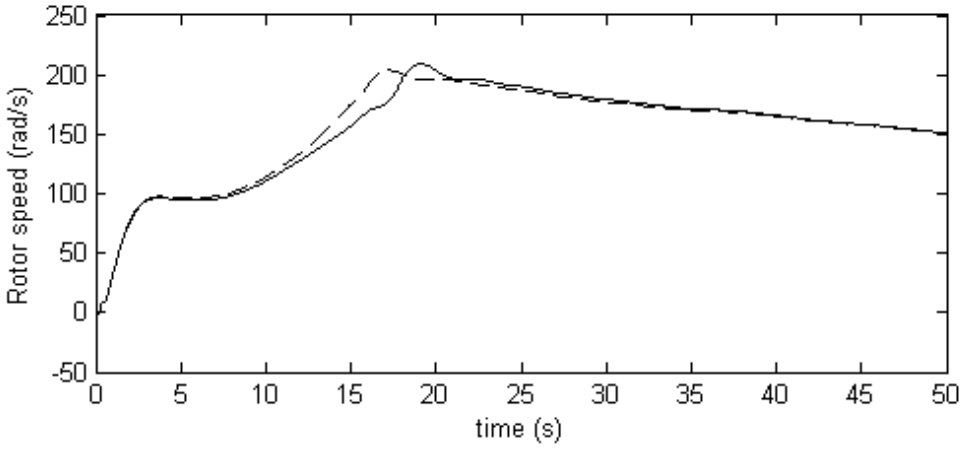

(b)

Figure 6-2: Wind turbine start-up (a) Reaction torque with and without PSS (b) Rotor speed with and without PSS

Solid line: Without PSS (optimal operation curve). Dashed line: With PSS

To avoid the PSS affecting wind turbine controller, a more efficient and possibly complex PSS concept must be designed for the wind turbine to provide a stabilizing contribution to grid.

6.3.2 Multi-band PSS design and modelling

The proposed multi-band PSS is based on the fact that power system oscillation modes and wind turbine structural loads are of different frequency ranges. The proposed PSS aims to achieve the precise control on the frequency that is under the effect of the PSS. The PSS is expected to provide multi-mode damping instead of generalized damping on all modes as conventional PSSs do.

The block diagram of the proposed multi-band PSS is shown in Figure 6-3. The structure of the multi-band PSS is based on IEEE PSS4b with modification.

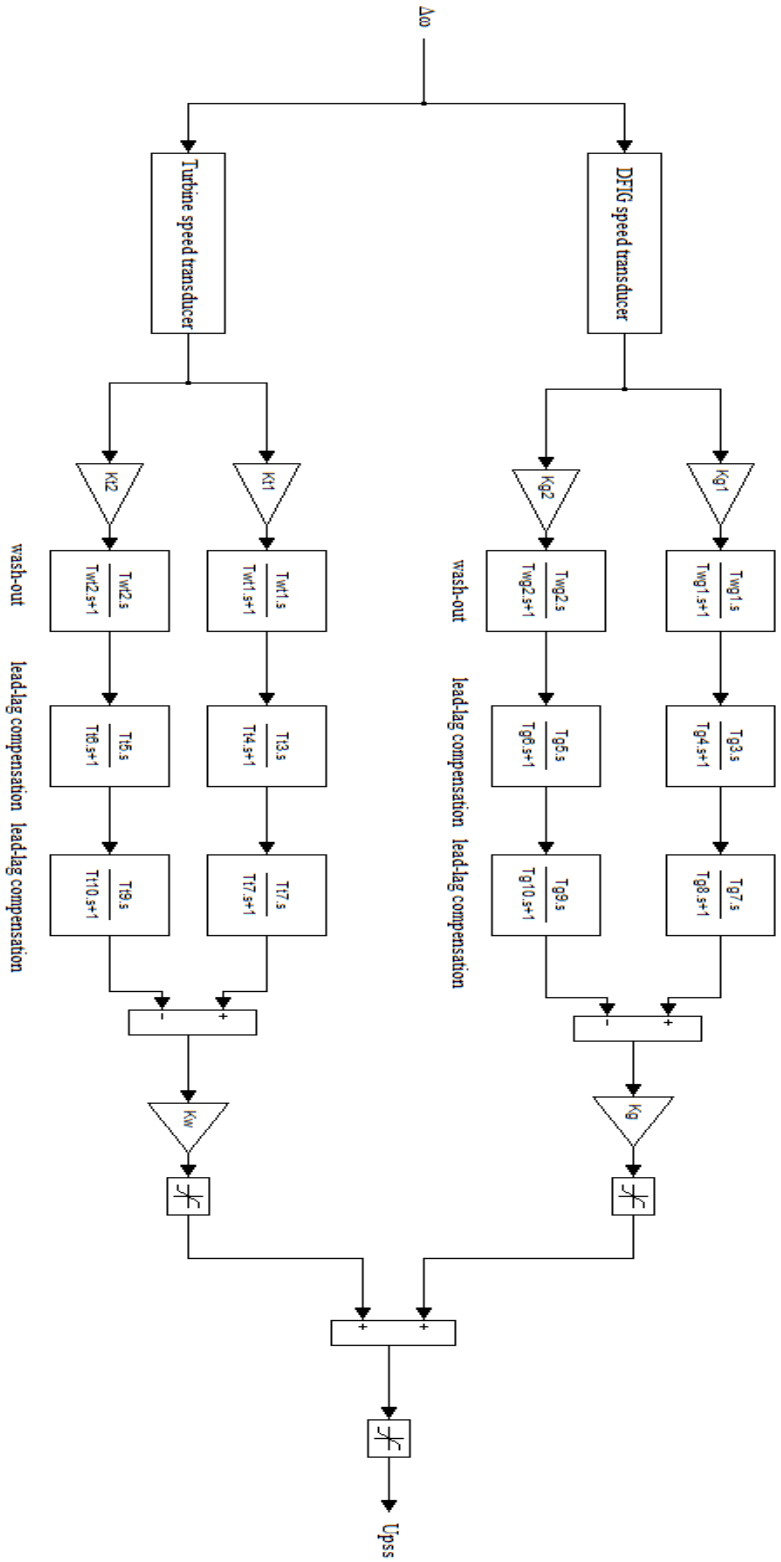

Figure 6-3: Block diagram of the multi-band PSS for wind turbine

There are two separate bands shown in the block diagram of the proposed PSS. The lower band is set at the power system oscillation mode. The upper band is set at the wind turbine drive-train mode. Many other modes exist in power system and wind turbine dynamics. These two major modes are taken as an example to introduce the concept of the multi-band PSS. The number of bands of the proposed PSS can be adjusted to deal with multiple oscillation modes.

To correctly implement the PSS, knowledge of the frequency response of the target power system and wind turbine is preferred. The rotational speed of the wind turbine high speed shaft is chosen as the input signal to the PSS as both the oscillations in the power system and the wind turbine mechanical components induce changes the input signal. A separated speed transducer can be mounted on wind turbine and generator shaft. A synthesized speed transducer is also acceptable when the measurement is not required to be very accurate, given that the input components within the frequencies of interest can be measured unchanged.

The PSS function is achieved by a series of cascaded lead-lag compensation blocks. The input signal goes through a wash-out block first so that the steady-state change of the rotor speed is not affected. The first pair of the lead-lag compensation blocks serves as a band-pass filter with phase compensation. The time constants define the frequency range where the damping on the speed oscillation is increased. The second pair of lead-lag compensation blocks is optional. The section can be used to further differentiate the behaviour of the PSS. For example, the signal in a specific frequency range can be enhanced or bypassed. When the modes of two wind turbine components are very close in frequency, the second lead-lag compensation block can be tuned to further improve the damping at that frequency based on the effect of the first lead-lag block.

An output limiter is placed before the output of the PSS. Different limits can be set separately for each wind turbine and DFIG. The PSS output limit for a wind turbine should ensure that the damping torque is not too large to affect the power tracking or speed regulation of the wind turbine. The limit for the DFIG should be set so that the PSS signal does not interact with the AVR signal. In the worst case the interaction between these two signals can lead to negative damping [62]. The conceptual diagram of the proposed PSS is plotted in Figure 6-4.

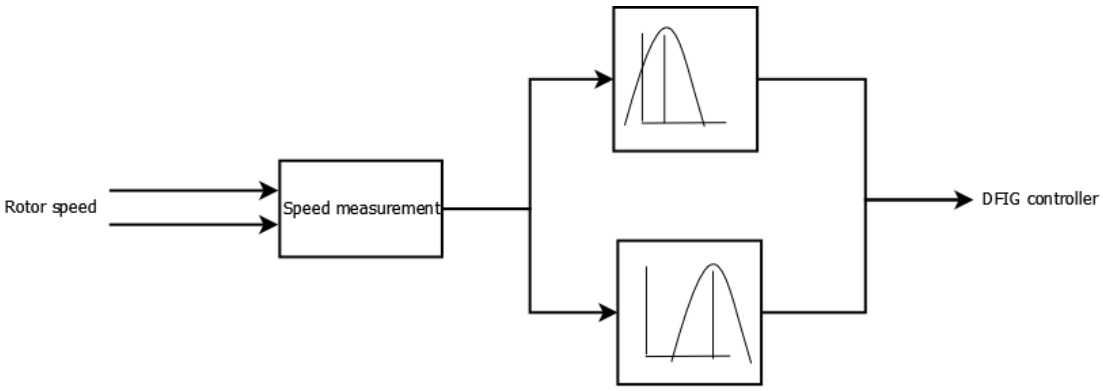

Figure 6-4: Conceptual block diagram of multi-band PSS

The rotor speed is measured as the input to the PSS. The rotor speed signal is processed by two band-pass filter to generate the negative feedback signal for the DFIG controller.

The PSS is integrated in the DFIG torque controller as an auxiliary control loop. The block diagram of the DFIG torque controller with PSS is shown in Figure 6-5. The PSS control signal is applied to the rotor voltage control loop directly to simulate the structure of conventional PSS for synchronous generator.

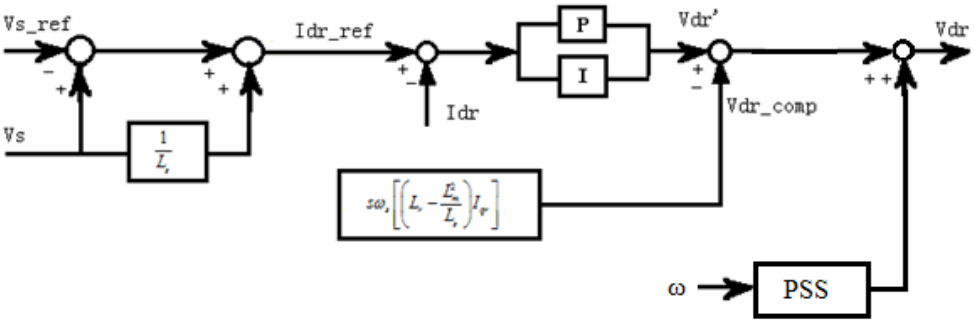

Figure 6-5: DFIG torque control including PSS

6.3.3 Frequency response analysis

The frequency response of the PSS and each band is shown in Figure 6-6. The PSS is tuned for a power system with an oscillation frequency of about 0.1Hz. The wind turbine connected to the power system is assumed to have a drive-train frequency of 1.5Hz, which is a typical value for a 2MW wind turbine. The same PSS gain is applied to both bands. In practice, the gain for each band of the PSS can be set flexibly according to the damping needed for the power system and the wind turbine drive-train.

The gain of each band is centred at the frequency to be damped. The symmetrical attenuation of the gain ensures that both low frequency and high frequency signals are not influenced by the PSS. The band for power system damping provides zero phase lead on its own. However, the band for wind turbine damping improved the phase lag at this frequency. The multi-band PSS is able to provide 45-degree phase lead at the power system oscillation frequency. The cut-off frequency for the PSS is recognized to be 0.076Hz and 1.83Hz. The result shows that the PSS only responds

to the frequency of interest. The gain of the PSS rapidly attenuates outside this frequency rang.

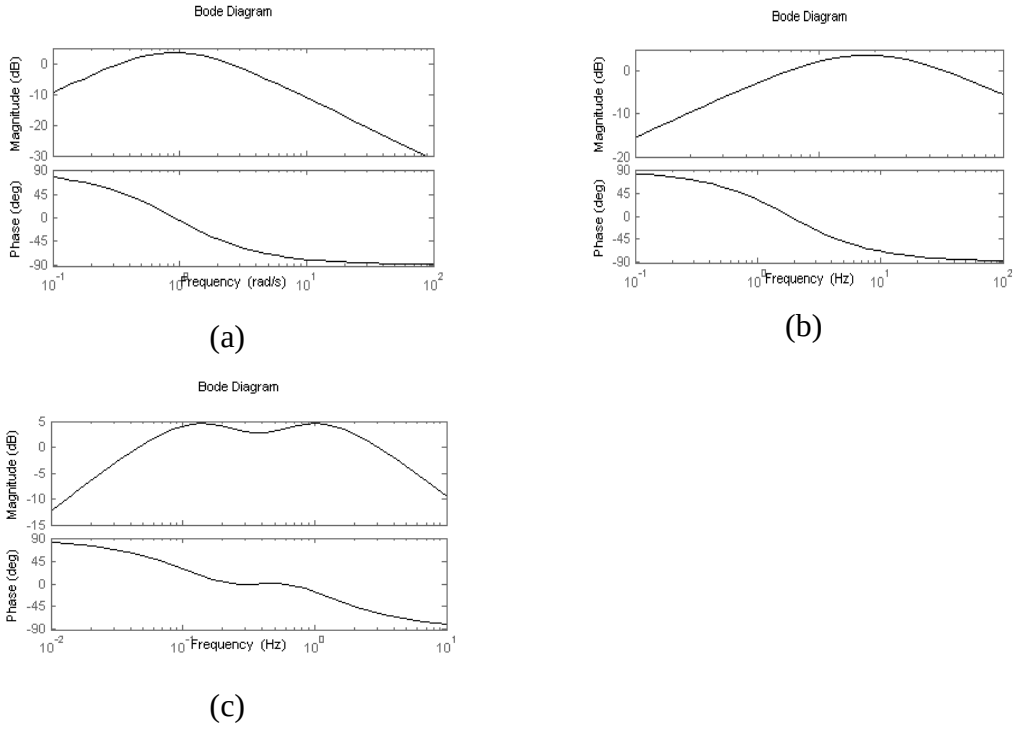

Figure 6-6: Frequency response of the multi-band PSS (a) Power system channel. (b) Wind turbine channel. (c) Combined response

The Bode plot of the conventional PSS type is shown in Figure 6-7 for comparison. The PSS comprises a wash-out block and a lead-lag block as introduced in Figure 6-1. This type of PSS shows the characteristic of a low-pass filter. The low frequency speed variation is amplified which is undesired. The gain decreases rapidly with the frequency increasing. This means that to gain appropriate damping on the power system oscillation mode, the damping on the wind turbine oscillation mode is sacrificed. We can conclude from the frequency response analysis that the characteristic of the conventional PSS is not suitable for the wind turbine. The wind turbine operation in steady state is deteriorated and the damping of the wind turbine mechanical load is attenuated.

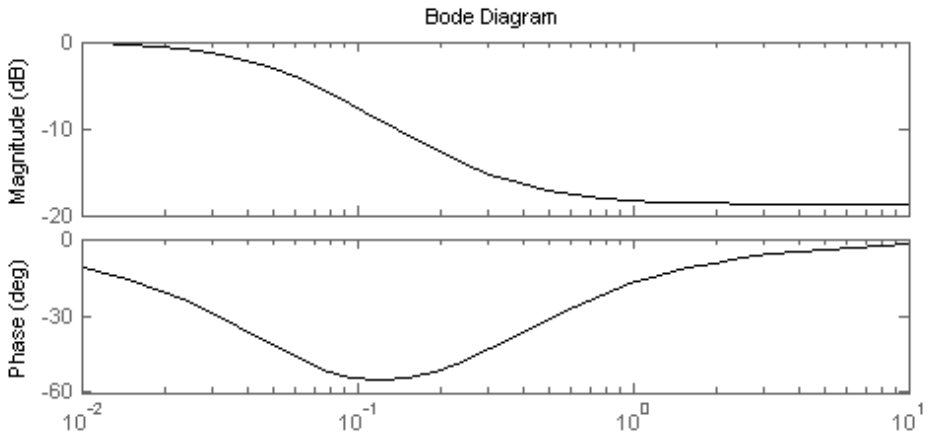

Figure 6-7: Frequency response of conventional PSS

6.3.4 Simulation result

6.3.4.1 Damping on power system oscillation

The proposed multi-band PSS is tested with the wind turbine and generic network model introduced in Chapter 3. The PSS is re-tuned according to the dynamics of the power system and the wind turbine. The PSS is installed in the DFIG wind turbine model, which represents the lumped Scottish wind farms. A symmetrical fault for is applied for 150 ms at the terminals of generator 3. The power oscillations in the power system with different PSS concepts are compared in Figure 6-8.

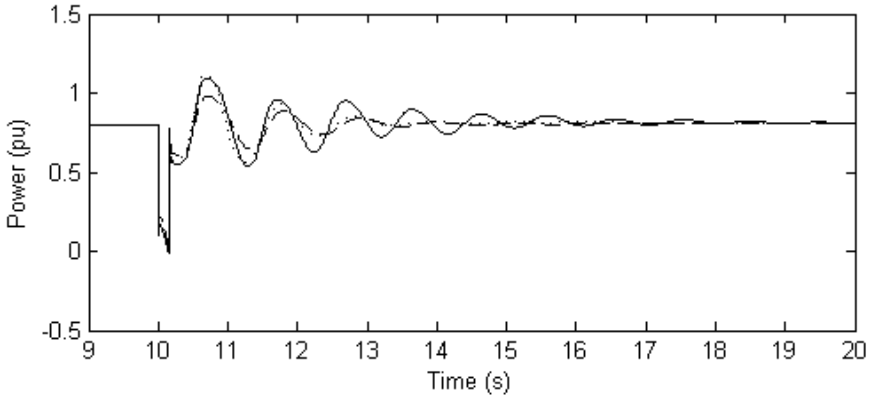

(a)

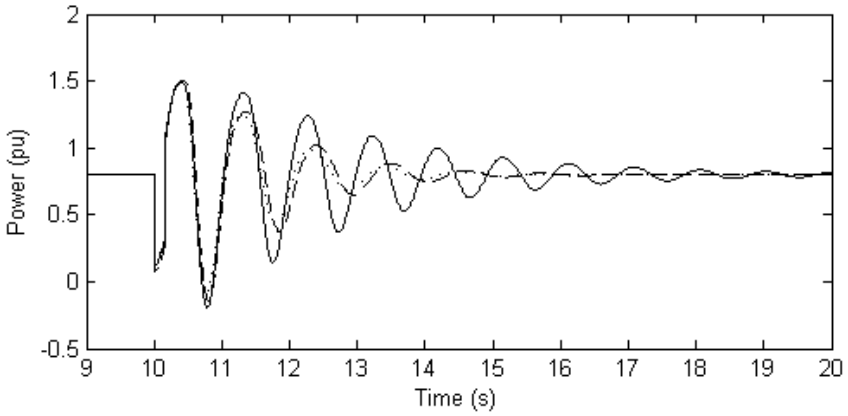

(b)

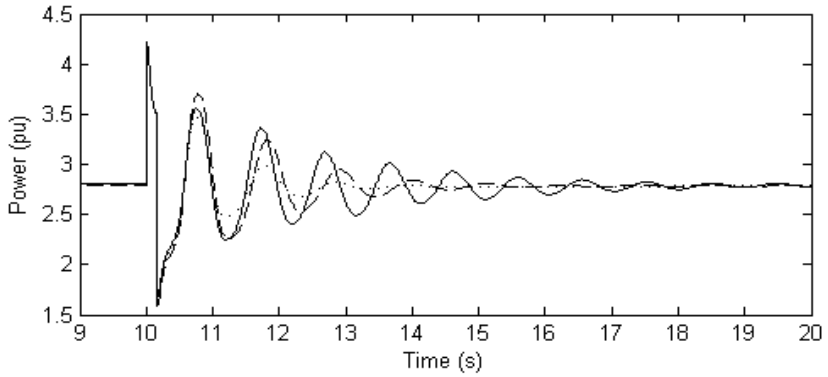

(c)

Figure 6-8: Power oscillation during fault (a) Scottish wind farm (b) Scottish conventional power plants (c) England &Wales power system

Solid line: No PSS on wind farm. Dashed line: single-band PSS on wind farm

Dotted line: multi-band PSS on wind farm

It is shown in Figure 6-8 that the multi-band PSS provides an equivalent amount of damping as a single-band PSS. The multi-band PSS performs similarly to the single-band PSS in terms of DFIG local damping. It is visible that the conventional single-band PSS responds with a time delay due to the phase lag it introduces to the system while the multi-band PSS responds immediately to the speed change. The result of the phase lag is shown more clearly in the power pattern of the main system (Figure 6-8c). The effect of the phase difference is amplified in the remote power system, causing the power oscillation duration to be extended. The multi-band PSS has an improved phase characteristic compared to the single-band PSS owing to the phase compensation provided by the additional band.

6.3.4.2 Damping on wind turbine drive-train

The damping improvement of the proposed PSS on the wind turbine drive train is illustrated in Figure 6-9. A grid fault occurs at 100 seconds. The electrical control is lost during the fault while the wind turbine controller functions as normal. The DFIG reaction torque is lost for 150ms. The wind turbine rotating speed and torque is shown.

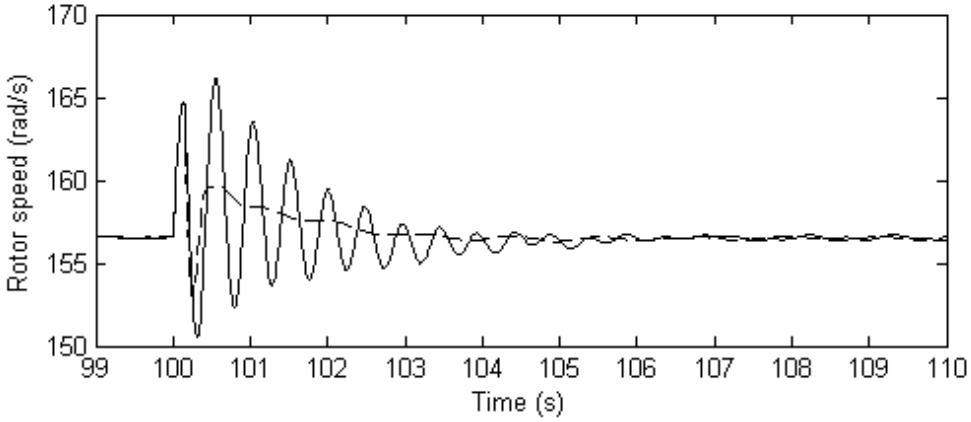

(a)

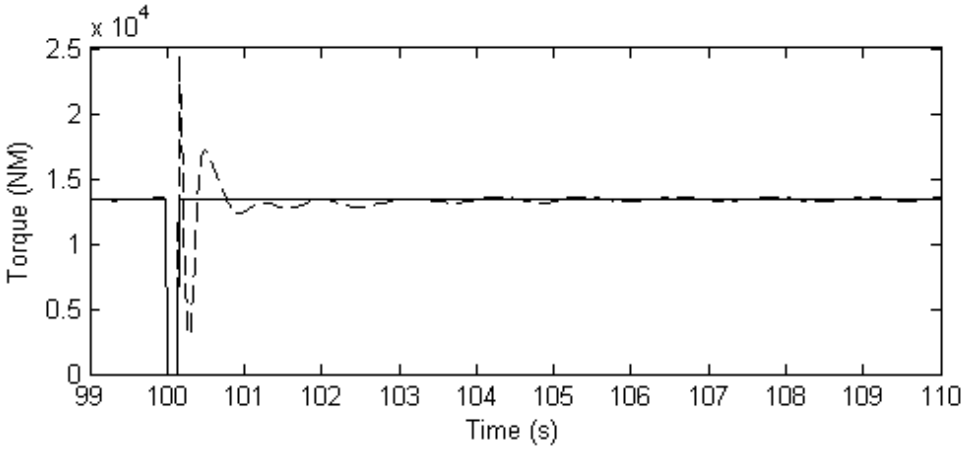

(b)

Figure 6-9: Multi-band PSS on wind turbine (a) Wind turbine rotor speed during fault (b) Wind turbine torque during fault

Solid line: without PSS. Dashed line: with Multi-band PSS

The improvement of the drive-train damping is clearly shown in the simulation result. The drive-train damping is increased substantially. The high frequency drive-train oscillation is significantly suppressed. The low-frequency speed control is barely affected. The damping is achieved at the cost of extra mechanical torque. However, the torque pulsation is not excessive in magnitude and only lasts for less than one second.

6.4 Summary

The PSS for a DFIG has been reported in several publications. However, the PSS design only focuses on increasing the damping to the power system, the mechanical damping of the wind turbine is not considered. A multi-band PSS concept for wind turbines is presented in this chapter. This type of PSS is able to produce damping to both wind turbine structural loads and various power system oscillation modes. This is helpful in terms of fatigue alleviation for large capacity wind turbines and large-scale integration of wind power.

The structure of the multi-band PSS is presented in this chapter. The PSS is designed to have multiple channels with each channel focusing on one oscillation model. With appropriate tuning, the PSS can accurately damp various oscillation frequencies existing in the power system and wind turbine mechanical system. The PSS provides a synthesis solution for the damping of the wind turbine and the power system. The combined analysis of the damping on the wind turbine mechanical load and electrical load is enabled.

CHAPTER 7: CONCLUSIONS AND FUTURE WORK

7.1 Conclusions

DFIG control strategies to improve the compatibility between a DFIG-based wind turbine and the power system under various conditions are developed in this thesis. Both the mechanical structure and the electrical equipment of the wind turbine are affected during grid disturbance. However, these two issues are often studied separately. This thesis contributes to the existing literature by providing a synthesized analysis of the fault ride-through and grid support of wind turbine considering both the generator protection and the mechanical load alleviation. The novelty and contribution of this thesis is summarized as follows:

- A holistic model including wind turbine mechanical dynamics, DFIG and power system is established in Chapter 3. The mathematical model of the DFIG-based wind turbine provides the baseline for FRT strategy design. The implementation of the model in Simulink enables the investigation of the interaction between wind turbine and electrical system. The exemplar SUPERGEN 2MW wind turbine model with controller is shown to be able to follow the operational curve for both below and above rated wind speed. The wind turbine dynamics presented by the mechanical model enabled the observation of the performance of the FRT controller. The DFIG model defines the electrical characteristic of the generator and the limitation on DFIG to ride-through grid fault. The power system model aims to represent the UK grid by lumped synchronous generator model and appropriate excitation system. The effect of wind farm operation on power system stability can be observed using this model.

- The fault ride-through during a short-term symmetrical fault for wind turbine is assessed in Chapter 4. A FRT strategy based on variable rotor resistance control is proposed. The FRT scheme employs an external rotor resistor to achieve wind turbine torque control during and after the grid fault. The rotor over-current which leads to generator shut down is limited by the incorporated resistor. The fast control over DFIG reaction torque is gained by controlling the resistance of the rotor. The problem of drive-train oscillation and rotor speed-up is solved with the proposed FRT strategy. A dynamic tuning method for the wind turbine drive-train damper to further enhance the wind turbine drive-train damping is reported. The damping of the wind turbine drive-train is adjusted according to the fault level. The drive-train damping is enhanced during the fault condition while the normal operation of wind turbine is not affected. A pitch filter to reduce the redundant pitching action due to grid faults is proposed. The blade pitching resulted from the wind turbine controller trying to reduce the torque variation caused by the grid fault but action is limited. The excessive load on the wind turbine blades during the grid fault is reduced using the pitch filter.

- A FRT strategy for DFIGs during asymmetrical grid faults is reported in Chapter 5. The FRT strategy is based on the existing DFIG controller, which avoids the implementation of a new controller in the dual reference frame. The controller employs DFIG rotor voltage compensation to suppress the double frequency torque oscillation induced by an asymmetrical grid fault. The drive-train load of the wind turbine during an asymmetrical grid fault is improved by the proposed FRT controller. A method to decouple the DFIG controller and the proposed FRT controller is also described in this chapter. The DFIG control is not influenced by the injection of the FRT control.

- A multi-band PSS design is proposed for a DFIG-based wind turbine to contribute to long-term power system stability without affecting wind turbine torque control or at the cost of significantly increased structural loads. The proposed multi-band PSS provides accurate control on various power system modes and wind turbine structural modes. The damping on each mode can be adjusted separately according to need. The multi-band PSS is shown to be able to reduce wind turbine drive-train load and improve power system damping at the same time. Moreover, the concept can be applied for wind turbines to meet future grid code requirements such as the ride-through of long-term grid fault/power system oscillation or provide inter-area damping to grid.

7.2 Future work

This thesis provides the investigation of the fault ride-through of the DFIG-based wind turbine from the combined mechanical and electrical perspectives. The baseline work such as modelling and basic FRT strategy on this issue is given. It is possible to extend the current research in the following aspects:

- The current research is based on software modelling and simulation. It would be useful to examine the proposed FRT strategy with an experimental test rig. The accurate model validation and performance test depend on the hardware experiment.

- The FRT strategies for various types of fault can be extended to PMG-based wind turbines. The PMG-based wind turbine naturally has enhanced fault ride-through capability due to the use of a fully-rated converter. The author did not investigate the fault ride-through of the PMG type wind turbine because of the present market share and the toughness of FRT. However, the

wind turbine based on a PMG has great potential in the future wind turbine market. It is possible to apply the proposed FRT strategies on PMG-based wind turbines to further improve the FRT and contribution to network.

- The FRT strategies in this thesis are implemented using the most popular and practical controller, which is the PID controller. The power electronics used are also mature equipment, which widely exists in industry. It is possible to use advanced control theory and advanced power electronics to improve the performance of the wind turbine FRT.

- Economics is not considered in this thesis. The cost-effectiveness of the proposed controllers should be tested for the commercialization of the FRT controller. The design of the FRT strategy can be further optimized by taking price into consideration.

REFERENCES

[1] Intergovernmental Panel on Climate Change, "Climate Change 2007: Synthesis Report," ed. Available: http://www.ipcc.ch/pdf/assessment-report/ar4/syr/ar4_syr.pdf

[2] United Nations Framework Convention on Climate Change, "Status of Ratification of the Kyoto Protocol," ed. Available: http://unfccc.int/kyoto_protocol/status_of_ratification/items/2613.php

[3] Renewable UK, "Wind: State of the Industry 2012," ed, 2012. Available: http://www.renewableuk.com/en/publications/reports.cfm/SOI2012

[4] European Wind Energy Association, "Wind in Power: 2011 European Statistics," ed. Available: http://www.ewea.org/fileadmin/files/library/publications/statistics/Wind_in_power_2011_European_statistics.pdf

[5] American Wind Energy Association, "Awea U.S. Wind Industry Third Quarter 2012 Market Report," ed. Available: https://www.awea.org/learnabout/publications/reports/upload/3Q2012-Market-Report_Public-Version.pdf

[6] Global Wind Energy Association, "Global Wind Report 2011 - Annual Market Update." Available: http://gwec.net/wp-content/uploads/2012/06/Annual_report_2011_lowres.pdf

[7] World Wind Energy Association. World Wind Energy Report 2012. Available: http://www.wwindea.org/webimages/WorldWindEnergyReport2012_final.pdf

[8] World Wind Energy Association, "World Wind Energy Report 2010," 26/Aug/2013 2010. Available: http://www.wwindea.org/home/images/stories/pdfs/worldwindenergyreport2010_s.pdf

[9] F.K.A. Lima, A. Luna, P. Rodriguez, E.H. Watanabe, and F. Blaabjerg, "Rotor Voltage Dynamics in the Doubly Fed Induction Generator During Grid Faults," *Power Electronics, IEEE Transactions on*, vol. 25, pp. 118-130, 2010.

[10] I.M. de Alegría, J. Andreu, J.L. Martín, P. Ibañez, J.L. Villate, and H. Camblong, "Connection Requirements for Wind Farms: A Survey on Technical Requierements and Regulation," *Renewable and Sustainable Energy Reviews*, vol. 11, pp. 1858-1872, 2007.

[11] National Grid Electricity Transmission plc,"The Grid Code, Issue 5, Rev. 1," 06 November 2012.

[12] TSO Scottish, "Scottish Grid Code," *Scottish Hydro-Electric Transmission Ltd*.

[13] D.G. Code, "Technical Regulations 3.2. 5 Wind Turbines Connected to Grids with Voltages Below 100 Kv," ed: Dec, 2010.

[14] D.G. Code, "Technical Regulations 3.2. 5 Wind Turbines Connected to Grids with Voltages above 100 Kv," 2010.
[15] E.ON Netz, "Grid Code High and Extra High Voltage," *E. ON Netz GmbH, Bayreuth*, 2006.
[16] E.ON Netz, "Requirements for Offshore Grid Connections in the Eon Netz Network," 2008.
[17] State Grid Corporation of China, "Technical Regulation for Interconnection of Wind Farms into Grid (Exposure Draft)," 2009.
[18] Federal Energy Regulatory Commission, "Interconnection for Wind Energy, Final Rule," June 2005.
[19] M. Altın, O. Goksu, R. Teodorescu, P. Rodriguez, B.B. Jensen, and L. Helle, "Overview of Recent Grid Codes for Wind Power Integration," in *Optimization of Electrical and Electronic Equipment (OPTIM), 2010 12th International Conference on*, 2010, pp. 1152-1160.
[20] W. Christiansen and D.T. Johnsen, "Analysis of Requirements in Selected Grid Codes," *Technical University of Denmark (DTU), Copenhagen*, p. 31, 2006.
[21] I. Erlich and U. Bachmann, "Grid Code Requirements Concerning Connection and Operation of Wind Turbines in Germany," in *Power Engineering Society General Meeting, 2005. IEEE*, 2005, pp. 1253-1257.
[22] F. Iov, A.D. Hansen, P.E. Sørensen, and N.A. Cutululis, "Mapping of Grid Faults and Grid Codes," Risø National Laboratory 8755036228, 2007.
[23] B. Singh and S.N Singh, "Wind Power Interconnection into the Power System: A Review of Grid Code Requirements," *The Electricity Journal*, vol. 22, pp. 54-63, 2009.
[24] A. Arulampalam, G. Ramtharan, N. Jenkins, V.K. Ramachandaramurthy, J.B. Ekanayake, and G. Strbac, "Trends in Wind Power Technology and Grid Code Requirements," in *Industrial and Information Systems, 2007. ICIIS 2007. International Conference on*, 2007, pp. 129-134.
[25] C. Jauch, J. Matevosyan, T. Ackermann, and S. Bolik, "International Comparison of Requirements for Connection of Wind Turbines to Power Systems," *Wind energy*, vol. 8, pp. 295-306, 2005.
[26] A. Johnson and N. Tleis, "The Development of Grid Code Requirements for New and Renewable Forms of Generation in Great Britain," *Wind Engineering*, vol. 29, pp. 201-216, 2005.
[27] M. Tsili, C. Patsiouras, and S. Papathanassiou, "Grid Code Requirements for Large Wind Farms: A Review of Technical Regulations and Available Wind Turbine Technologies," in *Proceedings of EWEC*, 2008.
[28] A. Causebrook and B. Fox, "Modernising Grid Codes to Accommodate Diverse Generation Technologies, Especially Modern Windfarms," *Wind Engineering*, vol. 28, pp. 75-86, 2004.

[29] M. Tsili and S. Papathanassiou, "A Review of Grid Code Technical Requirements for Wind Farms," *Renewable Power Generation, IET,* vol. 3, pp. 308-332, 2009.
[30] F. Zhang, W. E. Leithead, and O. Anaya-Lara, "Wind Turbine Control Design to Enhance the Fault Ride-through Capability," in *Renewable Power Generation (RPG 2011), IET Conference on*, 2011, pp. 1-6.
[31] T. Ackermann, *Wind Power in Power Systems* vol. 140: Wiley Online Library, 2005.
[32] ECAR Ltd., "Wind Integration: International Experience," ed, 2012.
[33] J. L. Dallachy and I. Tait, "Guidance Note for the Connection of Wind Farms," *SP Transmission and Distribution,* 2002.
[34] A. Sudrià, M. Chindris, A. Sumper, G. Gross, and F. Ferrer, "Wind Turbine Operation in Power Systems and Grid Connection Requirements," *IEEE Power and Energy Magazine,* vol. 5, pp. 47-51, 2007.
[35] J.G Slootweg, S.W.H De Haan, H. Polinder, and W.L Kling, "General Model for Representing Variable Speed Wind Turbines in Power System Dynamics Simulations," *Power Systems, IEEE Transactions on,* vol. 18, pp. 144-151, 2003.
[36] S. Muller, M. Deicke, and R.W. De Doncker, "Doubly Fed Induction Generator Systems for Wind Turbines," *Industry Applications Magazine, IEEE,* vol. 8, pp. 26-33, 2002.
[37] F. Van Hulle, "Large Scale Integration of Wind Energy in the European Power Supply: Analysis, Issues and Recommendations," *European Wind Energy Association (EWEA),* 2005.
[38] T. Burton, N. Jenkins, D. Sharpe, and E. Bossanyi, *Wind Energy Handbook*: Wiley, 2011.
[39] Z. Chen, J. M. Guerrero, and F. Blaabjerg, "A Review of the State of the Art of Power Electronics for Wind Turbines," *Power Electronics, IEEE Transactions on,* vol. 24, pp. 1859-1875, 2009.
[40] S. Seman, J. Niiranen, and A. Arkkio, "Ride-through Analysis of Doubly Fed Induction Wind-Power Generator under Unsymmetrical Network Disturbance," *Power Systems, IEEE Transactions on,* vol. 21, pp. 1782-1789, 2006.
[41] A.D. Hansen and G. Michalke, "Fault Ride-through Capability of Dfig Wind Turbines," *Renewable energy,* vol. 32, pp. 1594-1610, 2007.
[42] D.M. Robb and W.E. Leithead, "Derivation and Validation of Simple Correlated Wind Speed Models," Internal Report, Department of Electrical and Electronic Engineering, University of Strathclyde, Glasgow, Scotland.
[43] W.E Leithead and M.C.M. Rogers, "Drive-Train Characteristics of Constant Speed Hawt's: Part I-Representation by Simple Dynamic Models," *Wind Engineering,* vol. 20, pp. 149-174, 1996.

[44]W.E. Leithead and M.C.M. Rogers, "Drive-Train Characteristics of Constant Speed Hawt's: Part Ii-Simple Characterisation of Dynamics," *Wind Engineering,* vol. 20, p. 175, 1996.
[45]W.E. Leithead and B. Connor, "Control of Variable Speed Wind Turbines: Design Task," *International Journal of Control,* vol. 73, pp. 1189-1212, 2000.
[46]W.E. Leithead and B. Connor, "Control of Variable Speed Wind Turbines: Dynamic Models," *International Journal of Control,* vol. 73, pp. 1173-1188, 2000.
[47]D.J. Leith and W.E. Leithead, "Implementation of Wind Turbine Controllers," *International Journal of Control,* vol. 66, pp. 349-380, 1997.
[48]B. G. Rawn, P. W. Lehn, and M. Maggiore, "Control Methodology to Mitigate the Grid Impact of Wind Turbines," *Energy Conversion, IEEE Transactions on,* vol. 22, pp. 431-438, 2007.
[49]W.E. Leithead, S. De la Salle, and D. Reardon, "Role and Objectives of Control for Wind Turbines," in *IEE Proceedings C (Generation, Transmission and Distribution),* 1991, pp. 135-148.
[50]C. Nichita, D. Luca, B. Dakyo, and E. Ceanga, "Large Band Simulation of the Wind Speed for Real Time Wind Turbine Simulators," *Energy Conversion, IEEE Transactions on,* vol. 17, pp. 523-529, 2002.
[51]S. Dominguez, "Nm92 Controller Performance Analysis," University of Strathclyde.
[52]W.E. Leithead and S. Dominguez, "Active Regulation of Multi-Mw Wind Turbines: An Overview," *POWER SYSTEM TECHNOLOGY-BEIJING-*, vol. 31, p. 24, 2007.
[53]A.P.Chatzopoulos, "Full Envelope Wind Turbine Controller Design for Power Regulation and Tower Load Reduction," Doctor of Philosophy, Department of Electronic and Electrical Engineering,, University of Strathclyde, Glasgow, 2011.
[54]R. Pena, J.C. Clare, and G.M. Asher, "Doubly Fed Induction Generator Using Back-to-Back Pwm Converters and Its Application to Variable-Speed Wind-Energy Generation," in *Electric Power Applications, IEE Proceedings-*, 1996, pp. 231-241.
[55]F. Mei and B.C. Pal, "Modelling and Small-Signal Analysis of a Grid Connected Doubly-Fed Induction Generator," in *Power Engineering Society General Meeting, 2005. IEEE,* 2005, pp. 2101-2108.
[56]J. Morren, S.W.H. de Haan, P. Bauer, J.T.G. Pierik, and J. Bozelie, "Comparison of Complete and Reduced Models of a Wind Turbine with Doubly-Fed Induction Generator," *Proceed. of EPE,* vol. 3, 2003.
[57]F. Blaabjerg, R. Teodorescu, M. Liserre, and A.V. Timbus, "Overview of Control and Grid Synchronization for Distributed Power Generation Systems," *Industrial Electronics, IEEE Transactions on,* vol. 53, pp. 1398-1409, 2006.
[58]K. Elkington, V. Knazkins, and M. Ghandhari, "On the Stability of Power Systems Containing Doubly Fed Induction Generator-Based Generation," *Electric Power Systems Research,* vol. 78, pp. 1477-1484, 2008.

[59] S. Mechthild Bolik, *Modelling and Analysis of Variable Speed Wind Turbines with Induction Generator During Grid Fault*: Videnbasen for Aalborg UniversitetVBN, Aalborg UniversitetAalborg University, Det Teknisk-Naturvidenskabelige FakultetThe Faculty of Engineering and Science, Institut for EnergiteknikDepartment of Energy Technology, 2004.
[60] J.L. Blackburn, *Symmetrical Components for Power Systems Engineering* vol. 85: CRC, 1993.
[61] L. Holdsworth, XG Wu, JB Ekanayake, and N. Jenkins, "Comparison of Fixed Speed and Doubly-Fed Induction Wind Turbines During Power System Disturbances," in *Generation, Transmission and Distribution, IEE Proceedings-*, 2003, pp. 343-352.
[62] P. Kundur, N.J. Balu, and M.G. Lauby, *Power System Stability and Control* vol. 4: McGraw-hill New York, 1994.
[63] J.B. Ekanayake, L. Holdsworth, X.G. Wu, and N. Jenkins, "Dynamic Modeling of Doubly Fed Induction Generator Wind Turbines," *Power Systems, IEEE Transactions on,* vol. 18, pp. 803-809, 2003.
[64] O. Anaya-Lara, F.M. Hughes, N. Jenkins, and G. Strbac, "Rotor Flux Magnitude and Angle Control Strategy for Doubly Fed Induction Generators," *Wind energy,* vol. 9, pp. 479-495, 2006.
[65] A. Tapia, G. Tapia, J.X. Ostolaza, and J.R. Saenz, "Modeling and Control of a Wind Turbine Driven Doubly Fed Induction Generator," *Energy Conversion, IEEE Transactions on,* vol. 18, pp. 194-204, 2003.
[66] L. Congwei, W. Haiqing, S. Xudong, and L. Fahai, "Research of Stability of Double Fed Induction Motor Vector Control System," in *Electrical Machines and Systems, 2001. ICEMS 2001. Proceedings of the Fifth International Conference on,* 2001, pp. 1203-1206.
[67] A. Petersson, L. Harnefors, and T. Thiringer, "Evaluation of Current Control Methods for Wind Turbines Using Doubly-Fed Induction Machines," *Power Electronics, IEEE Transactions on,* vol. 20, pp. 227-235, 2005.
[68] J. Fortmann, "Validation of Dfig Model Using 1.5 Mw Turbine for the Analysis of Its Behaviour During Voltage Drops in the 110 Kv Grid," in *Proc. of 4th Int. Workshop on Large-Scale Integration of Wind Power and Transmission Networks for Offshore Wind*, 2003.
[69] A. Petersson, S. Lundberg, and T. Thiringer, "A Dfig Wind Turbine Ride‐through System. Influence on the Energy Production," *Wind energy,* vol. 8, pp. 251-263, 2005.
[70] A. Causebrook, D.J. Atkinson, and A.G. Jack, "Fault Ride-through of Large Wind Farms Using Series Dynamic Braking Resistors (March 2007)," *Power Systems, IEEE Transactions on,* vol. 22, pp. 966-975, 2007.

[71]O. Anaya-Lara, M. Hughes, and N. Jenkins, "Generic Network Model for Wind Farm Control Scheme Design and Performance Assessment," *Network,* vol. 1, p. C2, 2005.
[72]D.C. Lee, "Ieee Recommended Practice for Excitation System Models for Power System Stability Studies (Ieee Std 421.5-1992)," *Energy Development and Power Generating Committee of the Power Engineering Society,* 1992.
[73]V. Akhmatov, H. Knudsen, A. H. Nielsen, Jørgen Kaas Pedersen, and Niels Kjølstad Poulsen, "Modelling and Transient Stability of Large Wind Farms," *International Journal of Electrical Power & Energy Systems,* vol. 25, pp. 123-144, 2003.
[74]F. M. Hughes, O. Anaya-Lara, N. Jenkins, and G. Strbac, "A Power System Stabilizer for Dfig-Based Wind Generation," *Power Systems, IEEE Transactions on,* vol. 21, pp. 763-772, 2006.
[75]IEEE Project Working Group, "Electric Power System Compatibility with Industrial Process Equipment. Part I. Voltage Sags," in *Industrial and Commercial Power Systems Technical Conference*, 1994, pp. 261-266.
[76]J.C. Das, "Effects of Momentary Voltage Dips on the Operation of Induction and Synchronous Motors," *Industry Applications, IEEE Transactions on,* vol. 26, pp. 711-718, 1990.
[77]M. H.J. Bollen, "The Influence of Motor Reacceleration on Voltage Sags," *Industry Applications, IEEE Transactions on,* vol. 31, pp. 667-674, 1995.
[78]M. K. and Y. Liao, "A New Method for Classification and Characterization of Voltage Sags," *Electric Power Systems Research,* vol. 58, pp. 27-35, 2001.
[79]J. Lopez, P. Sanchis, X. Roboam, and L. Marroyo, "Dynamic Behavior of the Doubly Fed Induction Generator During Three-Phase Voltage Dips," *Energy Conversion, IEEE Transactions on,* vol. 22, pp. 709-717, 2007.
[80]D. Xiang, L. Ran, P.J. Tavner, and S. Yang, "Control of a Doubly Fed Induction Generator in a Wind Turbine During Grid Fault Ride-Through," *Energy Conversion, IEEE Transactions on,* vol. 21, pp. 652-662, 2006.
[81]J. López, E. Gubía, E. Olea, J. Ruiz, and L. Marroyo, "Ride through of Wind Turbines with Doubly Fed Induction Generator under Symmetrical Voltage Dips," *Industrial Electronics, IEEE Transactions on,* vol. 56, pp. 4246-4254, 2009.
[82]J. Liang, W. Qiao, and R. G. Harley, "Feed-Forward Transient Current Control for Low-Voltage Ride-through Enhancement of Dfig Wind Turbines," *Energy Conversion, IEEE Transactions on,* vol. 25, pp. 836-843, 2010.
[83]M. Mohseni, S. Islam, and MAS Masoum, "Fault Ride-through Capability Enhancement of Doubly-Fed Induction Wind Generators," *Renewable Power Generation, IET,* vol. 5, pp. 368-376, 2011.
[84]A.H. Kasem, E.F. El-Saadany, H.H. El-Tamaly, and M.A.A Wahab, "An Improved Fault Ride-through Strategy for Doubly Fed Induction Generator-Based Wind Turbines," *Renewable Power Generation, IET,* vol. 2, pp. 201-214, 2008.

[85]J. Yang, J.E. Fletcher, and J. O'Reilly, "A Series-Dynamic-Resistor-Based Converter Protection Scheme for Doubly-Fed Induction Generator During Various Fault Conditions," *Energy Conversion, IEEE Transactions on*, vol. 25, pp. 422-432, 2010.
[86]V. Akhmatov, *Analysis of Dynamic Behaviour of Electric Power Systems with Large Amount of Wind Power*: Electric Power Engineering, Ørsted-DTU, Technical University of Denmark, 2003.
[87]M.R. Khadraoui and M. Elleuch, "Comparison between Optislip and Fixed Speed Wind Energy Conversion Systems," 2008, pp. 1-6.
[88]K.V. Kumar, A.N. Rao, and MP Selvan, "Mitigation of Output Power Fluctuations in Wind Farms with Opti-Slip Induction Generator," 2009, pp. 1-5.
[89]A.D. Hansen, G. Michalke, P. Sørensen, T. Lund, and F. Iov, "Co‐Ordinated Voltage Control of Dfig Wind Turbines in Uninterrupted Operation During Grid Faults," *Wind energy*, vol. 10, pp. 51-68, 2007.
[90]C. Zhan and C.D. Barker, "Fault Ride-through Capability Investigation of a Doubly-Fed Induction Generator with an Additional Series-Connected Voltage Source Converter," in *AC and DC Power Transmission, 2006. ACDC 2006. The 8th IEE International Conference on*, 2006, pp. 79-84.
[91]C. Jin and P. Wang, "Enhancement of Low Voltage Ride-through Capability for Wind Turbine Driven Dfig with Active Crowbar and Battery Energy Storage System," in *Power and Energy Society General Meeting, 2010 IEEE*, 2010, pp. 1-8.
[92]X. Zhang and D. Xu, "Research on Control of Dfig with Active Crowbar under Symmetry Voltage Fault Condition," *Electric Machines and Control*, vol. 1, p. 020, 2009.
[93]Z. Peng and Y. He, "Control Strategy of an Active Crowbar for Dfig Based Wind Turbine under Grid Voltage Dips," in *Electrical Machines and Systems, 2007. ICEMS. International Conference on*, 2007, pp. 259-264.
[94]J. Yang, "Fault Analysis and Protection for Wind Power Generation Systems," University of Glasgow, 2011.
[95]O. Anaya-Lara, Z.F. Liu, G. Quinonez-Varela, and J.R. McDonald, "Optimal Dfig Crowbar Resistor Design under Different Controllers During Grid Faults," 2008, pp. 2580-2585.
[96]V. Akhmatov, "Variable-Speed Wind Turbines with Doubly-Fed Induction Generators Part Iii: Model with the Back-to-Back Converters," *Wind Engineering*, vol. 27, pp. 79-91, 2003.
[97]G. Tsourakis and C.D. Vournas, "Simulation of Low Voltage Ride through Capability of Wind Turbines with Doubly Fed Induction Generator," in *Proceedings of the 2006 European Wind Energy Conference, Athens*, 2006.
[98]M. R. Rathi and N. Mohan, "A Novel Robust Low Voltage and Fault Ride through for Wind Turbine Application Operating in Weak Grids," in *Industrial*

Electronics Society, 2005. IECON 2005. 31st Annual Conference of IEEE, 2005, p. 6 pp.
[99]T. Sun, Z. Chen, and F. Blaabjerg, "Voltage Recovery of Grid-Connected Wind Turbines with Dfig after a Short-Circuit Fault," in *Power Electronics Specialists Conference, 2004. PESC 04. 2004 IEEE 35th Annual*, 2004, pp. 1991-1997.
[100] O. Anaya-Lara, N. Jenkins, J. Ekanayake, P. Cartwright, and M. Hughes, *Wind Energy Generation: Modelling and Control*: Wiley, 2011.
[101] L. Holdsworth, N Jenkins, and G Strbac, "Electrical Stability of Large, Offshore Wind Farms," in *AC-DC Power Transmission, 2001. Seventh International Conference on (Conf. Publ. No. 485)*, 2001, pp. 156-161.
[102] A. Causebrook, "Fault Ride-through of Wind Farms Using Series Dynamic Braking Resistors," University of Newcastle-Upon-Tyne, 2008.
[103] V. Akhmatov, "Variable-Speed Windturbines with Doubly-Fed Induction Generators Part Ii: Power System Stability," *Wind Engineering*, vol. 26, pp. 171-188, 2002.
[104] A. D. Hansen and G. Michalke, "Voltage Grid Support of Dfig Wind Turbines During Grid Faults," in *2007 European Wind Energy Conference and Exhibition*, 2007.
[105] C. Feltes and I. Erlich, "Variable Frequency Operation of Dfig Based Wind Farms Connected to the Grid through Vsc-Hvdc Link," in *Power Engineering Society General Meeting, 2007. IEEE*, 2007, pp. 1-7.
[106] B. I. Næss, T. M. Undeland, and T. Gjengedal, "Methods for Reduction of Voltage Unbalance in Weak Grids Connected to Wind Plants," in *IEEE/CIGRE Workshop on Wind Power and the Impacts on Power Systems*, 2002.
[107] L. Xu and Y. Wang, "Dynamic Modeling and Control of Dfig-Based Wind Turbines under Unbalanced Network Conditions," *Power Systems, IEEE Transactions on*, vol. 22, pp. 314-323, 2007.
[108] M.R. Rathi, P. P. Jose, and N. Mohan, "A Novel H∞ Based Controller for Wind Turbine Applications Operating under Unbalanced Voltage Conditions," *Space*, vol. 1, p. 2, 2005.
[109] H. Song and K. Nam, "Dual Current Control Scheme for Pwm Converter under Unbalanced Input Voltage Conditions," *Industrial Electronics, IEEE Transactions on*, vol. 46, pp. 953-959, 1999.
[110] Y. Wang and L. Xu, "Control of Dfig-Based Wind Generation Systems under Unbalanced Network Supply," in *Electric Machines & Drives Conference, 2007. IEMDC'07. IEEE International*, 2007, pp. 430-435.
[111] T.K.A. Brekken and N. Mohan, "Control of a Doubly Fed Induction Wind Generator under Unbalanced Grid Voltage Conditions," *Energy Conversion, IEEE Transactions on*, vol. 22, pp. 129-135, 2007.
[112] E. Clarke, *Circuit Analysis of Ac Power Systems; Symmetrical and Related Components* vol. 1: Wiley, 1943.

[113] J. Hu, Y. He, L. Xu, and B.W. Williams, "Improved Control of Dfig Systems During Network Unbalance Using Pi–R Current Regulators," *Industrial Electronics, IEEE Transactions on,* vol. 56, pp. 439-451, 2009.
[114] C. Martinez, G. Joos, and B.T. Ooi, "Power System Stabilizers in Variable Speed Wind Farms," in *Power & Energy Society General Meeting, 2009. PES'09. IEEE,* 2009, pp. 1-7.
[115] F.M. Hughes, O. Anaya-Lara, G. Ramtharan, N. Jenkins, and G. Strbac, "Influence of Tower Shadow and Wind Turbulence on the Performance of Power System Stabilizers for Dfig-Based Wind Farms," *Energy Conversion, IEEE Transactions on,* vol. 23, pp. 519-528, 2008.
[116] B. Badrzadeh, S.K. Salman, and K.S. Smith, "Assessment and Enhancement of Grid Fault-Induced Torsional Oscillations for Induction Generator-Based Wind Turbines," in *Power Systems Conference and Exposition, 2009. PSCE'09. IEEE/PES*, 2009, pp. 1-7.
[117] A. F. Snyder, N. Hadjsaïd, D. Georges, L. Mili, A.G. Phadke, O. Faucon, and S. Vitet, "Inter-Area Oscillation Damping with Power System Stabilizers and Synchronized Phasor Measurements," in *Power System Technology, 1998. Proceedings. POWERCON'98. 1998 International Conference on*, 1998, pp. 790-794.
[118] M.Alivirdizadeh, B.Tousi, H.Ghahramani, J. Khazaie, and S.Rajebi, "A Novel Damping Controller for Inter-Area Oscillation by Means of Dfig-Based Wind Farm," *International Journal on Technical and Physical Problems of Engineering (IJTPE),* pp. 118-124.
[119] D.Ke, "Damping Controller Designs to Suppress Inter-Area Oscillations in Power Systems by Using Novel Eigenstructure-Based Indexes," 2012.
[120] A. Mendonca and J.A. Peças Lopes, "Robust Tuning of Power System Stabilisers to Install in Wind Energy Conversion Systems," *Renewable Power Generation, IET,* vol. 3, pp. 465-475, 2009.
[121] A.L.B.D. Bomfim, G.N. Taranto, and D.M. Falcao, "Simultaneous Tuning of Power System Damping Controllers Using Genetic Algorithms," *Power Systems, IEEE Transactions on,* vol. 15, pp. 163-169, 2000.
[122] Y. Mishra, S. Mishra, M. Tripathy, N. Senroy, and Z.Y. Dong, "Improving Stability of a Dfig-Based Wind Power System with Tuned Damping Controller," *Energy Conversion, IEEE Transactions on,* vol. 24, pp. 650-660, 2009.
[123] N. Kshatriya, U.D. Annakkage, F. M. Hughes, and A.M. Gole, "Optimized Partial Eigenstructure Assignment-Based Design of a Combined Pss and Active Damping Controller for a Dfig," *Power Systems, IEEE Transactions on,* vol. 25, pp. 866-876, 2010.
[124] "Computer Models for Representation of Digital-Based Excitation Systems " *Energy Conversion, IEEE Transactions on,* vol. 11, pp. 607 - 615 Sep 1996.

[125] P. Kundur, M. Klein, G.J. Rogers, and M.S. Zywno, "Application of Power System Stabilizers for Enhancement of Overall System Stability," *Power Systems, IEEE Transactions on,* vol. 4, pp. 614-626, 1989.
[126] E.V. Larsen and D.A. Swann, "Applying Power System Stabilizers Part Iii: Practical Considerations," *Power Apparatus and Systems, IEEE transactions on,* pp. 3034-3046, 1981.
[127] Y. Hsu and C. Chen, "Tuning of Power System Stabilizers Using an Artificial Neural Network," *Energy Conversion, IEEE Transactions on,* vol. 6, pp. 612-619, 1991.
[128] L. Cai and I. Erlich, "Simultaneous Coordinated Tuning of Pss and Facts Damping Controllers in Large Power Systems," *Power Systems, IEEE Transactions on,* vol. 20, pp. 294-300, 2005.
[129] Y. Hsu and C. Hsu, "Design of a Proportional-Integral Power System Stabilizer," *Power Systems, IEEE Transactions on,* vol. 1, pp. 46-52, 1986.
[130] P. Hoang and K. Tomsovic, "Design and Analysis of an Adaptive Fuzzy Power System Stabilizer," *Energy Conversion, IEEE Transactions on,* vol. 11, pp. 455-461, 1996.
[131] M.A. Abido and Y.L. Abdel-Magid, "A Hybrid Neuro-Fuzzy Power System Stabilizer for Multimachine Power Systems," *Power Systems, IEEE Transactions on,* vol. 13, pp. 1323-1330, 1998.
[132] R.K. Varma, S. Auddy, and Y. Semsedini, "Mitigation of Subsynchronous Resonance in a Series-Compensated Wind Farm Using Facts Controllers," *Power Delivery, IEEE Transactions on,* vol. 23, pp. 1645-1654, 2008.
[133] J. Conroy and R. Watson, "Torsional Damping Control of Gearless Full-Converter Large Wind Turbine Generators with Permanent Magnet Synchronous Machines," *Wind Engineering,* vol. 31, pp. 325-340, 2007.

APPENDIX A: PER-UNIT SYSTEM

The per-unit system (PU) is frequently used in power system analysis. The advantage of using per-unit system is the magnitude of variables is converted to a system regardless of the voltage level. The normalized quantities in per-unit system simplify the calculation by getting rid of conversion between different voltage levels. However, for mechanical analysis the international system of units (SI) is more convenient. The base values of the PU system and the conversion between PU and SI system is given in this section.

The base quality is defined first and other quantities are expressed as a fraction of the base quality in PU system. The base quality for the electrical system analysis and modelling in this thesis is shown in Table A-1. The traditional PU system does not contain the mechanical variables. The author defined a PU system for torque, rotational speed and frequency which is also described in Table A-1.

Table A-1: Per-unit system

Quantity	Notation	Derivation	Value
Power	P_{base}	Defined	10000000
Voltage	V_{base}	Defined	$575\sqrt{\frac{2}{3}}$
Current	I_{base}	$\frac{P_{base}}{V_{base}}$	14200
Resistance	R_{base}	$\frac{V_{base}}{I_{base}}$	0.03306
Frequency	f_{base}	Defined	60
Rotational Speed	w_{base}	$\frac{2\pi f_{base}}{p_{base}}$	125.6637
Inductance	L_{base}	$\frac{R_{base}}{2\pi f_{base}}$	0.00008769
Torque	T_{base}	$\frac{P_{base}}{w_{base}}$	13262.9

APPENDIX B: PARAMETERS OF THE WIND TURBINE AND ELECTRICAL SYSTEM

B.1 Electrical system parameters

Table B-1: DFIG parameters

Parameters of the electrical system (pu)	
DFIG	
Stator resistance	R_s=0.00491
Rotor resistance	R_r=0.00552
Stator inductance	L_s=0.09273
Rotor inductance	L_r=0.1
Mutual inductance	L_m=3.96545
Rotor speed limit	[0.5 1.5]
Stator self-inductance	$L_{ss}= L_s +L_m$
Rotor self-inductance	$L_{rr}= L_r +L_m$
DFIG controller	
Proportional gain	K_p=1

Integral gain	K_i=1
Limits for the DFIG control signal	[-1 1]
Voltage controller gain	K_{ivc}=0.01
Voltage controller gain	K_{pvc}=0.1
Voltage controller gain	K_{vc}=5
Synchronous generator	
Stator resistance	R_s=0.0037
Leakage inductance	L_{ls}=0.00003041
d-axis magnetizing inductance	L_{md}=0.001961
q-axis magnetizing inductance	L_{mq}=0.001634
Field resistance	R_f=0.001532
Leakage inductance	L_{lf}=0.0002729
d-axis resistance	Rd=0.1553
q-axis resistance	Rq=0.01569
d-axis leakage inductance	Lld=0.002244
q-axis leakage inductance	Llq=0.0001584

Excitation system	
AVR gain	K_a=250
AVR time constant	T_a=0.025
AVR time constant	T_b=5
AVR time constant	T_c=1.5
PSS time constant	T1=1.32
PSS time constant	T2=1.96
PSS time constant	T3=0.49
PSS time constant	T4=2.85
PSS gain	Kp=1
Turbine Governor	
Governor gain	Khp=0.3
Governor gain	Kd=100
Governor time constant	Thp=0.25
Governor time constant	Tg=0.2
Governor time constant	Tr=6

Turbine inertia	H=3.5
Multi-band PSS	
DFIG band gain	Kg1=100
DFIG band gain	Kg2=100
DFIG band time constant	Twg1=1
DFIG band time constant	Twg2=1
DFIG band time constant	Tg3=0.32
DFIG band time constant	Tg5=0.39
DFIG band time constant	Tg7=0.39
DFIG band time constant	Tg9=0.46
Wind turbine band gain	Kt1=100
Wind turbine band gain	Kt2=100
Wind turbine band time constant	Twt1=0.5
Wind turbine band time constant	Twt2=0.5
Wind turbine band time constant	Tt3=0.23333
Wind turbine band time constant	Tt5=0.28

Wind turbine band time constant	Tt7=0.28
Wind turbine band time constant	Tt9=0.336

B.2 Wind turbine parameters

The parameters of the 2MW exemplar 2MW SUPERGEN wind turbine are shown below. [126]

Table B-2: Wind turbine parameters

Parameters of the wind turbine	
Rotor	
Rotor radius [m]	R=37.5
Effective blade length (for wind speed correction) [m]	L=26.25
Distance of the centre of mass from the hub axis [m]	Rc=11.94
One blade mass [Kg]	Mblade=5320
One blade mass*3 [Kg]	Mbl = Mblade*3
Hub height [m]	h = 65
Tower/Rotor cross-coupling inertia [Kg*m^2]	Jc = Rc*h*Mbl
Flap natural frequency [rad/s]	w_f = 6.66

Rotor inertia [Kg*m^2]	J = 4.26849e+006
Blade flapwise stiffness [Nm/rad]	Kf = w_f^2*J
Edge natural frequency [rad/s]	w_e = 9.99
Blade edgewise stiffness [Nm/rad]	Ke = w_e^2*J
Rotor and nacelle mass [Kg]	Mr_n = 97961
Tower	
Tower fore-aft inertia [Kg*m^2]	Jt = h^2*(Mr_n-Mbl)
Tower fore-aft frequency [rad/s]	w_t = 2.5133
Tower fore-aft damping	Bt_param = 0.005
Tower fore-aft damping moment [Nm]	Bt = 2*Bt_param*w_t*Jt
Tower fore-aft stiffness [Nm/rad]	Kt = w_t^2*Jt
Tower side-side natural frequency [rad/s]	w_ts = 2.5133
Tower side-side inertia [Kg*m^2]	Jts = h^2*Mr_n
Tower side-side stiffness [Nm/rad]	Kts = w_ts^2*Jts
Tower side-side damping	Bts_param = 0.005
Tower side-side damping moment [Nm]	Bts = 2*Bts_param*w_ts*Jts

Coefficient to adjust tower/nacelle displacement	Ka = 1.4
Pitch actuator	
Pitch actuator transfer function	$G_{pa}(s) = \frac{39.48}{s^2 + 10.05s + 39.48}$
Operational parameters	
Minimum generator speed in generation mode [rad/s]	WMIN = 89.0118
Maximum generator speed in generation mode [rad/s]	WMAX = 157.07
Cut in wind speed [m/s]	WCUTIN = 4
Cut out wind speed [m/s]	WCUTOUT = 25
Nominal generator torque [Nm]	TQSET = 13403
Minimum pitch angle [deg]	PITMIN = -3
Maximum pitch angle [deg]	PITMAX = 90
Sampling time [s]	sample_time = 0.05
Air density [Kg/m^3]	rho = 1.225

Drive-train	
Hub inertia [Kg*m^2]	ILs = 12000
Low speed shaft damping	gls = 1e-007
High speed shaft damping	ghs = 5
Low speed shaft stiffness [Nm/rad]	KLsb = 1.9e+008
Low speed shaft material damping	g1s = 1.6e+006
High speed shaft material damping	g2s = 1000
High speed shaft stiffness [Nm/rad]	KHs = 1e+010
Gearbox ratio	N=n = 84.15
High speed shaft inertia [Kg*m^2]	J_Hs = 5
Generator inertia [Kg*m^2]	J_gen = 130
Drive-train efficiency below rated	EtaFL = 0.96
Drive-train efficiency above rated	EtaVS = 0.96
High speed shaft + generator inertia [Kg*m^2]	IHs = J_Hs+J_gen

APPENDIX C: TRANSFORMS

The transforms of DFIG mathematical equations between abc, αβ and dq frames are given below.

C.1 Clarke transformation[59]

Taking current as example, the Clarke transformation of DFIG from abc frame to αβ frame is

$$\begin{bmatrix} I_\alpha \\ I_\beta \\ I_0 \end{bmatrix} = M \begin{bmatrix} I_a \\ I_b \\ I_c \end{bmatrix}$$

where M is the Clarke transform matrix

$$M = \frac{2}{3}\begin{bmatrix} 1 & -\frac{1}{2} & -\frac{1}{2} \\ 0 & \frac{\sqrt{3}}{2} & -\frac{\sqrt{3}}{2} \\ \frac{1}{2} & \frac{1}{2} & \frac{1}{2} \end{bmatrix}$$

The inverse transform is

$$M^{-1} = \frac{2}{3}\begin{bmatrix} 1 & 0 & 1 \\ -\frac{1}{2} & \frac{\sqrt{3}}{2} & 1 \\ -\frac{1}{2} & -\frac{\sqrt{3}}{2} & 1 \end{bmatrix}$$

In balanced three-phase system , the zero term is zero and the Clarke transform becomes

$$\begin{bmatrix} I_\alpha \\ I_\beta \end{bmatrix} = M \begin{bmatrix} I_a \\ I_b \end{bmatrix}$$

The transformation matrix is

$$M = \begin{bmatrix} 1 & 0 \\ \frac{1}{\sqrt{3}} & \frac{2}{\sqrt{3}} \end{bmatrix}$$

And the inverse transformation matrix is

$$M^{-1} = \begin{bmatrix} 1 & 0 \\ -\frac{1}{2} & \frac{\sqrt{3}}{2} \\ -\frac{1}{2} & -\frac{\sqrt{3}}{2} \end{bmatrix}$$

C.2 dq0 transform[59]

The transformation between abc reference frame and synchronous rotating reference frame is referred to as park transformation or dqo transformation. The transformation is shown below in matrix form.

The park transform of current is expressed as

$$\begin{bmatrix} I_d \\ I_q \\ I_0 \end{bmatrix} = M \begin{bmatrix} I_a \\ I_b \\ I_c \end{bmatrix}$$

where

$$M = \frac{2}{3}\begin{bmatrix} \cos(\theta) & \cos\left(\theta - \frac{2\pi}{3}\right) & \cos\left(\theta + \frac{2\pi}{3}\right) \\ -\sin(\theta) & -\sin\left(\theta - \frac{2\pi}{3}\right) & -\sin\left(\theta + \frac{2\pi}{3}\right) \\ \frac{\sqrt{2}}{2} & \frac{\sqrt{2}}{2} & \frac{\sqrt{2}}{2} \end{bmatrix}$$

θ is the angle between d axis and a axis

The inverse park transform is expressed as

$$\begin{bmatrix} I_a \\ I_b \\ I_c \end{bmatrix} = M^{-1} \begin{bmatrix} I_d \\ I_q \\ I_0 \end{bmatrix}$$

where

$$M^{-1} = \frac{2}{3}\begin{bmatrix} \cos(\theta) & -\sin(\theta) & \frac{\sqrt{2}}{2} \\ \cos\left(\theta - \frac{2\pi}{3}\right) & -\sin\left(\theta - \frac{2\pi}{3}\right) & \frac{\sqrt{2}}{2} \\ \cos\left(\theta + \frac{2\pi}{3}\right) & -\sin\left(\theta + \frac{2\pi}{3}\right) & \frac{\sqrt{2}}{2} \end{bmatrix}$$